AD-A039 953 TDR INC LOS ANGELES CALIF F/G 1/3
FOUNDATION OF THE MAGNETIC FIELD INTEGRAL EQUATION CODE FOR THE--ETC(U)
APR 77 M I SANCER, S SIEGEL, A D VARVATSIS F29601-75-C-0067
UNCLASSIFIED AFWL-TR-76-279 NL

1 OF 2
AD
A039953

AFWL-TR-
76-279

FOUNDATION OF THE MAGNETIC FIELD INTEGRAL EQUATION CODE FOR THE CALCULATION OF ELECTROMAGNETIC PULSE EXTERNAL INTERACTION WITH AIRCRAFT

TDR, Incorporated
Los Angeles, CA 90049

April 1977

Final Report

AIR FORCE WEAPONS LABORATORY
Air Force Systems Command
Kirtland Air Force Base, NM 87117

This final report was prepared by TDR, Incorporated, Los Angeles, California, under Contract F29601-75-C-0067, Job Order 12090502 with the Air Force Weapons Laboratory, Kirtland Air Force Base, New Mexico. Captain Harrison (ELP) was the Laboratory Project Officer-in-Charge.

When US Government drawings, specifications, or other data are used for any purpose other than a definitely related Government procurement operation, the Government thereby incurs no responsibility nor any obligation whatsoever, and the fact that the Government may have formulated, furnished, or in any way supplied the said drawings, specifications, or other data is not to be regarded by implication or otherwise as in any manner licensing the holder or any other person or corporation or conveying any rights or permission to manufacture, use, or sell any patented invention that may in any way be related thereto.

This report has been reviewed by the Information Office (OI) and is releasable to the National Technical information Service (NTIS). At NTIS, it will be available to the general public, including foreign nations.

This technical report has been reviewed and is approved for publication.

Michael G. Harrison

MICHAEL G. HARRISON
Captain, USAF
Project Officer

FOR THE COMMANDER

Aaron B. Loggins

AARON B. LOGGINS
Lt Colonel, USAF
Chief, Phenomenology & Technology Branch

James L. Griggs

JAMES L. GRIGGS, JR.
Colonel, USAF
Chief, Electronics Division

DO NOT RETURN THIS COPY. RETAIN OR DESTROY.

UNCLASSIFIED

SECURITY CLASSIFICATION OF THIS PAGE (When Data Entered)

REPORT DOCUMENTATION PAGE

READ INSTRUCTIONS BEFORE COMPLETING FORM

1. REPORT NUMBER: AFWL-TR-76-279	2. GOVT ACCESSION NO.
3. RECIPIENT'S CATALOG NUMBER	
4. TITLE (and Subtitle): FOUNDATION OF THE MAGNETIC FIELD INTEGRAL EQUATION CODE FOR THE CALCULATION OF ELECTROMAGNETIC PULSE EXTERNAL INTERACTION WITH AIRCRAFT.	5. TYPE OF REPORT & PERIOD COVERED: Final Report.
	6. PERFORMING ORG. REPORT NUMBER
7. AUTHOR(s): Maurice I. Sancer, Scott Siegel, and A. D. Varvatsis	8. CONTRACT OR GRANT NUMBER(s): F29601-75-C-0067
9. PERFORMING ORGANIZATION NAME AND ADDRESS: TDR, Incorporated, 11777 San Vicente Blvd., Suite 725, Los Angeles, California 90049	10. PROGRAM ELEMENT, PROJECT, TASK AREA & WORK UNIT NUMBERS: 64747F, 12090502
11. CONTROLLING OFFICE NAME AND ADDRESS: Air Force Weapons Laboratory (ELP), Kirtland Air Force Base, NM 87117	12. REPORT DATE: Apr[illegible]77
	13. NUMBER OF PAGES: 148
14. MONITORING AGENCY NAME & ADDRESS (if different from Controlling Office)	15. SECURITY CLASS. (of this report): Unclassified
	15a. DECLASSIFICATION/DOWNGRADING SCHEDULE

16. DISTRIBUTION STATEMENT (of this Report)

Approved for public release; distribution unlimited.

17. DISTRIBUTION STATEMENT (of the abstract entered in Block 20, if different from Report)

18. SUPPLEMENTARY NOTES

19. KEY WORDS (Continue on reverse side if necessary and identify by block number)

Electromagnetic Fields and Waves
Aircraft Models
Numerical Analysis
Electromagnetic Pulse Interaction
Electromagnetic Pulse

20. ABSTRACT (Continue on reverse side if necessary and identify by block number)

This report presents the equations that are programmed along with their derivations and the underlying theory. The code determines the current density and charge density induced on a model of an aircraft. The equations that are programmed result from patch zoning the aircraft model in order to obtain a solution to the frequency domain representation of the magnetic field integral equation. The intent is to obtain solutions for a continuous spectrum that includes the low and resonant range of frequencies corresponding to the bulk of the energy in a typical EMP spectrum.

DD FORM 1 JAN 73 1473 EDITION OF 1 NOV 65 IS OBSOLETE

UNCLASSIFIED 392 622

SECURITY CLASSIFICATION OF THIS PAGE (When Data Entered)

ACKNOWLEDGEMENT

We would like to give Mike Harrison special thanks for his interest and encouragement concerning this work throughout its duration. We thank Bill Prather who, upon becoming involved with this project, gave us considerable support. This work evolved from previous efforts funded by AFWL and accordingly we thank Carl Baum and Phil Castillo for their continuing support.

CONTENTS

ILLUSTRATIONS

ILLUSTRATIONS (CONT.)

ILLUSTRATIONS (CONT.)

SECTION I

INTRODUCTION AND SUMMARY

This report accompanies a complete computer code to directly calculate the current density and charge density induced on the model of an aircraft depicted in figure 1. A description of the field incident on the model is presented in figure 2. The intent is to calculate these induced densities for a continuous spectrum that includes the low and resonant range of frequencies. The background establishing the need for the direct calculation of these quantities for EMP external coupling purposes is presented in reference 1. In that report, it was demonstrated that serious flaws existed in the prevalent stick model approach used to perform EMP external interaction calculations for aircraft. The essence of the error in that approach was the assumption that the current density distribution on the aircraft could be simply obtained from a knowledge of the bulk current. For this reason, the stick model approach was intended only to calculate the total current. In reference 1, it was demonstrated that methods employed to obtain the current density distribution from the bulk current made their largest error at low frequencies for which the density calculation was generally assumed to be the most accurate. The fact that an error becomes larger when it was expected to become smaller is an indication that the physics of the problem was not totally understood. Specifically, it was shown that the stick model approach could not yield a low frequency current density that was compatible with a magnetostatic solution.

The significance of the fact that current densities were incorrectly calculated will now be explained. It is the current density rather than the bulk current that is required by commonly employed deliberate antenna

---

1. Sancer, M. I., R. W. Latham and A. D. Varvatsis, Relationship Between Total Currents and Surface Current Densities Induced on Aircraft and Cylinders, Interaction Note 194, Air Force Weapons Laboratory, August 1974.

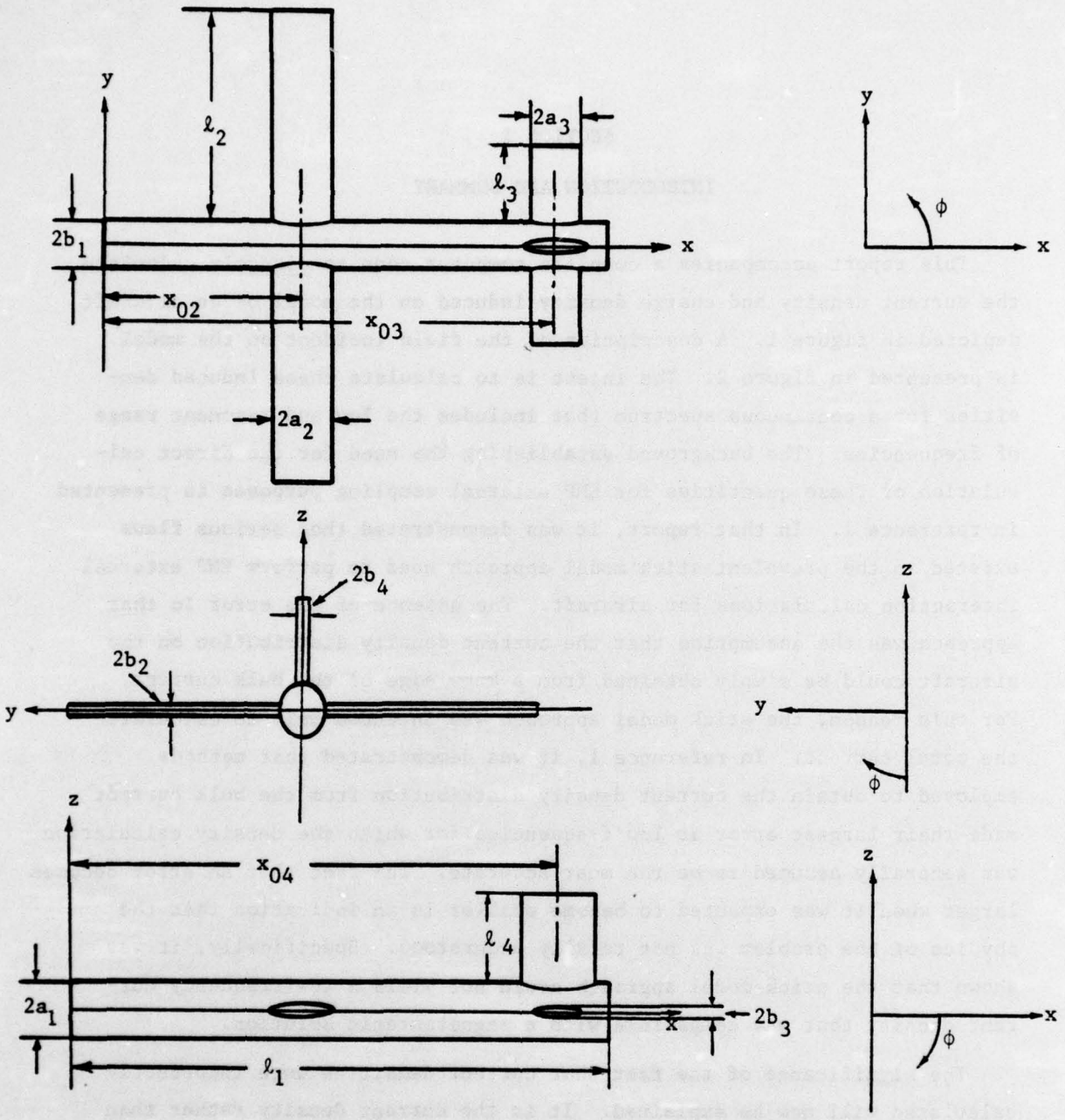

Figure 1: Aircraft model and input parameters.

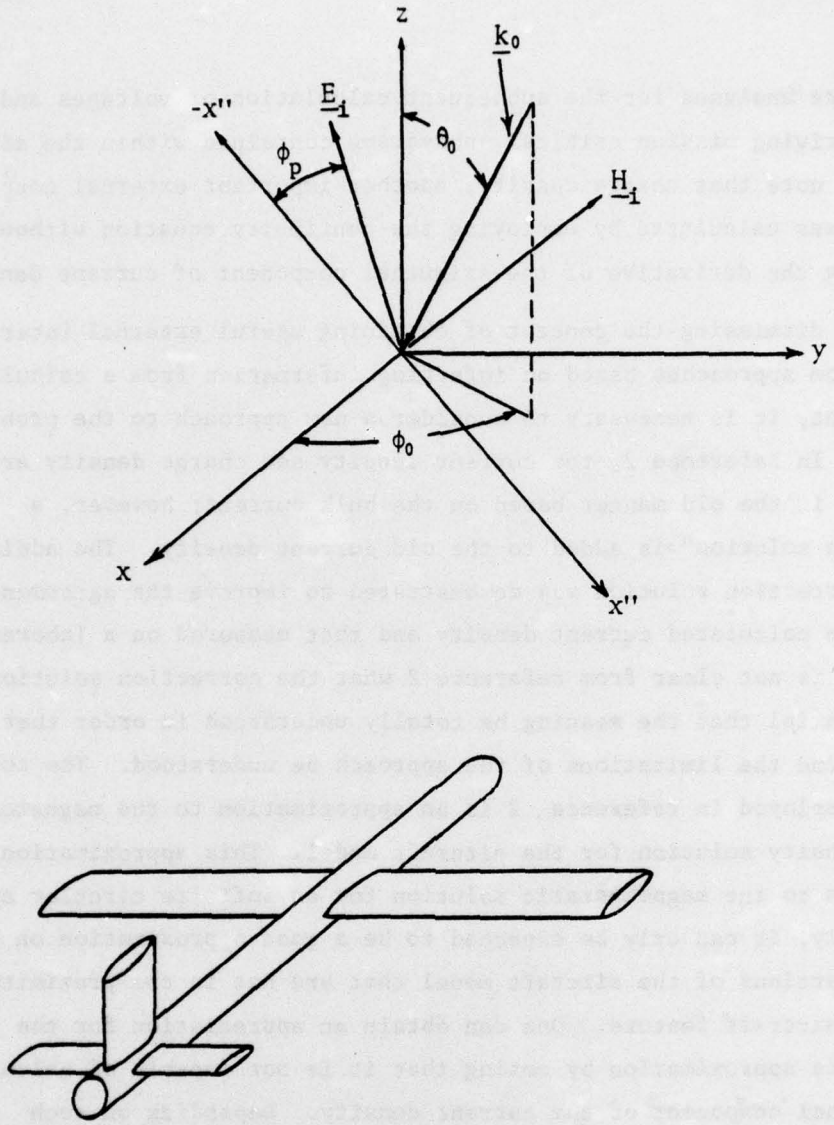

Figure 2: Description of the incident plane electromagnetic wave. Axis x'' is the intersection of the z,$\underline{k}$ plane and a plane perpendicular to $\underline{k}$ at the origin.

and aperture analyses for the subsequent calculation of voltages and currents driving mission critical subsystems contained within the aircraft. We note that charge density, another important external coupling quantity, was calculated by employing the continuity equation without considering the derivative of the azimuthal component of current density.

Before dismissing the concept of obtaining useful external interaction results from approaches based on inferring information from a calculated bulk current, it is necessary to consider a new approach to the problem (ref. 2). In reference 2, the current density and charge density are calculated in the old manner based on the bulk current; however, a "correction solution" is added to the old current density. The addition of this correction solution was demonstrated to improve the agreement between the calculated current density and that measured on a laboratory model. It is not clear from reference 2 what the correction solution means. It is essential that the meaning be totally understood in order that the potential and the limitations of the approach be understood. The correction solution employed in reference 2 is an approximation to the magnetostatic current density solution for the aircraft model. This approximation corresponds to the magnetostatic solution for an infinite circular cylinder. Consequently, it can only be expected to be a good approximation on circular cylinder portions of the aircraft model that are not in the proximity of any other aircraft feature. One can obtain an appreciation for the limitation of this approximation by noting that it is not capable of calculating the azimuthal component of the current density. Depending on such quantities as the incident field, frequency, and location of the body, the azimuthal component of the current density can be larger than the longitudinal component.

By understanding that the correction solution is an approximation to the magnetostatic solution, one can immediately appreciate one of the hidden difficulties of the approach. It is as difficult to obtain a

---

2. Taylor, C. D., K. T. Chen and T. T. Crow, Electromagnetic Pulse Interaction with the EC-135 Aircraft, AFWL-TR-75-205, Air Force Weapons Laboratory, June 1976.

magnetostatic solution for an aircraft model that includes important features, as it is to use our approach to calculate the current density directly. In fact, we obtain the magnetostatic current density for our aircraft model simply by setting the frequency equal to zero in our code. We see a possible benefit of adding our magnetostatic current density as the correction solution in order to obtain a better approximation to the current density using the modified bulk current approach of reference 2. The benefit of using our result in this manner would only be to save computer running time since we have to do as much analysis and programming to obtain the magnetostatic solution as to obtain the dynamic solution. The errors obtained would only be quantifiable by running our dynamic code at selected frequencies and comparing these results to those obtained by the improved approximate method. Finally, we note that the addition of the magnetostatic solution cannot improve the calculation of the charge density. This is the case because the divergence of the magnetostatic solution is zero.

The magnetostatic solution has considerably more significance than has already been discussed and this is a topic dealt with in a recent report (ref. 3). In that report it was demonstrated that the current density induced on a metallic body by an incident monochromatic plane wave behaved predominantly like a magnetostatic solution. It was shown that this was the case for an extended band of low frequencies and this frequency band can in turn be shown to correspond to a significant portion of the energy contained in a typical EMP spectrum. It is concluded that the magnetostatic response of a metallic system (aircraft, missile, etc.)

---

3. Sancer, M. I., Fundamental Errors Associated with the Gross Modeling of the Physical Features of Metallic Enclosures, AFWL-TR-76-297, Air Force Weapons Laboratory, December 1976.

should be considered in determining low frequency modeling requirements for EMP external coupling purposes. The primary significance of magnetostatic related modeling requirements is that they are much more severe than what has previously been thought justifiable as a result of considering long wavelength far zone scattering results. An appreciation concerning the impact of magnetostatics on determining modeling requirements can be obtained by noting the exact analogy between magnetostatics and irrotational and incompressible fluid flow around a rigid body. For a rigid perfectly conducting body, the velocity flow lines and the magnetic field lines in the vicinity of the body are identical. If certain features of aircraft or missiles would have a significant effect on fluid flow, then they would have a significant effect on the current density induced by an EMP. One should become concerned with modeling such features as missile tips and fins as well as aircraft features such as engines, wing cross sections, and extended junctions, particularly when the point of entry is in the proximity of these features.

In the process of developing the computer code described in this report, we became aware of the magnetostatic modeling consequences just discussed. This fact had an effect on our philosophy and approach in developing the computer code.

First, wherever possible we developed general results before restricting attention to our particular model. Second, we realized that our approach was dependent upon making zone sizes small enough to approximate the surface current density components as constants over the zone. In order to accommodate the possibility of rapidly changing current densities in the vicinity of edges, junctions, and high curvature we built a great deal of input controllable zoning into the code. This allows numerical experimentation to determine the effect of varying the zone size in the proximity of the above features and is potentially useful for obtaining zoning information for more complex models. An additional benefit of the zoning flexibility is that it permits one to increase the density of zones over the entire model, at the cost of increasing computer time, to either improve the accuracy of the solution or to obtain solutions for higher frequencies.

A description of the contents of the remaining part of this report will now be presented. In Section II we present the magnetic field integral equation (MFIE) for the current density and utilize the symmetry plane of the aircraft to transform this equation into a pair of more useful (for numerical purposes) integral equations for suitably defined fictitious current densities. The numerical solution for these integral equations only requires zoning of half of the aircraft. In Section III we trace the path that led us to the final zoning scheme on the surface of the aircraft. Section IV compares numerical solutions, obtained by using our MFIE patch zoning approach, with experimental data. These data were presented in two recent reports (refs. 4,5) and even though they refer to measurements of the current density on a finite metallic circular cylinder, rather than an aircraft model, they demonstrate the capability of our approach.

In Appendix A we demonstrate certain properties of the surface current density induced on a perfectly conducting body possessing one or more symmetry planes. These properties are useful in that they reduce computation time and also give insight as to the distribution of the induced current density on a perfectly conducting symmetric body. Part one of Appendix A considers a body with three planes of symmetry and places no restriction on the frequency of the incident wave. It assumes a wave vector perpendicular to a plane of symmetry and the electric field parallel to an axis of symmetry. The resulting relationships involve current densities at points symmetric to planes of symmetry other than the plane perpendicular to the wave vector. Part two considers the magnetostatic limit for a body with only one symmetry

---

4. Burton, R. W., R. W. P. King and D. Blejer, Surface Currents and Charges on a Thick Conducting Tube in an E-Polarized Plane-Wave Field, II. Measurements, progress report on contract F29601-75-C-0019, AFWL/ELPE, Kirtland Air Force Base, New Mexico, 1976.

5. King, R. W. P., Surface Currents and Charges on a Thick Conducting Tube in an E-Polarized Plane-Wave Field, IV. Generalization to Cylinders of Various Lengths, progress report on contract F29601-75-C-0019, AFWL/ELPE, Kirtland Air Force Base, New Mexico, 1976.

plane and an incident plane wave with a wave vector perpendicular to the symmetry plane. We show that the surface current density at points symmetric to the plane of symmetry are simply related. Since magnetostatics is a good approximation for an appreciable band of low frequencies, it follows that these relationships provide insight into the distribution of the current density on the surface of structures with a plane of symmetry including aircraft.

Appendix B presents the calculation of the surface current density induced on a perfectly conducting ellipsoid immersed in a magnetostatic field. This calculation was very helpful in predicting the magnetostatic current distribution on a finite elliptical cylinder which in turn was used to test the numerical results of the various zoning schemes as we explain in Section III.

Appendix C presents the method for numerical solution in detail. Specific topics treated are the model, zoning scheme, matrix equations for the current density, coordinates of centers and boundaries of zones, calculation of matrix elements, self-zone interaction considerations, interpolation scheme, calculation of charge density as well as edge and junction behavior. Finally, Appendix D supplements Appendix C by giving the coordinates and matrix elements for zones adjacent to junctions.

SECTION II

FORMULATION OF THE PROBLEM

The model of the aircraft we employ is depicted in figure 1. All components shown (fuselage, wings, horizontal stabilizers, vertical stabilizer) are perfectly conducting elliptical cylinders making perfect electric contact at the intersections. The aircraft is illuminated by a monochromatic plane electromagnetic wave of arbitrary direction and polarization. We are interested in calculating the surface current and charge densities everywhere on the surface of the aircraft. To do so we employ the magnetic field integral equation for the current density and utilize the symmetry of the aircraft about the xz-plane to transform this equation into a pair of more useful (for numerical purposes) integral equations for suitably defined fictitious current densities. Each of these equations lends itself to a numerical solution with a matrix (N/2) x (N/2) where (N x N) is the matrix of the original equation.

The magnetic field integral equation for a perfectly conducting body is

$$\frac{1}{2}\,\underline{J}(\underline{r}) = \underline{J}_i(\underline{r}) + \int_S \underline{\underline{K}}(\underline{r};\underline{r}_o) \cdot \underline{J}(\underline{r}_o)\, dS_o \qquad (1)$$

where $\underline{J}_i(\underline{r})$ is the incident current density, which serves as the source for the integral equation, given by

$$\underline{J}_i(\underline{r}) = \hat{n}(\underline{r}) \times \underline{H}_i(\underline{r}) \qquad (2)$$

$\hat{n}(\underline{r})$ is the unit normal to the surface at $\underline{r}$, $\underline{H}_i(\underline{r})$ is the incident magnetic field given by

$$\underline{H}_i(\underline{r}) = \underline{H}_o\, e^{i\underline{k}_o \cdot \underline{r}} \qquad (3)$$

$\underline{k}_o$ is the wave vector, $\underline{\underline{K}}$ is the kernel given by

$$\underline{\underline{K}}(\underline{r};\underline{r}_o) = \hat{n}(\underline{r}) \times [\nabla G_o(\underline{r};\underline{r}_o) \times \underline{\underline{I}}] = \hat{n}(\underline{r}) \times [\underline{R} \times \underline{\underline{I}}]\, Q(R) \tag{4}$$

$G_o = \exp[ik_oR]/4\pi R$ is the free space Green's function, $\underline{\underline{I}}$ is the identity operator and

$$Q(R) = \frac{e^{ik_oR}}{4\pi R^3}\,(ik_oR - 1)$$

$$\underline{R} = \underline{r} - \underline{r}_o$$

$$R = |\underline{R}| \tag{5}$$

The surface S extends over all components of the model shown in figure 1 including the flat caps.

It has been shown in reference 6 that for bodies possessing a symmetry plane say the xz-plane, equation (1) can be transformed into the following pair of equations

$$\left.\begin{aligned} \tfrac{1}{2}\,\underline{J}^+(\underline{r}^+) &= \underline{J}_i^+(\underline{r}^+) + \int_{S_+} \underline{\underline{K}}^+(\underline{r}^+;\underline{r}_o^+) \cdot \underline{J}^+(\underline{r}_o)\, dS_o \\ \tfrac{1}{2}\,\underline{J}^-(\underline{r}^-) &= \underline{J}_i^-(\underline{r}^+) + \int_{S_+} \underline{\underline{K}}^-(\underline{r}^+;\underline{r}_o^+) \cdot \underline{J}^-(\underline{r}_o)\, dS_o \end{aligned}\right\} \tag{6}$$

---

6. Sancer, M. I. and A. D. Varvatsis, Analytical and Numerical EMP Coupling Solutions for A Class of Structures Attached to the Wing of an Aircraft, AFWL-TR-74-298, July 1975 (also published as AFWL Interaction Note 197, October 1974).

where $\underline{J}^{\pm}(\underline{r}^{+}) = \frac{1}{2}\,[\underline{J}(\underline{r}^{+}) \pm \underline{\underline{R}}_y \cdot \underline{J}(\underline{\underline{R}}_y \cdot \underline{r}^{+})]$ (7)

$$\underline{J}_1^{\pm}(\underline{r}^{+}) = \frac{1}{2}\,[\underline{J}_1(\underline{r}) \pm \underline{\underline{R}}_y \cdot \underline{J}_1(\underline{\underline{R}}_y \cdot \underline{r})] \tag{8}$$

$$\underline{\underline{K}}^{\pm}(\underline{r}^{+};\underline{r}_o^{+}) = \underline{\underline{A}}(\underline{r}^{+};\underline{r}_o^{+}) \pm \underline{\underline{B}}(\underline{r}^{+};\underline{r}_o^{+}) \tag{9}$$

$$\underline{\underline{A}}(\underline{r}^{+};\underline{r}_o^{+}) = \underline{\underline{K}}(\underline{r}^{+};\underline{r}_o^{+})$$

$$\underline{\underline{B}}(\underline{r}^{+};\underline{r}_o^{+}) = \underline{\underline{K}}(\underline{r}^{+};\underline{\underline{R}}_y \cdot \underline{r}_o^{+}) \cdot \underline{\underline{R}}_y \tag{10}$$

$\underline{\underline{R}}_y$ is a reflection operator such that

$$\underline{\underline{R}}_y = \underline{\underline{I}} - 2\hat{e}_y\hat{e}_y$$

$$\underline{\underline{R}}_y \cdot \underline{r}^{+} = (x,-y,z), \quad \underline{r}^{+}(x,y \geq 0,z)$$

$$\underline{\underline{R}}_y \cdot \underline{a} = (a_x,-a_y,a_z), \quad \underline{a} = (a_x,a_y,a_z) \tag{11}$$

and S_+ is the surface of the body that corresponds to $y \geq 0$. Thus equations (6) are defined over the $y \geq 0$ half of the aircraft. Once we solve for $\underline{J}^{\pm}$ at $\underline{r}^{+}(x,y \geq 0,z)$ we can use equation (7) to calculate $\underline{J}$ at $\underline{r}^{+}$ and $\underline{\underline{R}}_y \cdot \underline{r}^{+}$, i.e., everywhere on the surface of the body:

$$\underline{J}(\underline{r}^{+}) = \underline{J}^{+}(\underline{r}^{+}) + \underline{J}^{-}(\underline{r}^{+})$$

$$\underline{J}(\underline{r}^{-}) = \underline{\underline{R}}_y \cdot [\underline{J}^{+}(\underline{r}^{+}) - \underline{J}^{-}(\underline{r}^{+})] \tag{12}$$

where $\underline{r}^{-} = \underline{\underline{R}}_y \cdot \underline{r}^{+} = (x,-y,z)$.

We solve equation (6) for two orthogonal surface components $\hat{s} \cdot \underline{J}^{\pm}(\underline{r}^{+})$ and $\hat{t} \cdot \underline{J}^{\pm}(\underline{r}^{+})$ where $\hat{s}$ and $\hat{t}$ are unit surface vectors forming an orthonormal triad with the unit normal $\hat{n}$: $\hat{n} = \hat{s} \times \hat{t}$. For each component of the aircraft the $\hat{s}$ vector is defined as the tangent unit vector at the intersection of

a cylinder with a plane perpendicular to its axis, i.e.,

$$\hat{s} = \frac{\partial \underline{r}/\partial\phi}{|\partial \underline{r}/\partial\phi|} \tag{13}$$

This definition is true for the fuselage, vertical stabilizer and the $y > 0$ wing and horizontal stabilizer. For the $y < 0$ wing and horizontal stabilizer $\hat{s}$ is given by equation (13) with a minus sign. The $\hat{t}$-vector is obtained through the relationship $\hat{t} = \hat{n} \times \hat{s}$. Referring to figures 1 and 3 we can show that

Fuselage

$$\left.\begin{array}{llll}
x = x & y = b_1 r \sin\phi & z = -a_1 r \cos\phi & r = 1 \text{ on walls} \\
 & & & 0 \leq r \leq 1 \text{ on caps} \\
s_x = 0 & s_y = \dfrac{b_1 \cos\phi}{N_1(\phi)} & s_z = \dfrac{a_1 \sin\phi}{N_1(\phi)} & \text{on walls and caps} \\
t_x = 1 & t_y = 0 & t_z = 0 & \text{on walls} \\
t_x = 0 & t_y = \dfrac{a_1 \sin\phi}{N_1(\phi)} & t_z = \dfrac{-b_1 \cos\phi}{N_1(\phi)} & \text{on } x = 0 \text{ cap} \\
t_x = 0 & t_y = -\dfrac{a_1 \sin\phi}{N_1(\phi)} & t_z = \dfrac{b_1 \cos\phi}{N_1(\phi)} & \text{on } x = \ell_1 \text{ cap}
\end{array}\right\} \tag{14}$$

Wing for $y > 0$

$$\begin{array}{llll}
x = a_2 r \cos\phi + x_{02} & y = y & z = -b_2 r \sin\phi & r = 1 \text{ on walls} \\
 & & & 0 \leq r \leq 1 \text{ on cap} \\
s_x = -\dfrac{a_2 \sin\phi}{N_2(\phi)} & s_y = 0 & s_z = -\dfrac{b_2 \cos\phi}{N_2(\phi)} & \text{on walls and cap} \\
t_x = 0 & t_y = 1 & t_z = 0 & \text{on walls} \\
t_x = -\dfrac{b_2 \cos\phi}{N_2(\phi)} & t_y = 0 & t_z = \dfrac{a_2 \sin\phi}{N_2(\phi)} & \text{on cap}
\end{array} \tag{15}$$

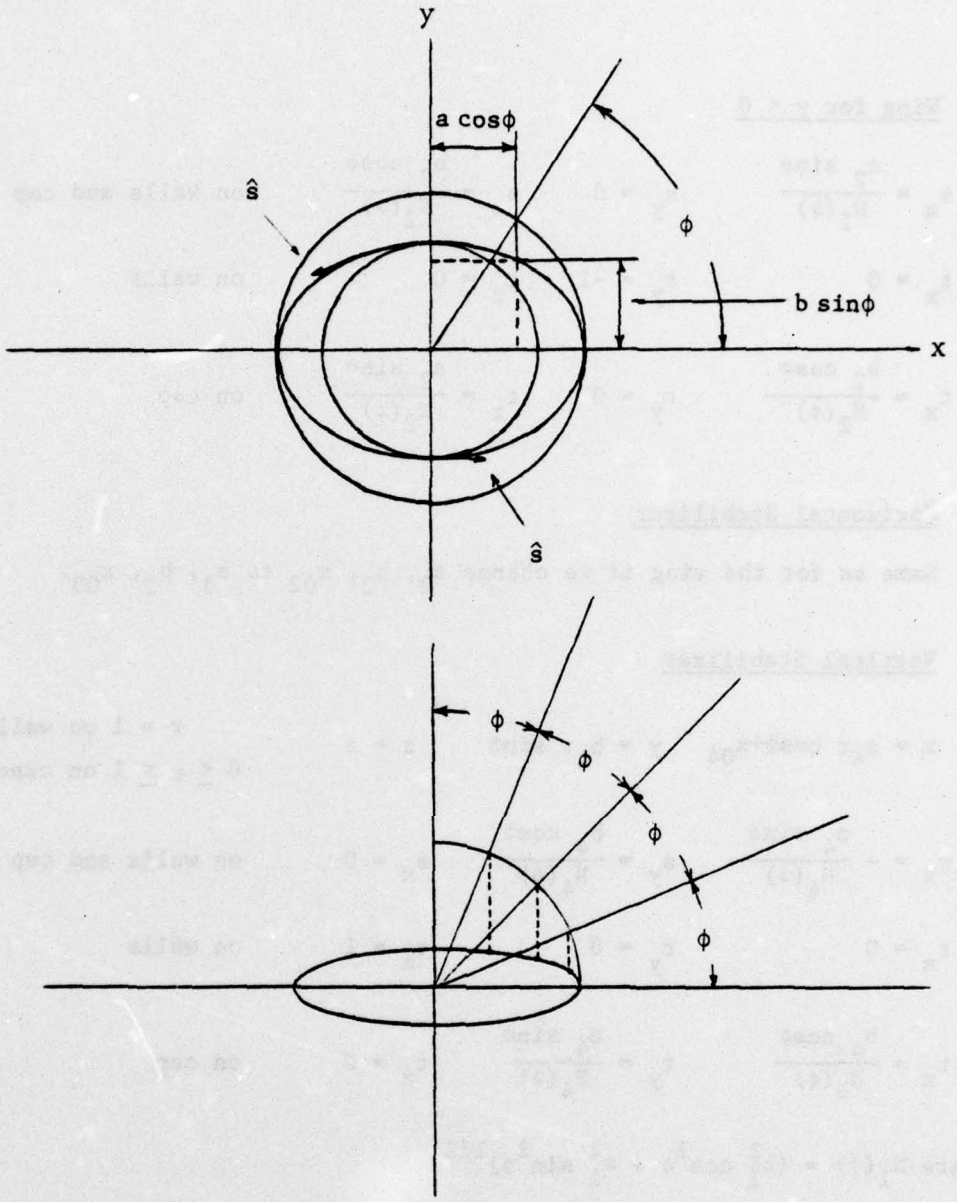

Figure 3: Definition of the elliptical angle ϕ such that $x = a\cos\phi$, $y = b\sin\phi$. Notice that equal increments in ϕ over a quadrant do not correspond to equal arc lengths.

Wing for $y < 0$

$$s_x = \frac{a_2 \sin\phi}{N_2(\phi)} \qquad s_y = 0 \qquad s_z = \frac{b_2 \cos\phi}{N_2(\phi)} \qquad \text{on walls and cap}$$

$$t_x = 0 \qquad t_y = -1 \qquad t_z = 0 \qquad \text{on walls}$$

$$t_x = \frac{b_2 \cos\phi}{N_2(\phi)} \qquad t_y = 0 \qquad t_z = \frac{a_2 \sin\phi}{N_2(\phi)} \qquad \text{on cap} \qquad (15)$$

Horizontal Stabilizer

Same as for the wing if we change a_2, b_2, x_{02} to a_3, b_3, x_{03}.

Vertical Stabilizer

$$x = a_4 r \cos\phi + x_{04} \qquad y = b_4 r \sin\phi \qquad z = z \qquad \begin{array}{r} r = 1 \text{ on walls} \\ 0 \le r \le 1 \text{ on caps} \end{array}$$

$$s_x = -\frac{a_4 \sin\phi}{N_4(\phi)} \qquad s_y = \frac{b_4 \cos\phi}{N_4(\phi)} \qquad s_x = 0 \qquad \text{on walls and cap}$$

$$t_x = 0 \qquad t_y = 0 \qquad t_z = 1 \qquad \text{on walls}$$

$$t_x = \frac{b_4 \cos\phi}{N_4(\phi)} \qquad t_y = \frac{a_4 \sin\phi}{N_4(\phi)} \qquad t_z = 0 \qquad \text{on cap} \qquad (16)$$

where $N_1(\phi) = (b_1^2 \cos^2\phi + a_1^2 \sin^2\phi)^{1/2}$

$$N_2(\phi) = (a_2^2 \sin^2\phi + b_2^2 \cos^2\phi)^{1/2}$$

$$N_4(\phi) = (a_4^2 \sin^2\phi + b_4^2 \cos^2\phi)^{1/2} \qquad (17)$$

Equations (12) can be rewritten in component form

$$J_t(\underline{r}^+) = J_t^+(\underline{r}^-) + J_t^-(\underline{r}^+)$$

$$J_t(\underline{r}^-) = \hat{t}(\underline{r}^-) \cdot \underline{R}_y \cdot [\underline{J}^+(\underline{r}^+) - \underline{J}^-(\underline{r}^+)] \qquad (18)$$

$$J_s(\underline{r}^+) = J_s^+(\underline{r}^-) + J_s^-(\underline{r}^+)$$

$$J_s(\underline{r}^-) = \hat{s}(\underline{r}^-) \cdot \underline{\underline{R}}_y \cdot [\underline{J}^+(\underline{r}^+) - \underline{J}^-(\underline{r}^+) \tag{19}$$

From relationships (14) through (16) we see that

Fuselage

$$s_y(\underline{r}^+) = s_y(\underline{r}^-),\ s_z(\underline{r}^+) = -s_z(\underline{r}^-) \qquad \text{on walls and caps}$$

$$t_x(\underline{r}^+) = t_x(\underline{r}^-) \qquad \text{on walls}$$

$$t_y(\underline{r}^+) = -t_y(\underline{r}^+),\ t_z(\underline{r}^+) = t_z(\underline{r}^-) \qquad \text{on caps} \tag{20}$$

Wings and Horizontal Stabilizer

$$s_x(\underline{r}^+) = -s_x(\underline{r}^-),\ s_z(\underline{r}^+) = -s_z(\underline{r}^-) \qquad \text{on walls and caps}$$

$$t_y(\underline{r}^+) = -t_y(\underline{r}^-) \qquad \text{on walls}$$

$$t_x(\underline{r}^+) = t_x(\underline{r}^-),\ t_z(\underline{r}^+) = t_z(\underline{r}^-) \tag{21}$$

Vertical Stabilizer

$$s_x(\underline{r}^+) = -s_x(\underline{r}^-),\ s_y(\underline{r}^+) = s_y(\underline{r}^-) \qquad \text{on walls and caps}$$

$$t_z(\underline{r}^+) = t_z(\underline{r}^-) \qquad \text{on walls}$$

$$t_x(\underline{r}^+) = t_x(\underline{r}^-),\ t_y(\underline{r}^+) = t_y(\underline{r}^-) \qquad \text{on cap} \tag{22}$$

From the above relationships we see that in general

$$\begin{aligned} s_x(\underline{r}^+) &= -s_x(\underline{r}^-) & t_x(\underline{r}^+) &= t_x(\underline{r}^-) \\ s_y(\underline{r}^+) &= s_y(\underline{r}^-) & t_y(\underline{r}^+) &= -t_y(\underline{r}^-) \\ s_z(\underline{r}^+) &= -s_z(\underline{r}^-) & t_z(\underline{r}^+) &= t_z(\underline{r}^-) \end{aligned} \tag{23}$$

and consequently

$$\hat{t}(\underline{r}^-) \cdot \underline{\underline{R}}_y = [\underline{t}_x(\underline{r}^-) + \underline{t}_y(\underline{r}^-) + \underline{t}_z(\underline{r}^-)] \cdot \underline{\underline{R}}_y = \underline{t}_x(\underline{r}^-) - \underline{t}_y(\underline{r}^-)$$

$$+ \underline{t}_z(\underline{r}^-) = \underline{t}_x(\underline{r}^+) + \underline{t}_y(\underline{r}^+) + \underline{t}_z(\underline{r}^+) = \hat{t}(\underline{r}^+)$$

Similarly

$$\hat{s}(\underline{r}^-) \cdot \underline{\underline{R}}_y = -\hat{s}(\underline{r}^+)$$

Thus equations (18) and (19) can be rewritten as

$$J_t(\underline{r}^+) = J_t^+(\underline{r}^+) + J_t^-(\underline{r}^+)$$

$$J_t(\underline{r}^-) = J_t^+(\underline{r}^+) - J_t^-(\underline{r}^+)$$

$$J_s(\underline{r}^+) = J_t^+(\underline{r}^+) + J_s^-(\underline{r}^+)$$

$$J_s(\underline{r}^-) = -[J_s^+(\underline{r}^+) - J_s^-(\underline{r}^+)] \qquad (24)$$

In order to solve numerical equations (6) we first write them in component form and then transform them into a system of simultaneous algebraic equations for the components of the fictitious current densities evaluated at the centers of zones into which we have divided the entire aircraft. That is, we assume that the current components $J_t^{\pm}$, $J_s^{\pm}$ are constant over a zone and equal to their values at the center of the zone. Appendix C presents the numerical solution in detail.

SECTION III

HIGHLIGHTS OF THE NUMERICAL SOLUTION

In this section we present some of the highlights of the path that led us to our final computer code. In particular, we discuss how we decided on the number and size of zones, and the accuracy we employ for the calculation of matrix elements.

Our first task was to decide on the number of zones on the surface of our model: how many we needed, what their optimum size was as a function of location and whether the resulting matrix to be inverted would be too large to assure confidence that the round off error would be negligible.

To assess this error we considered the problem of calculating the current densities on a circular cylinder, illuminated by a plane wave with broadside incidence and the electric field polarized along the axis of the cylinder, by employing two debugged computer codes. One took advantage of <u>one</u> symmetry plane and solved for $\underline{J}^{\pm}$ defined in Section I. The other utilized three symmetry planes. The details of the latter approach are given in Appendix A where it is shown that one need only calculate two fictitious quantities $\underline{J}^{-+-}$ and $\underline{J}^{-++}$ over 1/8 of the surface of the cylinder whereas the first approach requires calculation of $\underline{J}^{+}$ and $\underline{J}^{-}$ over half the surface. The three-symmetry-plane code involved the inversion of a matrix 108 x 108 whereas the one-symmetry-plane code required the inversion of a (4 x 108) x (4 x 108) = 432 x 432 matrix. We displayed our results with eight significant figures and did not observe any roundoff error.

Once we gained confidence that large matrices of the type generated by our approach could be inverted accurately we proceeded to determine the minimum number of zones on the aircraft. To that end we had to decide how many zones we should use on the elliptical cylinders modeling the aircraft components. The choice of the size of a zone is based on the requirement that the current density components should not vary appreciably over a zone. The variation of the current density depends on geometrical

and wavelength considerations. Geometrical considerations determine the minimum number of zones and wavelength considerations can increase this number. The geometric requirements are exactly the ones required in order to obtain a magnetostatic solution. As an example, in the past, it has been common practice to require that the size of a zone, both longitudinal and azimuthal, on the surface of a circular cylinder should not be larger than the diameter of the cross section, independently of the wavelength. The wavelength requirement was that we should have at least ten zones per wavelength. Thus the wavelength requirement was automatically satisfied via the geometry requirement for wavelengths larger than ten times the diameter of the cylinder. For smaller wavelengths the wavelength requirement determined the total number of zones. It should be noted that the factor of ten associated with the wavelength requirement is somewhat arbitrary. There is no restriction built into the code based on the factor being equal to ten. To the contrary, the zoning flexibility built into the code allows one to assess whether a smaller factor (corresponding to higher frequencies for fewer zones) yields sufficient accuracy.

For an elliptical cylinder a geometrical condition that has been imposed in the past requires that the linear size of a zone should not exceed the minor axis of the ellipse. In order to test this condition we decided to compare our computer code (with a variable number of zones) to the exact magnetostatic solution for an ellipsoid immersed in a uniform magnetic field (see Appendix B). The basis for the comparison was that for ellipsoids with large c/a ($c > a > b$) the variation of the current density around the central cross section was insensitive to c/a. Thus we had reason to believe that the variation of the current density at the central cross section of the ellipsoid approximated, to a high degree of accuracy, the variation of the current density at the central cross section of a finite elliptical cylinder with $h/a = c/a$ (h is the cylinder half length). The computer code we used employed all three planes of symmetry for broadside incidence with an electric field parallel to the axis of the cylinder. This was done to minimize the cost for each

run as we varied the number of zones and naturally we ran the code for $\omega = 0$. By examining the exact solution we noticed that the current density varied most rapidly near points of high curvature. This meant that our zoning should be nonuniform with zone size diminishing as we approached the point of highest curvature. This was an important observation but it led to the following problem. In the past we had subzoned each zone in order to accurately calculate the neighboring zone interaction. As for the self-zone calculation we had realized the need to analytically treat the integrable singularity of the integrand in order to secure a high degree of accuracy. We had accomplished that by dividing the two-dimensional integral into two integrals: one with a two-dimensional nonsingular integrand that was calculated by subzoning and one with a singular but integrable integrand that could be reduced to a one-dimensional integral with a nonsingular integrand. No such precaution had been taken for neighboring zone interaction because the integrands involved did not vary appreciably and allowed accurate calculation through subzoning. For an elliptical cylinder with a large a/b (say larger than 4) the required zone size in regions of high curvature may be so small that neighboring zone interaction could require a large number of subzones to evaluate the integrals whose integrands now can vary appreciably. The code automatically prescribes the same number of subzones for all zones and this is clearly unnecessary for neighboring zone interaction (in regions of small curvature) where the zone size is not small. This would cause the code to be unnecessarily costly. We decided to examine whether we could calculate the matrix element without subzoning the zones. We found that the two-dimensional integrals over a zone on the walls or the caps of the cylinder could be reduced to one-dimensional integrals with nonsingular integrands without dividing the original integrals into two integrals as we did in the past. (See Appendix C, Section 5 for details.) Thus we were in a position to calculate the matrix elements for self-zone and zone-to-zone interactions by evaluating well-behaved one-dimensional integrals with a high degree of accuracy. An additional benefit of making the matrix elements to this degree of accuracy was

also achieved. We found that the improved accuracy of the evaluation of the matrix elements improved the accuracy of the phase of the solution. We observed situations where it could have been erroneously concluded that the matrix elements were calculated with sufficient accuracy based on comparing the magnitude of the resulting solution with known results. We calculated the same quantities with a code that utilized more accurate matrix elements and noticed a significant effect on the phase of the solution while the magnitude was minimally affected.

Now we will describe the flexibility built into our code and present guidelines for utilizing this flexibility. A general description of the flexibility is that the zoning of the aircraft model can be specified with input data cards to cause more dense zoning in regions near junctions and edges as well as the regions of rapidly varying curvature near the leading and trailing edges of the elliptic cylinder components. The zoning density over the entire aircraft model can also be increased through input data cards to accommodate frequencies higher than those determined by the geometry limited zoning. The primary reason that we have this flexibility is that our method of accurately calculating the matrix elements is insensitive to the size of our zones. A penalty that is paid for having this flexibility of nonuniform zoning is that the benefit of using symmetries to reduce the matrix generation time is reduced.

We conclude this section by presenting guidelines for the geometry limited zoning. The presentation of these guidelines is facilitated by considering the following categories of surfaces that require zoning: cylinder walls, junctions, edges and end caps.

The zoning of the cylinder walls is first determined without regard to junctions and edges. A description of the initial zoning of the walls is assisted by considering figure 3. We will describe the zoning of the elliptic cylinder walls with the zoning of the circular cylinder walls being a special case. Our code allows that the full range for ϕ can be subdivided as finely as desired. This has utility for zoning in the

vicinity of junctions; however, for determining the number and size of the zones independently of the junctions,we can consider that each wall is divided into either two or four subdivisions corresponding to a ϕ range of 90° (quadrants). On the fuselage and on the vertical stabilizer we have two quadrants; on the wings as well as on the horizontal stabilizers we have four quadrants. For each of the quadrants we choose the number of ϕ zone divisions according to the ratio of the major to minor axis of the ellipse. Specifically the number of zone divisions is the nearest integer to half of the sum of one plus this ratio. Once this number is specified as an input parameter, the code chooses the size of these zones so that they are smallest in the region of the most rapidly varying curvature. Specifically, it chooses them to be equal increments in the elliptic angle ϕ. The longitudinal length of a zone is taken to be no larger than the major axis of the ellipse. These guidelines are meant to represent an initial estimate of the geometry limited zoning. The adequacy of the zoning can be determined by running the code at zero frequency with the initial geometry limited zoning estimate and then running the code with a more dense zoning.

The zoning of junctions, edges and end caps is determined by utilizing the zoning flexibility of the code and performing numerical experiments. We single out the zoning of the end caps for special consideration only because they are necessarily in the vicinity of an edge. Now we make a further distinction between the numerical experiments in the vicinity of junctions and edges. As explained in Appendix C, Section 9, neither component of current density becomes unbounded in the vicinity of a junction; however, the component parallel to an edge does become unbounded. We believe that this singular behavior should be given special analytic and numerical treatment. We attempted a numerical subtractive procedure to treat this edge difficulty and obtained unsatisfactory results. Due to time limitations, we have not yet numerically determined whether a multiplicative procedure would allow us to trust our solution for points arbitrarily close to the edge. Despite the fact we have misgivings about our solution arbitrarily close to an edge, the comparison between our calculations and measured data (presented in the next section) is

quite good at a distance corresponding to half of an ordinary zone length.

SECTION IV

COMPARISON WITH EXPERIMENTAL DATA

In this section we compare numerical solutions, obtained by using our MFIE patch zoning approach, with experimental data. Even though these measurements and calculations were not for the complete geometry of the aircraft model they demonstrate the capability of the approach. It should be noted that the quantities that will be compared correspond to measurements and calculations on the surface of an object. It is more difficult to calculate surface distributions than far zone scattering results, thus the excellent degree of agreement to be demonstrated is very encouraging. To further relate the calculations used in the comparison to our final code, we note that through the use of input data cards our complete aircraft code can be reduced to yield results for the geometry used in the comparison. At this time an experimental program is underway to measure the current density induced on the complete aircraft model for which we developed our code.

The comparison of the calculated and measured data is facilitated by considering figures 4 through 8. All of these figures contain material that was presented in references 4 and 5. The curves in figures 5, 6a, 7a, and 8a were traced from Xerox copies of curves presented in those reports. The figure containing the description of the experiment pertaining to the data presented in these figures is also redrawn based on a figure presented in reference 4. All of these figures were originally redrawn for presentation in reference 3.

The intent of the experiment is to simulate a monochromatic plane wave incident on a tube having a total length of 2h. By referring to figure 4, we can see that the angle θ is defined so that 0° corresponds to the deep shadow region and 180° corresponds to direct illumination. The θ in figures 6a, 7a, and 8a correspond to this definition and z is the axial distance ranging from 0 at the ground plane to h at the top of the cylinder. The quantities $|K_z|$, $|K_\theta|$, and θ_z plotted in these figures are the magnitude of the axial component of the current density,

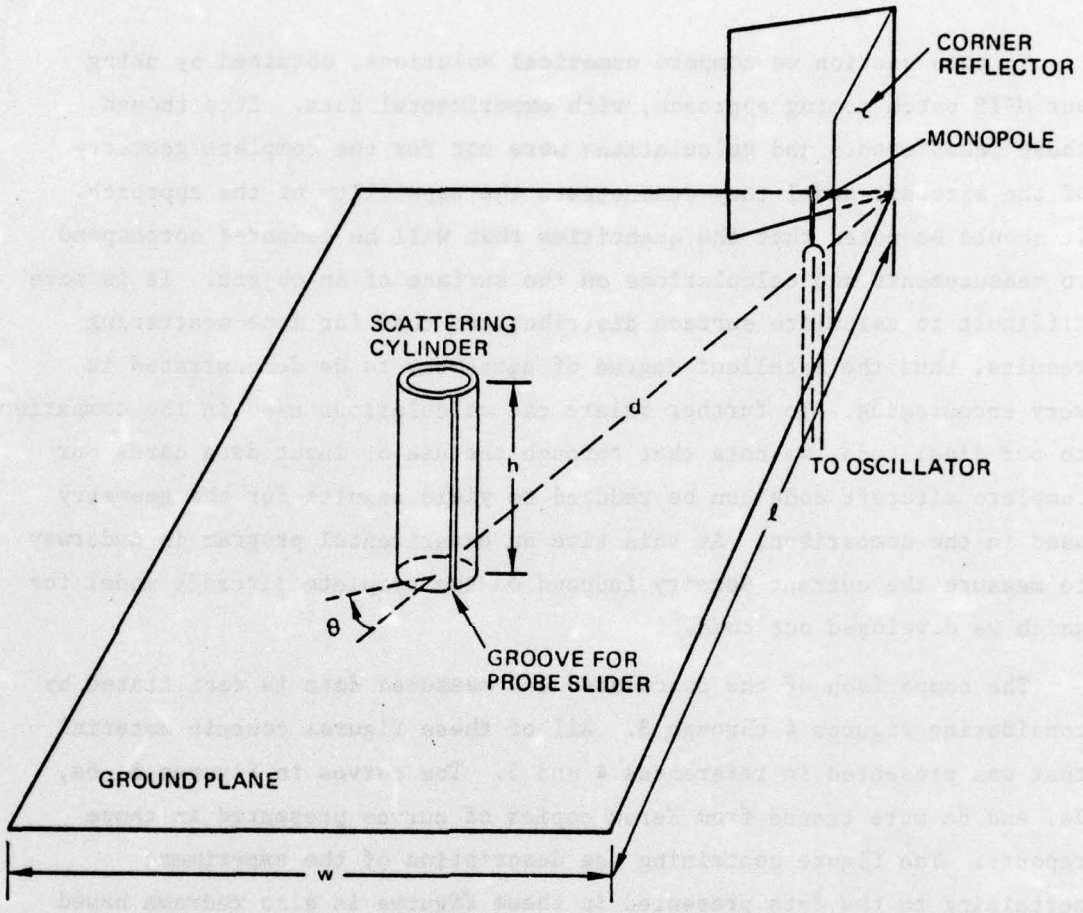

Figure 4: Schematic diagram of scattering cylinder on ground plane.

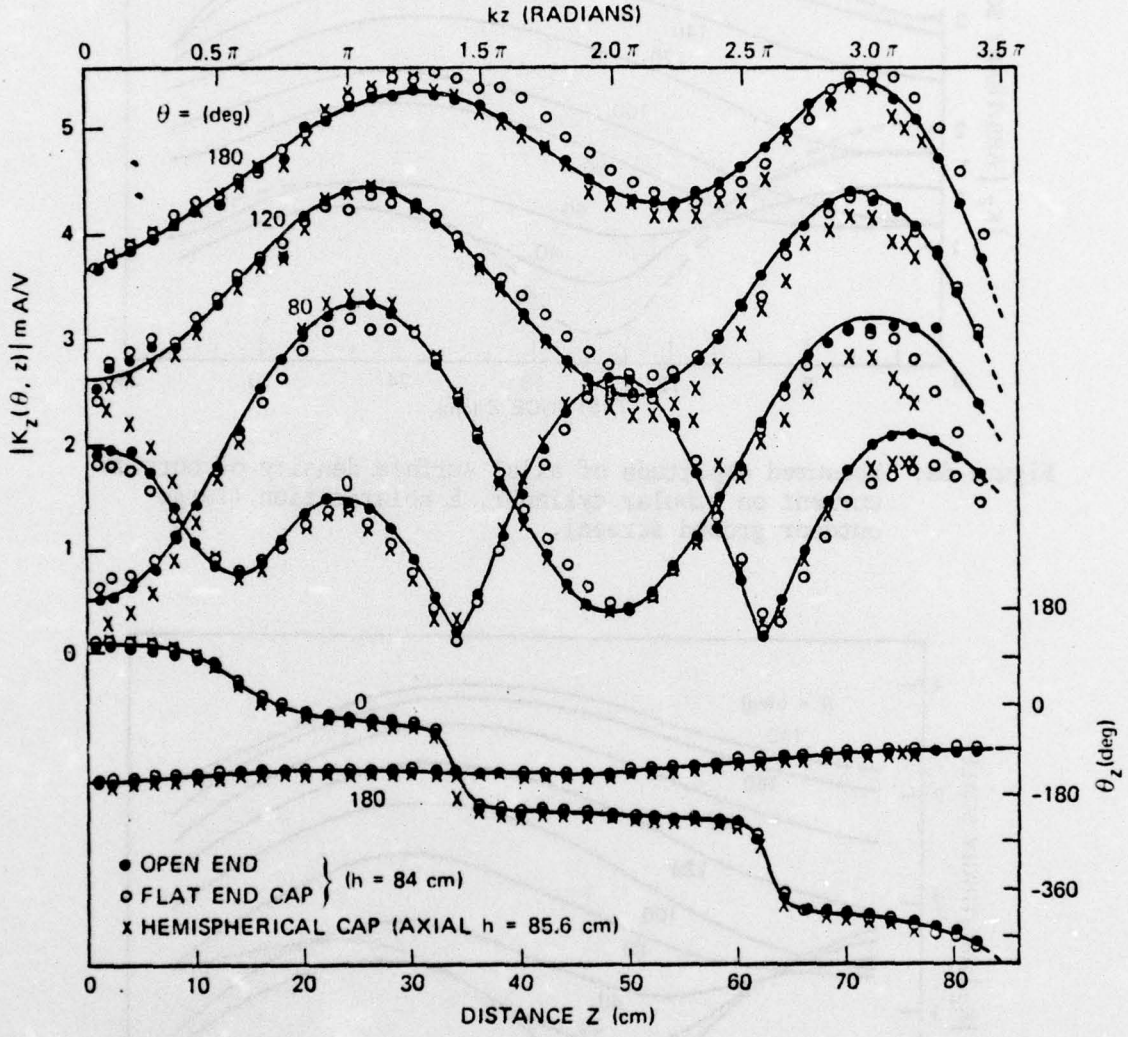

Figure 5: Measured magnitude and phase of surface density of outside axial current on tubular cylinder with open end, flat and hemispherical end caps. E-polarization.

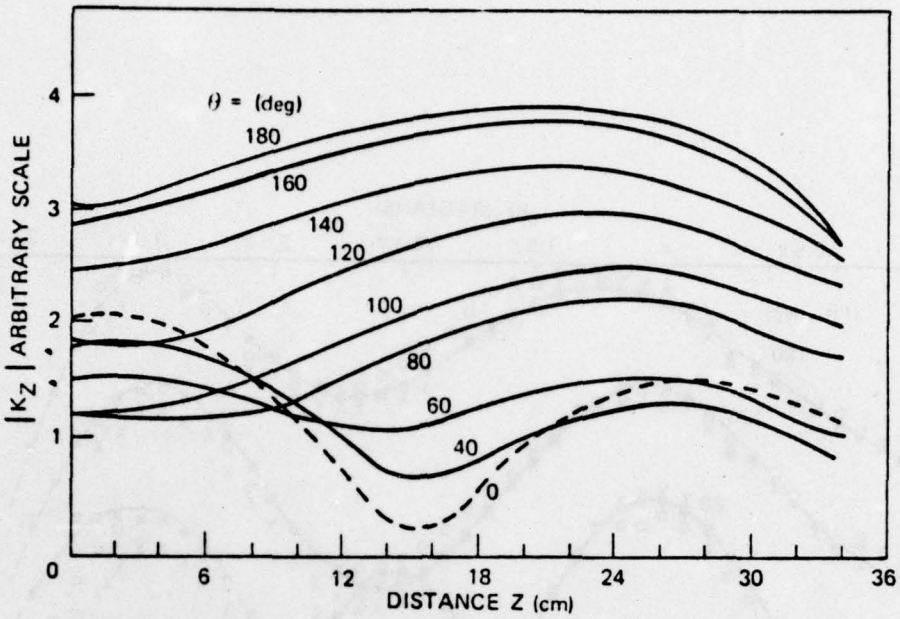

Figure 6a: Measured amplitude of axial surface density of outside current on tubular cylinder, E-polarization (large outdoor ground screen).

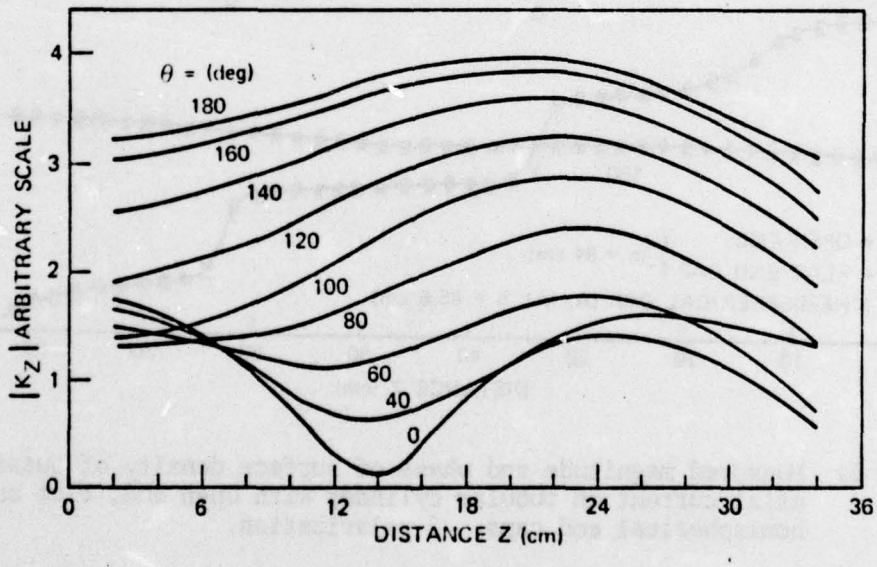

Figure 6b: Calculated amplitude of axial surface current density on a finite circular cylinder.

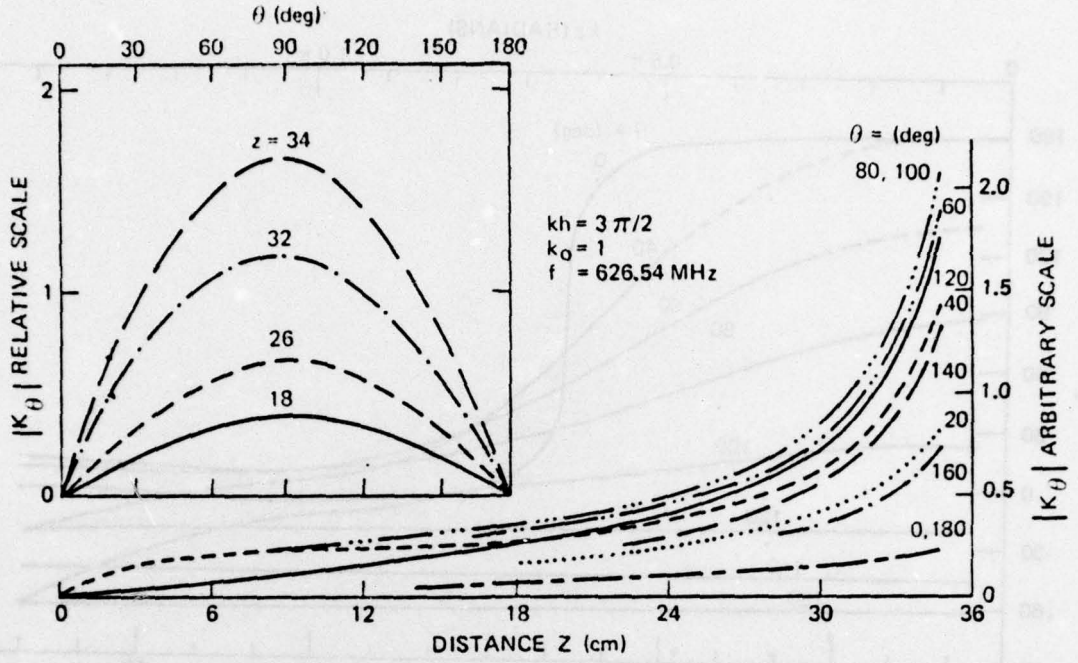

Figure 7a: Measured amplitude of surface density of transverse current on tubular cylinder, E-polarization; normal incidence (large outdoor ground screen).

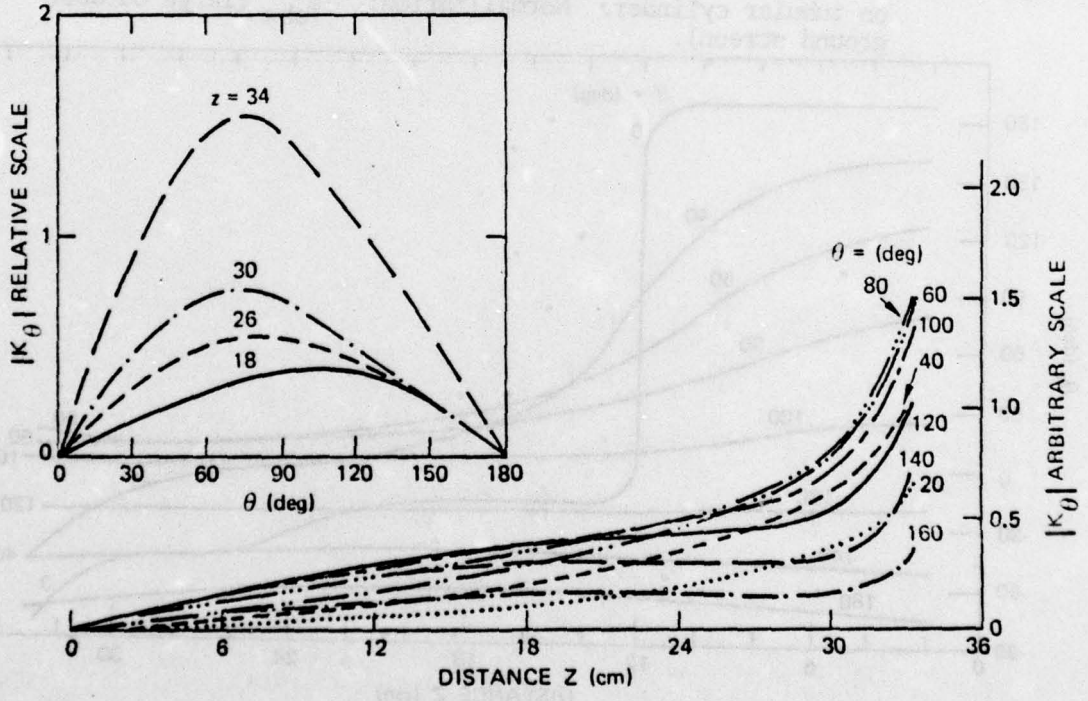

Figure 7b: Calculated amplitude of transverse surface current density on a finite circular cylinder.

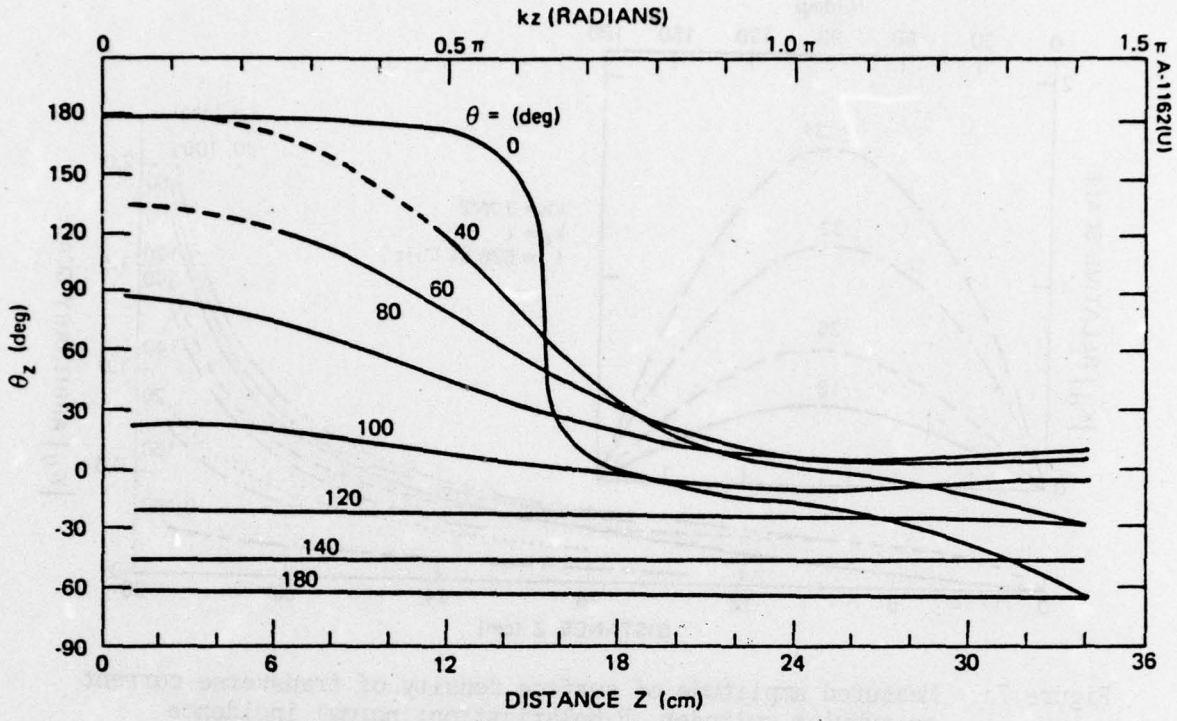

Figure 8a: Measured phase of axial surface density of outside current on tubular cylinder. Normalization: $-\phi_{obs}$ (large outdoor ground screen).

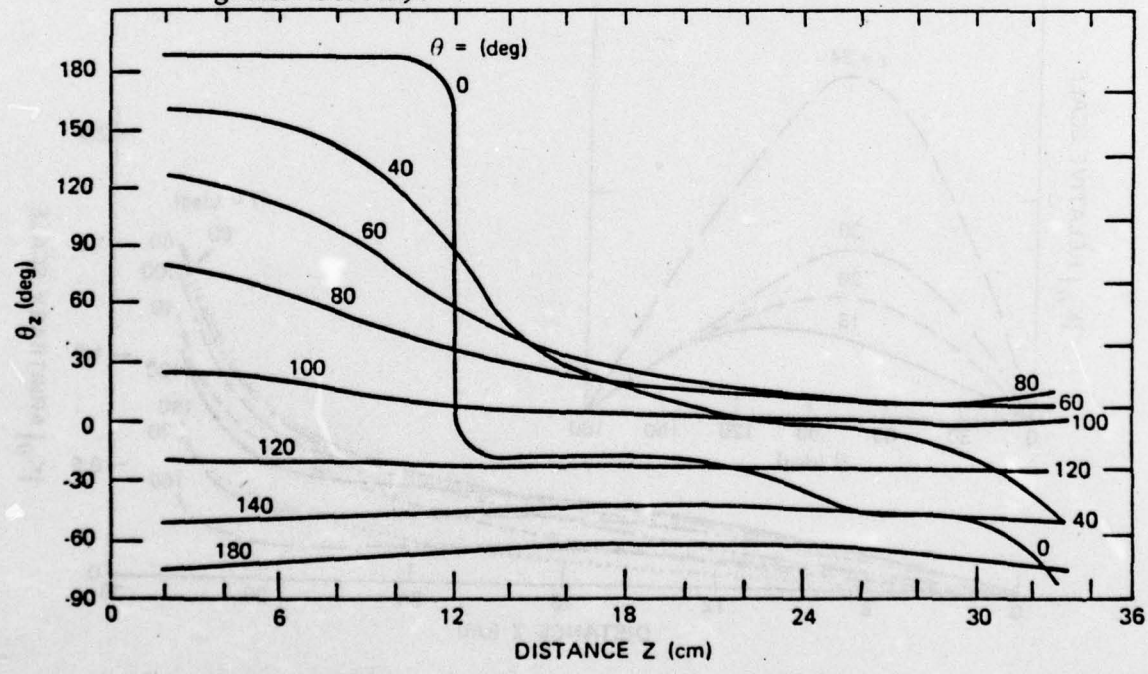

Figure 8b: Calculated phase of axial surface current density on a finite circular cylinder.

the magnitude of the transverse component of the current density, and the phase of the axial component of the current density. The same quantities calculated by our MFIE computer code for the current density induced by the same source on a flatly capped cylinder having the same length and diameter as the tube of the experiment are presented in figures 6b, 7b, and 8b. In these figures we employ the symbol $\underline{K}$ rather than $\underline{J}$ to denote the current density in order to conform to the notation of the measured data. The scales of our calculations were adjusted to the scales of the experimental data by using three numbers, a multiplicative factor for each set of the magnitude comparisons and an additive factor for the set of phase comparisons. These three numbers were determined by forcing one point of the experimental data to match one point of our calculated data on only one curve of each of the three sets of curves. The reason we include figure 5 in this paper is to show that there is only a minimal measured effect of capping the tube, thus justifying our comparing our capped tube calculations to the uncapped measurements. It should be noted that our comparisons with the data were for $h = 36$ cm while data in figure 5 corresponds to $h = 84$ cm. It is possible that capping the shorter tube could have a greater effect on the measured surface distributions. This could account for some of the differences between the experimental data and the calculations; however, as can be seen the difference is already quite small.

Now it is necessary for us to discuss the frequency at which we made the comparison between our calculations and the experimental data. The normalized value $kh = 1.5\,\pi$ determines the frequency. First we note, without scaling h to missile or aircraft size dimension, that the comparison was made well beyond the primary resonance of the cylinder. Next we mention that if h is taken to be in the 10 to 20 meter range, the frequency scales to the 20 to 10 MHz range. In this regard, we claim that our MFIE approach can only perform better as the frequency is decreased according to the explanation contained in the previous section.

APPENDIX A

SYMMETRY RELATIONSHIPS

In this appendix we derive certain properties of the surface current density induced on a perfectly conducting body possessing one or more symmetry planes. The symmetry properties are true when the body is illuminated by a plane electromagnetic wave of a particular direction of propagation and polarization as we will explain shortly. These properties are useful in that they reduce computation time and also give insight as to the distribution of the induced current density on the perfectly conducting body. (See reference 7 for a one symmetry plane analysis used in a different context.)

We divide this appendix into two parts. In the first part we consider a body with three planes of symmetry with an incident wave vector $\underline{k}$ perpendicular to a plane of symmetry and the electric field parallel to an axis of symmetry. We derive the symmetry relationships for a circular cylinder, because a circular cylinder is relevant to this report, but analogous properties can similarly be derived for any body with three planes of symmetry. These relationships involve the surface current densities at points symmetric to planes of symmetry other than the plane perpendicular to the $\underline{k}$ vector. In the second part we consider a body with only one plane of symmetry with an incident wave vector perpendicular to the plane of symmetry and the electric field parallel to a suitably defined axis. We show that the surface current densities at points symmetric to the plane of symmetry are simply related to each other as the frequency $\omega \to 0$ (magnetostatic limit).

Before we tackle each part in detail we present certain important results whose derivation can be found in reference 3. Starting with the magnetic field integral equation for the surface current density

$$\frac{1}{2}\,\underline{J}(\underline{r}) = \underline{J}_{inc}(\underline{r}) + \int_S \underline{\underline{K}}(\underline{r};\underline{r}_o) \cdot \underline{J}(\underline{r}_o)\, dS_o \qquad \text{(A-1)}$$

---

7. Baum, C. E., Interaction of Electromagnetic Fields with an Object Which has an Electromagnetic Symmetry Plane, Interaction Note 63, Air Force Weapons Laboratory, March 1971.

and assuming that the xy-plane is a plane of symmetry for the body, one obtains the following set of integral equations

$$\frac{1}{2}\,\underline{J}^{+}(\underline{r}^{+}) = \underline{J}^{+}_{inc}(\underline{r}^{+}) + \int_{S_+} \underline{\underline{K}}^{+}(\underline{r}^{+};\underline{r}^{+}_{o}) \cdot \underline{J}^{+}(\underline{r}^{+}_{o})\, dS_o \tag{A-2}$$

$$\frac{1}{2}\,\underline{J}^{-}(\underline{r}^{+}) = \underline{J}^{-}_{inc}(\underline{r}^{+}) + \int_{S_+} \underline{\underline{K}}^{-}(\underline{r}^{+};\underline{r}^{+}_{o}) \cdot \underline{J}^{-}(\underline{r}^{+}_{o})\, dS_o \tag{A-3}$$

where

$$\underline{J}^{+}(\underline{r}^{+}) + \frac{1}{2}\left[\underline{J}(\underline{r}^{+}) + \underline{\underline{R}}_z \cdot \underline{J}(\underline{\underline{R}}_z \cdot \underline{r}^{+})\right] \tag{A-4}$$

$$\underline{J}^{-}(\underline{r}^{+}) = \frac{1}{2}\left[\underline{J}(\underline{r}^{+}) - \underline{\underline{R}}_z \cdot \underline{J}(\underline{\underline{R}}_z \cdot \underline{r}^{+})\right] \tag{A-5}$$

$\underline{r}^{+}$, $\underline{r}^{+}_{o}$ are radius vectors at points with $z \geq 0$, $\underline{\underline{R}}_z$ is a reflection operator defined by

$$\underline{\underline{R}}_z = \underline{\underline{I}} - 2\,\hat{e}_z\,\hat{e}_z \tag{A-6}$$

$\underline{\underline{I}}$ is the identity operator, S_+ is half the surface defined by $z \geq 0$, $\underline{J}^{\pm}_{inc}$ are defined through the incident current density $\underline{J}_{inc}$ by expressions analogous to equations (A-4), (A-5) and

$$\underline{\underline{K}}^{\pm}(\underline{r}^{+};\, \underline{r}^{+}_{o}) = \underline{\underline{A}}(\underline{r}^{+};\, \underline{r}^{+}_{o}) \pm \underline{\underline{B}}(\underline{r}^{+};\, \underline{r}^{+}_{o}) \tag{A-7}$$

$$\underline{\underline{A}}(\underline{r}^{+};\, \underline{r}^{+}_{o}) = \underline{\underline{K}}(\underline{r}^{+};\, \underline{r}^{+}_{o}) \tag{A-8}$$

$$\underline{\underline{B}}(\underline{r}^{+};\, \underline{r}^{+}_{o}) = \underline{\underline{K}}(\underline{r}^{+};\, \underline{\underline{R}}_z \cdot \underline{r}^{+}_{o}) \cdot \underline{\underline{R}}_z \tag{A-9}$$

Notice that $\underline{r}^+ = x,y,z(\geq 0)$, $\underline{\underline{R}}_z \cdot \underline{r}^+ = x,y,-z$.

The above relationships show that instead of solving equation (A-1) for points over the entire cylindrical surface, we can solve equations (A-2) and (A-3) at points over half the surface and calculate the current density at any point by inverting equations (A-6) and (A-5), i.e.

$$\underline{J}(\underline{r}^+) = \underline{J}^+ + \underline{J}^-$$

$$\underline{J}(\underline{\underline{R}}_z \cdot \underline{r}^+) = \underline{\underline{R}}_z \cdot (\underline{J}^+ - \underline{J}^-)$$

With the above as background information we now consider part one in detail.

1. THREE PLANES OF SYMMETRY

The geometry is depicted in figure A1 where

$$\underline{H}_{inc} = - H_o \hat{e}_y e^{-ikz} \tag{A-10}$$

We define the unit surface vectors $\hat{t}$, $\hat{s}$ such that

$$\hat{n} = \hat{s} \times \hat{t} \tag{A-11}$$

where $\hat{n}$ is the unit outward normal. Thus

$$\left.\begin{aligned} \hat{t} &= \hat{e}_x \\ \hat{s} &= \hat{e}_\phi \\ \hat{n} &= \hat{e}_\rho \end{aligned}\right\} \quad \text{on the walls} \tag{A-12}$$

$$\left.\begin{aligned} \hat{t} &= -\hat{e}_\rho \\ \hat{s} &= \hat{e}_\phi \\ \hat{n} &= \hat{e}_x \end{aligned}\right\} \quad \text{on } x > 0 \text{ cap} \tag{A-13}$$

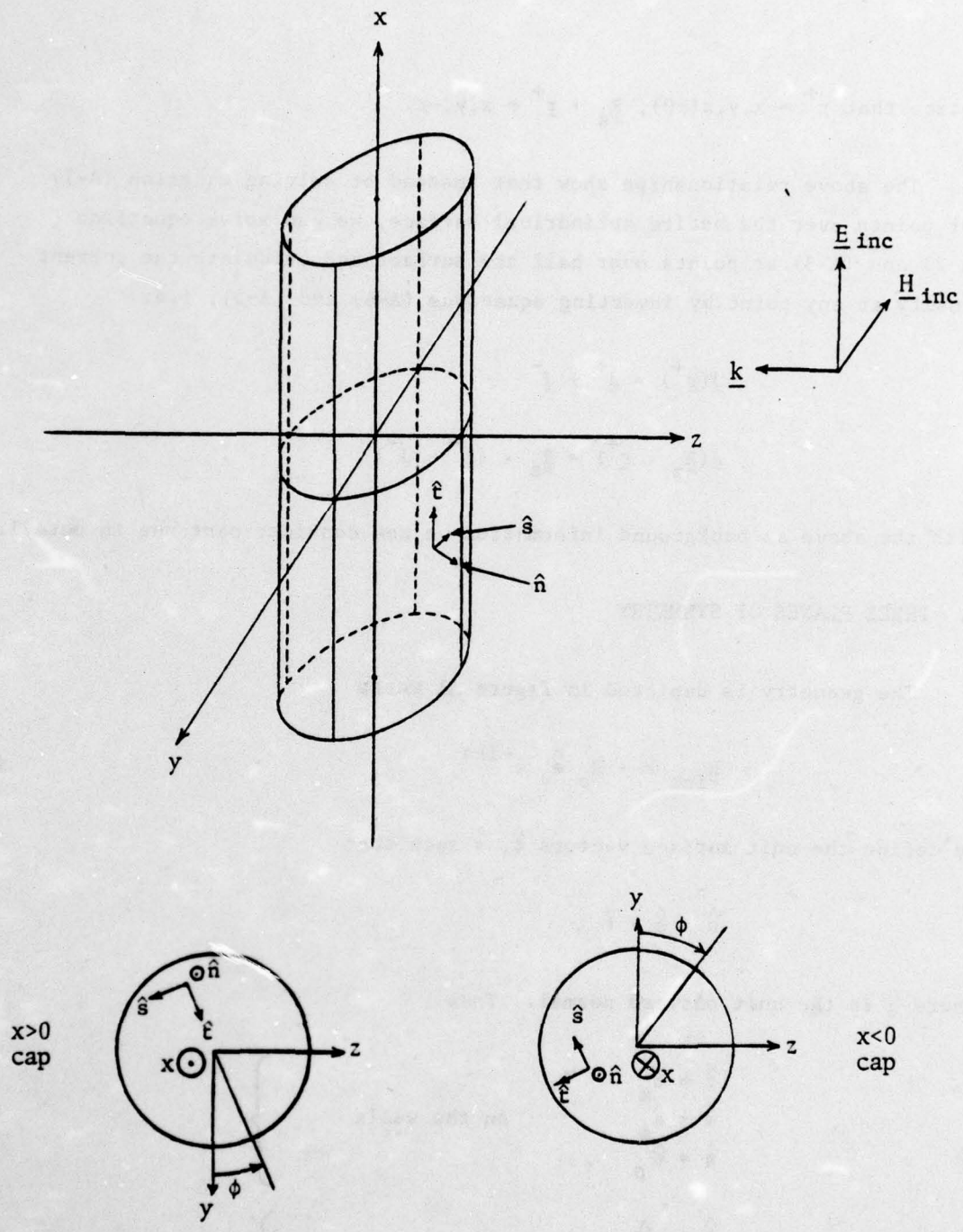

Figure A1: A finite circular cylinder possessing three planes of symmetry illuminated by a plane wave $\underline{H}_{inc} = -\hat{e}_y H_o \exp(-ikz)$ and orientation of the orthonormal triad $\hat{n},\hat{s},\hat{t}$.

$$\left.\begin{aligned} \hat{t} &= \hat{e}_r \\ \hat{s} &= \hat{e}_\phi \\ \hat{n} &= -\hat{e}_x \end{aligned} \qquad \text{on } x < 0 \text{ cap} \right\} \tag{A-14}$$

We will show that

$$J_t(x,y,z) = J_t(x,-y,z) = J_t(-x,y,z) = J_t(-x,-y,z) \tag{A-15}$$

$$J_s(x,y,z) = -J_s(x,-y,z) = -J_s(-x,y,z) = J_s(-x,-y,z) \tag{A-16}$$

everywhere on the cylinder (walls and caps).

These relationships give us a lot of information concerning the distribution of the surface current density. For example, along the intersection of the $y = 0$ plane with the cylinder, $J_s(x,o,z) = 0$. Similarly, along the intersection with the $x = 0$ plane the azimuthal component $J_s(o,y,z)$ is zero. Notice, however, that equations (A-15) and (A-16) involve points symmetric to either the $x = 0$ or the $y = 0$ planes <u>not</u> the $z = 0$ plane. Part two deals with symmetries across the $z = 0$ plane in the limit $\omega = 0$.

First we consider points symmetric to the $y = 0$ plane. The following preliminary calculations are necessary.

a. **Walls**

Let us calculate the incident current density $\underline{J}_{inc}$ and the auxiliary currents $\underline{J}^{\pm}_{inc}$.

$$\underline{J}_{inc}(x,y,z) = \hat{n}(x,y,z) \times \underline{H}_{inc}(x,y,z) \tag{A-17}$$

$$\underline{\underline{R}}_y \cdot \underline{J}_{inc}(\underline{\underline{R}}_y \cdot \underline{r}) = \underline{\underline{R}}_y \cdot \left[\hat{n}(\underline{\underline{R}}_y \cdot \underline{r}) \times \underline{H}_{inc}(\underline{\underline{R}}_y \cdot \underline{r})\right] \tag{A-18}$$

where $\underline{\underline{R}}_y \cdot \underline{r} = x,-y,z$.

With the aid of figure A2 we see that

$$\hat{n}(\underline{\underline{R}}_y \cdot \underline{r}) \times \hat{e}_y = \hat{n}(\underline{r}) \times \hat{e}_y$$

and

$$\underline{\underline{R}}_y \cdot \left[\hat{n}(\underline{\underline{R}}_y \cdot r) \times \hat{e}_y\right] = \hat{n}(R_y \cdot r) \times \hat{e}_y$$

since $\hat{n}(\underline{\underline{R}}_y \cdot \underline{r}) \times \hat{e}_y$ is in the x-direction.

Thus

$$\underline{J}_{inc}(\underline{r}) = -\left[\hat{n}(\underline{r}) \times \hat{e}_y\right] H_o e^{-ikz}$$

$$\underline{\underline{R}}_y \cdot \underline{J}_{inc}(\underline{\underline{R}}_y \cdot \underline{r}) = -\left[\hat{n}(\underline{r}) \times \hat{e}_y\right] H_o e^{-ikz} = \underline{J}_{inc}(\underline{r})$$

If we recall definitions (A-4) and (A-5) we see that

$$\underline{J}^{+}_{inc}(x,y,z) = \underline{J}_{inc}(x,y,z) \qquad \text{(A-19)}$$

$$\underline{J}^{-}_{inc}(x,y,z) = 0 \qquad \text{(A-20)}$$

b. $x > 0$ Cap

With the aid of figure 10 we see that

$$\underline{\underline{R}}_y \cdot \left[\hat{n}(\underline{\underline{R}}_y \cdot \underline{r}) \times \hat{e}_y\right] = \hat{n}\,(\underline{\underline{R}}_y \cdot \underline{r}) \times \hat{e}_y$$

$$\hat{n}\,(\underline{\underline{R}}_y \cdot \underline{r}) \times \hat{e}_y = \hat{n}(\underline{r}) \times \hat{e}_y$$

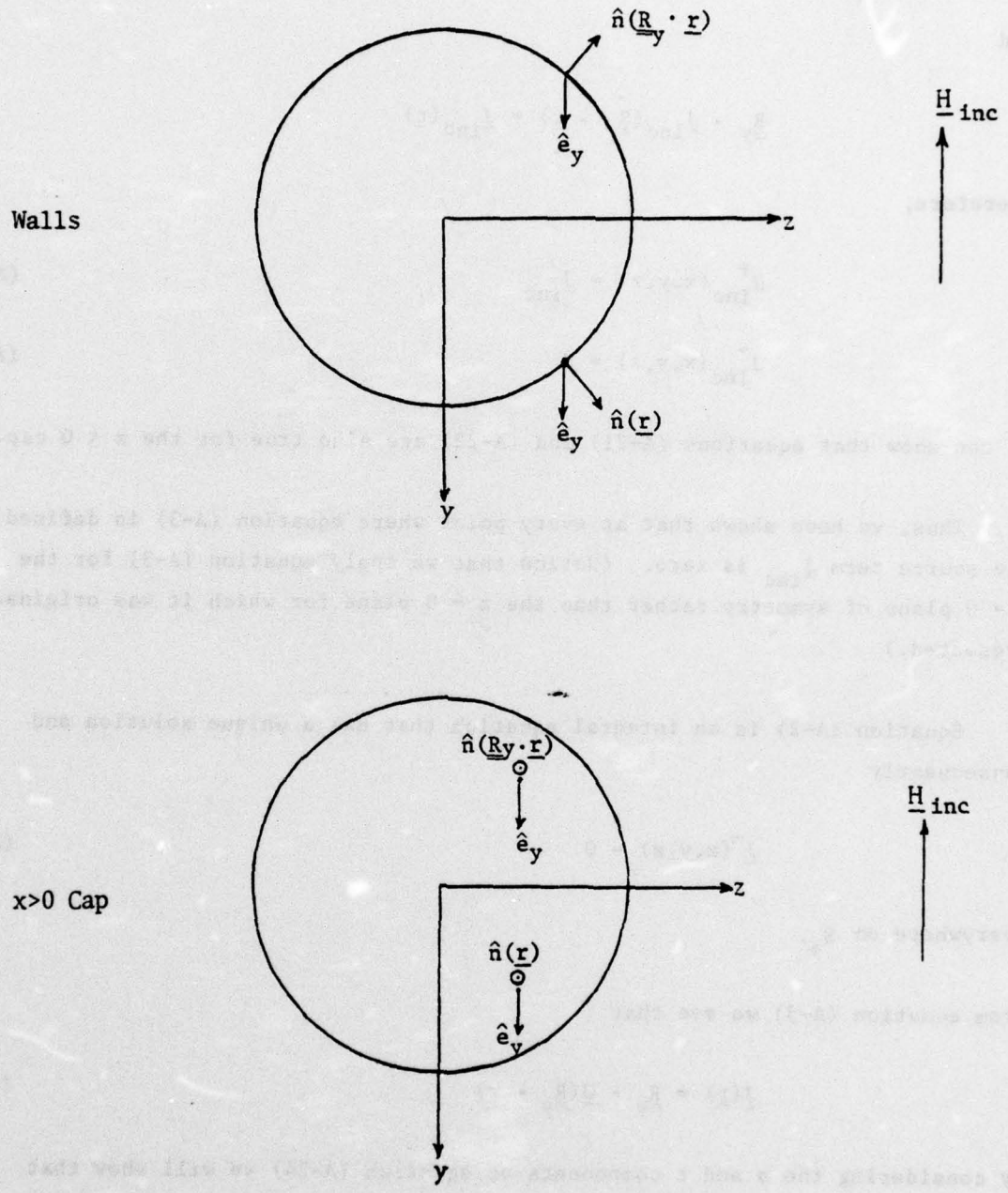

Figure A2: Orientation of the unit normal $\hat{n}$ at symmetric positions with respect to the xz-plane.

and

$$\underline{\underline{R}}_y \cdot \underline{J}_{inc}(\underline{\underline{R}}_y \cdot \underline{r}) = \underline{J}_{inc}(\underline{r})$$

Therefore,

$$J^{+}_{inc}(x,y,z) = \underline{J}_{inc} \tag{A-21}$$

$$J^{-}_{inc}(x,y,z) = 0 \tag{A-22}$$

We can show that equations (A-21) and (A-22) are also true for the $x < 0$ cap.

Thus, we have shown that at every point where equation (A-3) is defined the source term $\underline{J}_{inc}$ is zero. (Notice that we apply equation (A-3) for the $y = 0$ plane of symmetry rather than the $z = 0$ plane for which it was originally presented.)

Equation (A-2) is an integral equation that has a unique solution and consequently

$$\underline{J}^{-}(x,y,z) = 0 \tag{A-23}$$

everywhere on S_+.

From equation (A-5) we see that

$$\underline{J}(\underline{r}) = \underline{\underline{R}}_y \cdot \underline{J}(\underline{\underline{R}}_y \cdot \underline{r}) \tag{A-24}$$

By considering the s and t components of equation (A-24) we will show that

$$J_t(x,y,z) = J_t(x,-y,z) \tag{A-25}$$

$$J_s(x,y,z) = -J_s(x,-y,z) \tag{A-26}$$

everywhere on the cylinder (walls and caps).

c. Walls

(1) t-Components

If we take the inner product of equation (A-24) with $\hat{t}(\underline{r})$ we obtain

$$J_t(\underline{r}) = \hat{t}(\underline{r}) \cdot \underline{\underline{R}}_y \cdot \underline{J}(x,-y,z) \tag{A-27}$$

Recalling that $\hat{t} = \hat{e}_x$ on the walls we see that

$$\hat{t}(\underline{r}) \cdot \underline{\underline{R}}_y = \hat{t}(\underline{r}) = \hat{t}(\underline{\underline{R}}_y \cdot \underline{r})$$

and from equation (A-27)

$$J_t(x,y,z) = J_t(x,-y,z) \tag{A-25}$$

(2) s-Components

From equation (A-24) we obtain

$$J_s(\underline{r}) = \hat{s}(\underline{r}) \cdot \underline{\underline{R}}_y \cdot \underline{J}(x,-y,z) \tag{A-29}$$

With the aid of figure A3 we see that

$$\begin{aligned}
\hat{s}(\underline{r}) \cdot \underline{\underline{R}}_y &= \left[\underline{s}_y(\underline{r}) + \underline{s}_z(\underline{r})\right] \cdot \underline{\underline{R}}_y \\
&= -\underline{s}_y(\underline{r}) + \underline{s}_z(\underline{r}) \\
&= -\underline{s}_y(x,-y,z) - \underline{s}_z(x,-y,z) \\
&= -\hat{\underline{s}}(x,-y,z)
\end{aligned}$$

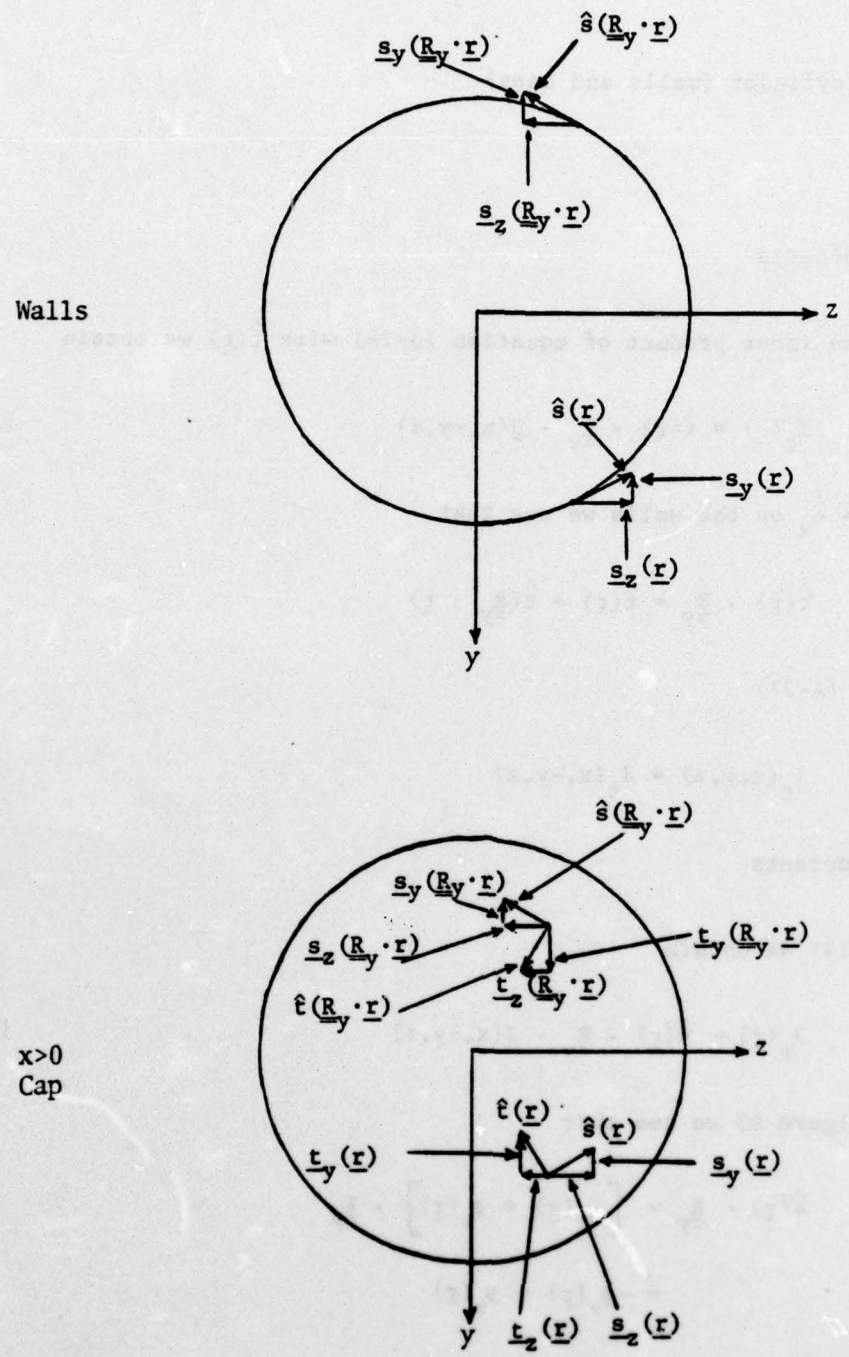

Figure A3: Orientation of $\hat{s}$ and $\hat{t}$ at positions symmetric to the xz-plane.

and equation (A-29) gives

$$J_s(x,y,z) = -J_s(x,-y,z) \tag{A-26}$$

c. Caps

(1) $x > 0$, t-Components

Writing equation (A-27) for this case and with the aid of figure A3 we obtain

$$\hat{t}(\underline{r}) \cdot \underline{\underline{R}}_y = \left[\underline{t}_y(\underline{r}) + \underline{t}_z(\underline{r})\right] \cdot \underline{\underline{R}}_y$$

$$= -\underline{t}_y(\underline{r}) + \underline{t}_z(\underline{r})$$

$$= t_y(\underline{\underline{R}}_y \cdot \underline{r}) + \underline{t}_z(\underline{\underline{R}}_y \cdot \underline{r})$$

$$= \underline{t}(\underline{\underline{R}}_y \cdot \underline{r})$$

and equation (A-27) gives

$$J_t(x,y,z) = J_t(x,-y,z) \tag{A-25}$$

(2) $x > 0$, s-Components

Again we use equation (A-29) and figure A3

$$\hat{s}(\underline{r}) \cdot \underline{\underline{R}}_y = \left[\underline{s}_y(\underline{r}) + \underline{s}_z(\underline{r})\right] \cdot \underline{\underline{R}}_y$$

$$= -\underline{s}_y(\underline{r}) + \underline{s}_z(\underline{r})$$

$$= -\hat{s}(\underline{\underline{R}}_y \cdot \underline{r})$$

and

$$J_s(x,y,z) = -J_s(x,-y,z) \tag{A-26}$$

We can show that equations (A-25) and (A-26) are also true for the bottom cap $x < 0$.

The proof for

$$J_t(x,y,z) = J_t(-x,y,z) \tag{A-30}$$

$$J_s(x,y,z) = -J_s(-x,y,z) \tag{A-31}$$

that relate the current density components at points symmetric to the $x = 0$ plane is similar to the proof we gave for the $y = 0$ plane. In the $x = 0$ case we can show that $\underline{J}^{+}_{inc} = 0$ everywhere instead of $\underline{J}^{-}_{inc} = 0$ as in the case of $y = 0$ but otherwise the proof follows the same lines. Equations (A-25), (A-26), (A-30), and (A-31) are the same as equations (A-25) and (A-16).

5. INTEGRAL EQUATIONS WITH FULL REDUCTION

We will now employ equations(A-15) and (A-16) along with the reduction scheme given by equations (A-2) through (A-9) to derive a pair of integral equations for two fictitious current densities, defined only over the part of the surface of the cylinder that corresponds to the first octant, i.e. $x \geq 0$, $y \geq 0$, $z \geq 0$ and show that from a knowledge of the current density over the surface of the cylinder that corresponds to only two octants ($x \geq 0$, $y \geq 0$, $z \geq 0$ and $x \geq 0$, $y \geq 0$, $z \leq 0$) we can calculate the current density at any point on the remaining six octants. As we mentioned earlier, the surface integrals in equations (A-2) and (A-3) are evaluated over S_+ which is defined for $z_o \geq 0$. By applying the same reduction scheme we can substitute equation (A-2) by two integral equations for $\underline{J}^{++}$, $\underline{J}^{+-}$ and equation (A-3) by two integral equations for $\underline{J}^{-+}$, $\underline{J}^{--}$ by considering the symmetries about the

$x = 0$ plane and evaluating the resulting surface integrals over S_{++} defined by $x_o \geq 0$, $z_o \geq 0$. We can go one step further and consider symmetries about the $y = 0$ plane. Then the original equation (A-1) for $\underline{J}$ is transformed into eight integral equations for $\underline{J}^{+++}$, $\underline{J}^{++-}$, $\underline{J}^{+-+}$, $\underline{J}^{+--}$, $\underline{J}^{-++}$, $\underline{J}^{-+-}$, $\underline{J}^{--+}$, $\underline{J}^{---}$ with kernels $\underline{\underline{K}}^{+++}$, $\underline{\underline{K}}^{++-}$, $\underline{\underline{K}}^{+-+}$, $\underline{\underline{K}}^{+--}$, $\underline{\underline{K}}^{-++}$, $\underline{\underline{K}}^{-+-}$, $\underline{\underline{K}}^{--+}$, $\underline{\underline{K}}^{---}$ respectively. The surface integrals will be evaluated over S_{+++} defined by $x_o \geq 0$, $y_o \geq 0$, $z_o \geq 0$. By repeated application of defining equations like equations (A-4) and (A-5) we can derive the following relationship

$$\begin{aligned}\underline{J}^{\alpha\beta\gamma} = \frac{1}{8}\Big[&\underline{J}(\underline{r}) + \alpha\underline{\underline{R}}_x \cdot \underline{J}(\underline{\underline{R}}_x \cdot \underline{r}) + \beta\underline{\underline{R}}_y \cdot \underline{J}(\underline{\underline{R}}_y \cdot \underline{r}) \\ &+ \gamma\underline{\underline{R}}_z \cdot \underline{J}(\underline{\underline{R}}_z \cdot \underline{r}) + \alpha\beta\underline{\underline{R}}_x \cdot \underline{\underline{R}}_y \cdot \underline{J}(\underline{\underline{R}}_x \cdot \underline{\underline{R}}_y \cdot \underline{r}) \\ &+ \alpha\gamma\underline{\underline{R}}_x \cdot \underline{\underline{R}}_z \cdot \underline{J}(\underline{\underline{R}}_x \cdot \underline{\underline{R}}_z \cdot \underline{r}) + \beta\gamma\underline{\underline{R}}_y \cdot \underline{\underline{R}}_z \cdot \underline{J}(\underline{\underline{R}}_y \cdot \underline{\underline{R}}_z \cdot \underline{r}) \\ &+ \alpha\beta\gamma\underline{\underline{R}}_x \cdot \underline{\underline{R}}_y \cdot \underline{\underline{R}}_z \cdot \underline{J}(\underline{\underline{R}}_x \cdot \underline{\underline{R}}_y \cdot \underline{\underline{R}}_z \cdot \underline{r})\Big] \qquad \text{(A-32)}\end{aligned}$$

where on the left hand side α, β, γ are + or - and on the right hand side they are equal to +1 or -1. Also notice that in deriving equation (A-32) the $x = 0$ plane symmetry was considered first followed by the $y = 0$ plane symmetry and finally the $z = 0$ plane symmetry but the order is not important.

We want to show that of the eight currents defined by equation (A-32) six are identically equal to zero. We will do so by considering the t and s components of equation (A-32). By following a procedure similar to the one that led to symmetry relationships (A-15) and (A-16) one can show that

$$\left.\begin{aligned}\hat{t}(\underline{r}) \cdot \underline{\underline{R}}_x &= -\hat{t}(\underline{\underline{R}}_x \cdot \underline{r}) \\ \hat{t}(\underline{r}) \cdot \underline{\underline{R}}_y &= \hat{t}(\underline{\underline{R}}_y \cdot \underline{r}) \\ \hat{t}(\underline{r}) \cdot \underline{\underline{R}}_z &= \hat{t}(\underline{\underline{R}}_z \cdot \underline{r})\end{aligned}\right\} \qquad \text{(A-33)}$$

and consequently

$$\hat{t}(\underline{r}) \cdot \underline{\underline{R}}_x \cdot \underline{\underline{R}}_y = -\hat{t}(\underline{\underline{R}}_x \cdot \underline{r}) \cdot \underline{\underline{R}}_y = -\hat{t}(\underline{\underline{R}}_y \cdot \underline{\underline{R}}_x \cdot \underline{r})$$

$$= -\hat{t}(\underline{\underline{R}}_x \cdot \underline{\underline{R}}_y \cdot \underline{r}) \qquad \text{(A-34)}$$

since $\underline{\underline{R}}_x$, $\underline{\underline{R}}_y$, $\underline{\underline{R}}_z$ commute, and

$$\left.\begin{aligned} \hat{t}(\underline{r}) \cdot \underline{\underline{R}}_x \cdot \underline{\underline{R}}_z &= -\hat{t}(\underline{\underline{R}}_x \cdot \underline{\underline{R}}_z \cdot \underline{r}) \\ \hat{t}(\underline{r}) \cdot \underline{\underline{R}}_y \cdot \underline{\underline{R}}_z &= \hat{t}(\underline{\underline{R}}_y \cdot \underline{\underline{R}}_z \cdot \underline{r}) \\ \hat{t}(\underline{r}) \cdot \underline{\underline{R}}_x \cdot \underline{\underline{R}}_y \cdot \underline{\underline{R}}_z &= -\hat{t}(\underline{\underline{R}}_x \cdot \underline{\underline{R}}_y \cdot \underline{\underline{R}}_z \cdot \underline{r}) \end{aligned}\right\} \qquad \text{(A-35)}$$

Similarly

$$\left.\begin{aligned} \hat{s}(\underline{r}) \cdot \underline{\underline{R}}_x &= \hat{s}(\underline{\underline{R}}_x \cdot \underline{r}) \\ \hat{s}(\underline{r}) \cdot \underline{\underline{R}}_y &= -\hat{s}(\underline{\underline{R}}_y \cdot \underline{r}) \\ \hat{s}(\underline{r}) \cdot \underline{\underline{R}}_z &= -\hat{s}(\underline{\underline{R}}_z \cdot \underline{r}) \end{aligned}\right\} \qquad \text{(A-36)}$$

and consequently

$$\left.\begin{aligned} \hat{s}(\underline{r}) \cdot \underline{\underline{R}}_x \cdot \underline{\underline{R}}_y &= -\hat{s}(\underline{\underline{R}}_x \cdot \underline{\underline{R}}_y \cdot \underline{r}) \\ \hat{s}(\underline{r}) \cdot \underline{\underline{R}}_x \cdot \underline{\underline{R}}_z &= -\hat{s}(\underline{\underline{R}}_x \cdot \underline{\underline{R}}_z \cdot \underline{r}) \\ \hat{s}(\underline{r}) \cdot \underline{\underline{R}}_y \cdot \underline{\underline{R}}_z &= \hat{s}(\underline{\underline{R}}_y \cdot \underline{\underline{R}}_z \cdot \underline{r}) \end{aligned}\right\} \qquad \text{(A-37)}$$

$$\hat{s}(\underline{r}) \cdot \underline{\underline{R}}_x \cdot \underline{\underline{R}}_y \cdot \underline{\underline{R}}_z = -\hat{s}(\underline{\underline{R}}_x \cdot \underline{\underline{R}}_y \cdot \underline{\underline{R}}_z \cdot \underline{r})$$

Before we consider the t and s components of equation (A-32) we also recall equations(A-15) and (A-16) which we can rewrite as

$$\left.\begin{aligned}
&J_t(\underline{r}) = J_t(\underline{\underline{R}}_x \cdot \underline{r}) = J_t(\underline{\underline{R}}_y \cdot \underline{r}) = J_t(\underline{\underline{R}}_x \cdot \underline{\underline{R}}_y \cdot \underline{r}) \\
&J_t(\underline{\underline{R}}_z \cdot \underline{r}) = J_t(\underline{\underline{R}}_x \cdot \underline{\underline{R}}_z \cdot \underline{r}) = J_t(\underline{\underline{R}}_y \cdot \underline{\underline{R}}_z \cdot \underline{r}) = J_t(\underline{\underline{R}}_x \cdot \underline{\underline{R}}_y \cdot \underline{\underline{R}}_z \cdot \underline{r}) \\
&J_s(\underline{r}) = -J_s(\underline{\underline{R}}_x \cdot \underline{r}) = -J_s(\underline{\underline{R}}_y \cdot \underline{r}) = J_s(\underline{\underline{R}}_x \cdot \underline{\underline{R}}_y \cdot \underline{r}) \\
&J_s(\underline{\underline{R}}_z \cdot \underline{r}) = -J_s(\underline{\underline{R}}_x \cdot \underline{\underline{R}}_z \cdot \underline{r}) = -J_s(\underline{\underline{R}}_y \cdot \underline{\underline{R}}_z \cdot \underline{r}) = J_s(\underline{\underline{R}}_x \cdot \underline{\underline{R}}_y \cdot \underline{\underline{R}}_z \cdot \underline{r})
\end{aligned}\right\} \quad \text{(A-38)}$$

In view of equations (A-33) through (A-38), equation (A-32) gives

$$J_t^{\alpha\beta\gamma} = \frac{1}{8}\left[(1 + \beta - \alpha - \alpha\beta)\, J_t(\underline{r}) + (\gamma + \beta\gamma - \alpha\gamma - \alpha\beta\gamma)\, J_t(\underline{\underline{R}}_z \cdot \underline{r})\right] \quad \text{(A-39)}$$

$$J_s^{\alpha\beta\gamma} = \frac{1}{8}\left[(1 + \beta - \alpha - \alpha\beta)\, J_s(\underline{r}) - (\gamma + \beta\gamma - \alpha\gamma - \alpha\beta\gamma)\, J_s(\underline{\underline{R}}_z \cdot \underline{r})\right] \quad \text{(A-40)}$$

From equations (A-39) and (A-40) we can see that only $\underline{J}^{-++}$ and $\underline{J}^{-+-}$ are non-zero and that

$$\left.\begin{aligned}
J_t^{-++} &= \frac{1}{2}\left[J_t(\underline{r}) + J_t(\underline{\underline{R}}_z \cdot \underline{r})\right] \\
J_s^{-++} &= \frac{1}{2}\left[J_s(\underline{r}) - J_s(\underline{\underline{R}}_z \cdot \underline{r})\right] \\
J_t^{-+-} &= \frac{1}{2}\left[J_t(\underline{r}) - J_t(\underline{\underline{R}}_z \cdot \underline{r})\right] \\
J_s^{-+-} &= \frac{1}{2}\left[J_s(\underline{r}) + J_s(\underline{\underline{R}}_z \cdot \underline{r})\right]
\end{aligned}\right\} \quad \text{(A-41)}$$

Thus we can evaluate $J_t(\underline{r})$ at any $\underline{r}$ on the entire cylindrical surface if we know $\underline{J}^{-+\pm}$. Symmetry relationships (A-38) show that this is possible if we know $J(\underline{r})$ and $J(\underline{\underline{R}}_z \cdot \underline{r})$ where $\underline{r} = (x \geq 0, y \geq 0, z \geq 0)$. Thus from a knowledge of the current density over the surface of the cylinder corresponding to only two octants ($x \geq 0$, $y \gtrless 0$, $z \geq 0$ and $x \geq 0$, $y \geq 0$, $z \leq 0$) we can calculate the current density at any point on the remaining six octants. From

equation (A-41) we obtain

$$
\begin{aligned}
J_t(\underline{r}) &= J_t^{-++} + J_t^{-+-} \\
J_t(\underline{\underline{R}}_z \cdot \underline{r}) &= J_t^{-++} - J_t^{-+-} \\
J_s(\underline{r}) &= J_s^{-++} + J_s^{-+-} \\
J_s(\underline{\underline{R}}_z \cdot \underline{r}) &= -(J_s^{-++} - J_s^{-+-})
\end{aligned}
\qquad \text{(A-42)}
$$

Equations (A-42) give $\underline{J}(\underline{r})$ and $\underline{J}(\underline{\underline{R}}_z \cdot \underline{r})$ ($\underline{r} \equiv (x > 0,\ y \geq 0,\ z \geq 0)$) in terms of $\underline{J}^{-+\pm}$. In order to write down the equations satisfied by $\underline{J}^{-++}$ and $\underline{J}^{-+-}$ we must calculate the corresponding source terms and kernels. One can show that the incident current density also satisfies relationships (A-15) and (A-16) or their equivalent ones given by equations (A-38). Thus

$$
\begin{aligned}
J_{inc,t}^{-++} &= \frac{1}{2}\left[J_{inc,t}(\underline{r}) + J_{inc,t}(\underline{\underline{R}}_z \cdot \underline{r})\right] \\
&= i\, H_o s_y(\underline{r}) \sin kz \\
J_{inc,s}^{-++} &= \frac{1}{2}\left[J_{inc,s}(\underline{r}) + J_{inc,s}(\underline{\underline{R}}_z \cdot \underline{r})\right] \\
&= H_o\, t_y(\underline{r}) \cos kz \\
J_{inc,t}^{-+-} &= \frac{1}{2}\left[J_{inc,t}(\underline{r}) - J_{inc,t}(\underline{\underline{R}}_z \cdot \underline{r})\right] \\
&= -H_o\, s_y(\underline{r}) \cos kz \\
J_{inc,s}^{-+-} &= \frac{1}{2}\left[J_{inc,s}(\underline{r}) - J_{inc,s}(\underline{\underline{R}}_z \cdot \underline{r})\right] \\
&= -i\, H_o t_y(\underline{r}) \sin kz
\end{aligned}
$$

By repeated application of equations (A-7) through (A-9) one obtains

$$\begin{aligned}\underline{\underline{K}}^{-++} = {} & \underline{\underline{K}}(\underline{r};\underline{r}_o) - \underline{\underline{K}}(\underline{r};\underline{\underline{R}}_x \cdot \underline{r}_o) \cdot \underline{\underline{R}}_x + \underline{\underline{K}}(\underline{r};\underline{\underline{R}}_y \cdot \underline{r}_o) \cdot \underline{\underline{R}}_y \\ & \pm \underline{\underline{K}}(\underline{r};\underline{\underline{R}}_z \cdot \underline{r}_o) \cdot \underline{\underline{R}}_z - \underline{\underline{K}}(\underline{r};\underline{\underline{R}}_x \cdot \underline{\underline{R}}_y \cdot \underline{r}_o) \cdot \underline{\underline{R}}_x \cdot \underline{\underline{R}}_y \\ & \mp \underline{\underline{K}}(\underline{r};\underline{\underline{R}}_x \cdot \underline{\underline{R}}_z \cdot \underline{r}_o) \cdot \underline{\underline{R}}_x \cdot \underline{\underline{R}}_z \pm \underline{\underline{K}}(\underline{r};\underline{\underline{R}}_y \cdot \underline{\underline{R}}_z \cdot \underline{r}_o) \cdot \underline{\underline{R}}_y \cdot \underline{\underline{R}}_z \\ & \mp \underline{\underline{K}}(\underline{r};\underline{\underline{R}}_x \cdot \underline{\underline{R}}_y \cdot \underline{\underline{R}}_z \cdot \underline{r}_o) \cdot \underline{\underline{R}}_x \cdot \underline{\underline{R}}_y \cdot \underline{\underline{R}}_z \end{aligned} \qquad \text{(A-43)}$$

In order to exhibit the integral equation for $\underline{J}^{-+\pm}$ in component form we must calculate the inner products

$$\hat{s}(\underline{r}) \cdot \underline{\underline{K}}^{-++} \cdot \hat{s}(\underline{r}_o), \; \hat{s}(\underline{r}) \cdot \underline{\underline{K}}^{-++} \cdot \hat{t}(\underline{r}_o)$$

$$\hat{t}(\underline{r}) \cdot \underline{\underline{K}}^{-++} \cdot \hat{s}(\underline{r}_o), \; \hat{t}(\underline{r}) \cdot \underline{\underline{K}}^{-++} \cdot \hat{t}(\underline{r}_o)$$

Recalling that

$$\underline{\underline{K}}(\underline{r};\underline{r}_o) = \hat{n}(\underline{r}) \times \left[\nabla G(\underline{r};\underline{r}_o) \times \underline{\underline{I}}\right].$$

where

$$\nabla G(\underline{r};\underline{r}_o) = Q(R)\underline{R}$$

$$Q(R) = \frac{e^{ikR}}{4\pi R^3}(-1 + ikR)$$

$$\underline{R} = \underline{r} - \underline{r}_o, \; R = |\underline{R}|$$

we have

$$\left[\hat{s}(\underline{r}),\ \hat{t}(\underline{r})\right] \cdot \underline{\underline{K}}(\underline{r};\underline{r}_o) \cdot \left[\hat{s}(\underline{r}_o),\ \hat{t}(\underline{r}_o)\right]$$

$$= \left[\hat{s}(\underline{r}),\ \hat{t}(\underline{r})\right] \cdot \left\{\hat{n}(\underline{r}) \left[\underline{R} \times \left[\hat{s}(\underline{r}_o),\ \hat{t}(\underline{r}_o)\right]\right]\right\} Q(R)$$

$$= \left[\left[\hat{s}(\underline{r}),\ \hat{t}(\underline{r})\right] \times \hat{n}(\underline{r})\right] \cdot \left[\underline{R} \times \left[\hat{s}(\underline{r}_o),\ \hat{t}(\underline{r}_o)\right]\right] Q(R)$$

$$= \left[-\hat{t}(\underline{r}),\ \hat{s}(\underline{r})\right] \cdot \left[\underline{R} \times \left[\hat{s}(\underline{r}_o),\ \hat{t}(\underline{r}_o)\right]\right] Q(R)$$

$$= \left[-\hat{t}(\underline{r}),\ \hat{s}(\underline{r})\right] \times \left[\hat{s}(\underline{r}_o),\ \hat{t}(\underline{r}_o)\right] \cdot \underline{R}\ Q(R)$$

In view of the above relationships we finally obtain

$$\begin{aligned} J_s^{-++}(\underline{r}) &= H_o t_y \cos kz + \int_S \left[M(t,s_o)\ J_s(\underline{r}_o) + M(t,t_o)\ J_t(\underline{r}_o)\right] dS_o \\ J_t^{-++}(\underline{r}) &= iH_o s_y \sin kz + \int_S \left[M(s,-s_o) J_s(\underline{r}_o) + M(s,-t_o) J_t(\underline{r}_o)\right] dS_o \end{aligned} \tag{A-44}$$

$$\begin{aligned} J_s^{-+-}(\underline{r}) &= -iH_o t_y \sin kz + \int_S \left[N(t,s_o)\ J_s(\underline{r}_o) + N(t,t_o)\ J_t(\underline{r}_o)\right] dS_o \\ J_t^{-+-}(\underline{r}) &= -H_o s_y \cos kz + \int_S \left[N(s,-s_o) J_s(\underline{r}_o) + N(s,-t_o)\ J_t(\underline{r}_o)\right] dS_o \end{aligned} \tag{A-45}$$

where

$$\left.\begin{aligned} M(p,\phi_o) = {} & Q_1(\hat{\phi}_1 \times \hat{p}) \cdot \underline{R}_1 - Q_2(\hat{\phi}_2 \times \hat{p}) \cdot \underline{R}_2 + Q_3(\hat{\phi}_3 \times \hat{p}) \cdot \underline{R}_3 \\ & - Q_4(\hat{\phi}_4 \times \hat{p}) \cdot \underline{R}_4 - Q_5(\hat{\phi}_5 \times \hat{p}) \cdot \underline{R}_5 - Q_6(\hat{\phi}_6 \times \hat{p}) \cdot \underline{R}_6 \\ & + Q_7(\hat{\phi}_7 \times \hat{\rho}) \cdot \underline{R}_7 - Q_8(\hat{\phi}_8 \times \hat{\rho}) \cdot \underline{R}_8 \end{aligned}\right\} \tag{A-46}$$

$$N(p,\phi_o) = Q_1(\hat{\phi}_1 \times \hat{p}) \cdot \underline{R}_1 - Q_2(\hat{\phi}_2 \times \hat{p}) \cdot R_2 - Q_3(\phi_3 \times p) \cdot \underline{R}_3$$
$$- Q_4(\hat{\phi}_4 \times \hat{p}) \cdot \underline{R}_4 + Q_5(\hat{\phi}_5 \times \hat{p}) \cdot \underline{R}_5 - Q_6(\phi_6 \times p) \cdot \underline{R}_6 \qquad \text{(A-47)}$$
$$- Q_7(\hat{\phi}_7 \times \hat{p}) \cdot \underline{R}_7 + Q_8 (\hat{\phi}_8 \times \hat{p}) \cdot \underline{R}_8$$

and

$$\begin{aligned} \underline{R}_1 &= \underline{r} - \underline{r}_o & \underline{R}_5 &= \underline{r} - \underline{\underline{R}}_x \cdot \underline{\underline{R}}_y \cdot \underline{r}_o \\ \underline{R}_2 &= \underline{r} - \underline{\underline{R}}_x \cdot \underline{r}_o & \underline{R}_6 &= \underline{r} - \underline{\underline{R}}_x \cdot \underline{\underline{R}}_z \cdot \underline{r}_o \\ \underline{R}_3 &= \underline{r} - \underline{\underline{R}}_y \cdot \underline{r}_o & \underline{R}_7 &= \underline{r} - \underline{\underline{R}}_y \cdot \underline{\underline{R}}_z \cdot \underline{r}_o \\ \underline{R}_4 &= \underline{r} - \underline{\underline{R}}_z \cdot \underline{r}_o & \underline{R}_8 &= \underline{r} - \underline{\underline{R}}_x \cdot \underline{\underline{R}}_y \cdot \underline{\underline{R}}_z \cdot \underline{r}_o \end{aligned} \qquad \text{(A-48)}$$

$$\begin{aligned} \hat{\phi}_1 &= \hat{\phi}_1(\underline{r}_o) & \hat{\phi}_5 &= \underline{\underline{R}}_x \cdot \underline{\underline{R}}_y \cdot \hat{\phi}_1 \\ \hat{\phi}_2 &= \underline{\underline{R}}_x \cdot \hat{\phi}_1 & \hat{\phi}_6 &= \underline{\underline{R}}_x \cdot \underline{\underline{R}}_z \cdot \hat{\phi}_1 \\ \hat{\phi}_3 &= \underline{\underline{R}}_y \cdot \hat{\phi}_1 & \hat{\phi}_7 &= \underline{\underline{R}}_y \cdot \underline{\underline{R}}_z \cdot \hat{\phi}_1 \\ \hat{\phi}_4 &= \underline{\underline{R}}_z \cdot \hat{\phi}_1 & \hat{\phi}_8 &= \underline{\underline{R}}_x \cdot \underline{\underline{R}}_y \cdot \underline{\underline{R}}_z \cdot \hat{\phi}_1 = -\hat{\phi}_1 \end{aligned} \qquad \text{(A-49)}$$

The explicit forms (A-46) and (A-47) define our notation for $M(p,\phi_o)$ and $N(p,\phi_o)$ which admittedly is not impeccably clear. To obtain $M(s,-s_o)$, for example, we substitute $\hat{p}$ by $\hat{s}(\underline{r})$ and $\hat{\phi}_i (i = 1, 2, \ldots, 8)$ by $-\hat{s}_i$ where $\hat{s}_1$ is the unit vector $\hat{s}$ evaluated at $\underline{r}_o = (x_o \geq 0, y_o \geq 0, z_o \geq 0)$! The integrals are evaluated over the part of the cylindrical surface defined by $x_o \geq 0$, $y_o \geq 0$, $z_o \geq 0$.

Thus the existence of three symmetry planes and broadside incidence (see figure A1) allows one to reduce the problem of calculating the current density on the cylindrical surface to equations (A-44) and (A-45) which involve integrating over one eighth of the cylindrical surface whereas the original equation (A-1) is defined over the entire surface. Once we know $\underline{J}^{-++}$ and $\underline{J}^{-+-}$ we can employ equation (A-42) to evaluate $\underline{J}(\underline{r})$ and $\underline{J}(\underline{\underline{R}}_z \cdot \underline{r})$ where $\underline{r} = (x \geq 0,$

$y \geq 0$, $z \geq 0$). The current density at any point is then obtained by using symmetry relationships (A-38). If the $\underline{k}$ vector is still perpendicular to the xy-plane but the electric field has x and y-components we can consider the two components separately and employ the relevant symmetries for each case. The final current density is then given by superposition of the current densities corresponding to the two electric field components. If the incident wave has arbitrary direction and polarization symmetry relationships (A-38) are no longer valid. One can still reduce equation (A-1) to integral equations over the $x \geq 0$, $y \geq 0$, $z \geq 0$ part of the surface and solve for the eight current densities $\underline{J}^{\pm\pm\pm}$. From equations (A-32) one can solve for the real current density J evaluated at points over all eight octants in terms of the $\underline{J}^{\pm\pm\pm}$ current densities. For a specific plane wave some of the symmetry relationships given by equation (A-38) may hold and this would reduce the number of non-zero $\underline{J}^{\pm\pm\pm}$ current densities.

2. ONE PLANE OF SYMMETRY. MAGNETOSTATIC LIMIT

Consider a perfectly conducting body, possessing a plane of symmetry xy, illuminated by a plane wave with the wave vector $\underline{k}$ perpendicular to the plane of symmetry and the H vector parallel to the y-axis as depicted in figure A4. The x-axis is chosen conveniently, for example for aircraft it is the axis of the fuselage.

We will show that in the limit $\omega = 0$, where ω is the radian frequency, the surface current density at points symmetric to the xy plane, are simply related to each other. The specific relationship will be presented shortly. The surface components at the surface current density J will be denoted J_s and J_t, that is at each point on the surface we have

$$\underline{J} = J_s \hat{s} + J_t \hat{t} \qquad \text{(A-50)}$$

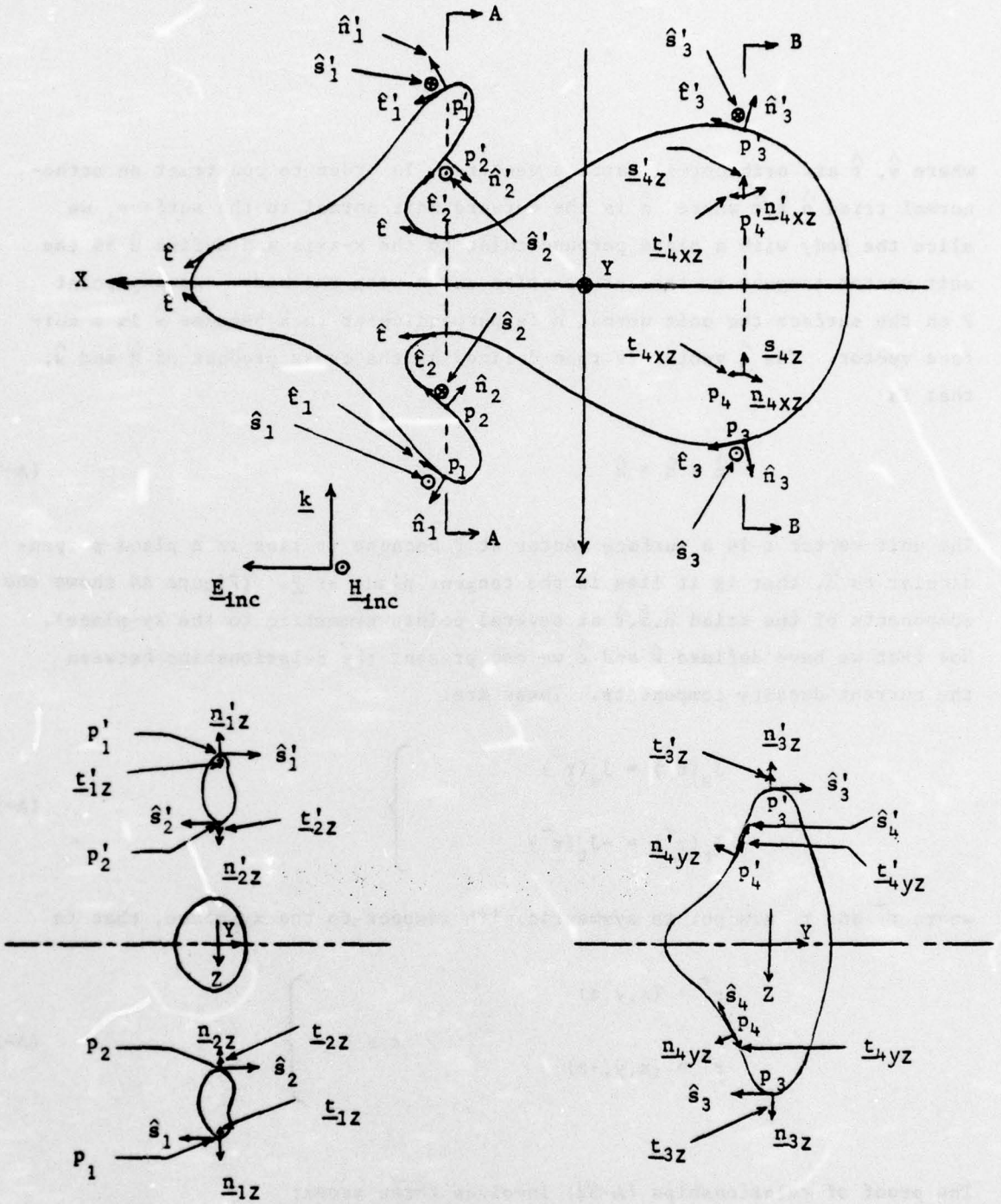

Figure A4: A body possessing a plane of symmetry (xy-plane) and orientation of unit vectors $\hat{n}$, $\hat{s}$ and $\hat{t}$.

where $\hat{s}$, $\hat{t}$ are orthonormal surface vectors. In order to construct an orthonormal triad $\hat{n},\hat{s},\hat{t}$ where $\hat{n}$ is the outward unit normal to the surface, we slice the body with a plane perpendicular to the x-axis and define $\hat{s}$ as the unit vector tangent to the intersection curve with the body. At any point P on the surface the unit normal $\hat{n}$ is perpendicular to $\hat{s}$ because $\hat{s}$ is a surface vector. The $\hat{c}$ vector is then defined as the cross product of $\hat{n}$ and $\hat{s}$, that is

$$\hat{t} = \hat{n} \times \hat{s} \tag{A-51}$$

The unit vector $\hat{t}$ is a surface vector at $\underline{P}$ because it lies in a plane perpendicular to $\hat{n}$, that is it lies in the tangent plane at $\underline{P}$. (Figure A4 shows the components of the triad $\hat{n},\hat{s},\hat{c}$ at several points symmetric to the xy-plane). Now that we have defined $\hat{s}$ and $\hat{c}$ we can present the relationships between the current density components. These are:

$$\left.\begin{aligned} J_s(\underline{r}^+) &= J_s(\underline{r}^-) \\ J_t(\underline{r}^+) &= -J_t(\underline{r}^-) \end{aligned}\right\} \tag{A-52}$$

where $\underline{r}^+$ and $\underline{r}^-$ are points symmetric with respect to the xy-plane, that is

$$\left.\begin{aligned} \underline{r}^+ &= (x,y,z) \\ \underline{r}^- &= (x,y,-z) \end{aligned}\right\} \quad z \geq 0 \tag{A-53}$$

The proof of relationships (A-52) involves three steps:

(a) Use of certain symmetry arguments through which the usual magnetic field integral equation for $\underline{J}(\underline{r})$ is substituted by two integral equations for $\underline{J}^+$ and $\underline{J}^-$ on the positive ($z \geq 0$) half of the surface S where

$$\underline{J}^{\pm} = \frac{1}{2}\left[\underline{J}(r^{+}) \pm \underline{\underline{R}}_z \cdot \underline{J}(\underline{r}^{-})\right] \tag{A-54}$$

and R_z is a reflection operator about the symmetry plane

$$R_z = \underline{\underline{I}} - 2\,\hat{e}_z\,\hat{e}_z \tag{A-55}$$

($\underline{\underline{I}}$ is the identify operators.)

(b) Proof that at $\omega = 0$ the source term $\underline{J}^{+}_{inc}$, for the $\underline{J}^{+}$ integral equation, is zero everywhere on the ($z \geq 0$) surface of the body and consequently $\underline{J}^{+} = 0$.

(c) Inner multiplication of equation(A-54)for $\underline{J}^{+}$ with $\hat{s}$ and $\hat{t}$ and use of geometrical properties of these unit vectors to finally show the validity of equation (A-52).

We now present the above three steps in detail. The magnetic field integral equation for $\underline{J}$ is

$$\frac{1}{2}\,\underline{J}(\underline{r}) = \underline{J}_i(\underline{r}) + \int_S \underline{\underline{K}}(\underline{r},\underline{r}_o) \cdot \underline{J}(\underline{r}_o)\,dS_o \tag{A-1}$$

where

$$\underline{J}_{inc}(\underline{r}) = \hat{n}(\underline{r}) \times \underline{H}_{inc}(\underline{r}) \tag{A-56}$$

and S is the surface of the perfectly conducting body.

Equation (A-1) as we mentioned earlier can be transformed into the following pair of equations:

$$\frac{1}{2}\,\underline{J}^{+}(\underline{r}^{+}) = \underline{J}^{+}_{inc}(\underline{r}^{+}) + \int_{S_+} \underline{\underline{K}}^{+}(\underline{r}^{+};\, \underline{r}_o^{+}) \cdot \underline{J}^{+}(\underline{r}_o^{+})\,dS_o \tag{A-2}$$

$$\frac{1}{2}\,\underline{J}^{-}(\underline{r}^{+}) = \underline{J}^{-}_{inc}(\underline{r}^{+}) + \int_{S_+} \underline{\underline{K}}^{-}(\underline{r}^{+};\, \underline{r}_o^{+}) \cdot \underline{J}^{-}(\underline{r}_o^{+})\, dS_o \qquad \text{(A-3)}$$

where $\underline{\underline{K}}^{\pm}(\underline{r}^{+}, \underline{r}_o^{+})$ are defined by equations (A-7) through (A-9).

Next we calculate $\underline{J}^{+}_{inc}(\underline{r}^{+})$ from

$$\underline{J}^{+}_{inc}(\underline{r}^{+}) = \frac{1}{2}\left[\underline{J}_{inc}(\underline{r}^{+}) + \underline{\underline{R}}_z \cdot \underline{J}_{inc}(\underline{\underline{R}}_z \cdot \underline{r}^{+})\right] \qquad \text{(A-57)}$$

$$\begin{aligned} \underline{J}_{inc}(\underline{r}^{+}) &= \hat{n}(\underline{r}^{+}) \times \underline{H}_{inc}(\underline{r}^{+}) \\ &= -\left[\hat{n}(\underline{r}^{+}) \times \hat{e}_y\right] H_o e^{-ikz} \end{aligned} \qquad \text{(A-58)}$$

and

$$\begin{aligned} \underline{\underline{R}}_z \cdot \underline{J}_{inc}(\underline{r}^{-}) &= \underline{\underline{R}}_z \cdot \left\{-\left[\hat{n}(\underline{r}^{-}) \times \hat{e}_y\right] H_o e^{ikz}\right\} \\ &= \underline{\underline{R}}_z \cdot \left\{-\left[\underline{n}_x(\underline{r}^{-}) \times \hat{e}_y + \underline{n}_z(\underline{r}^{-}) \times \hat{e}_y\right] H_o e^{ikz}\right\} \end{aligned} \qquad \text{(A-59)}$$

where

$$\hat{n} = \underline{n}_x + \underline{n}_y + \underline{n}_z$$

From figure A4 we see that

$$\underline{n}_x(\underline{r}^{-}) \times \hat{e}_y = \underline{n}_x(\underline{r}^{+}) \times \hat{e}_y$$

$$\underline{n}_z(\underline{r}^{-}) \times \hat{e}_y = -\,\underline{n}_z(\underline{r}^{+}) \times \hat{e}_y$$

and from the definition of $\underline{\underline{R}}_z$ given by equation (A-55)

$$\underline{\underline{R}}_z \cdot \left[\underline{n}_x(\underline{r}^+) \times \hat{e}_y \right] = - \underline{n}_x(\underline{r}^+) \times \hat{e}_y$$

$$\underline{\underline{R}}_z \cdot \left[\underline{n}_z(\underline{r}^+) \times \hat{e}_y \right] = \underline{n}_z(\underline{r}^+) \times \hat{e}_y$$

Using these relationships, equation (A-59) can be written as

$$\underline{\underline{R}}_z \cdot \underline{J}_{inc}(\underline{r}^-) = \left[\hat{n}(\underline{r}^+) \times \hat{e}_y \right] H_o e^{ikz}$$

and from equation (A-57)

$$J^+_{inc}(r^+) = - \frac{1}{2} H_o \left[\hat{n}(\underline{r}^+) \times \hat{e}_y \right] (e^{-ikz} - e^{ikz})$$

$$= i H_o \left[\hat{n}(\underline{r}^+) \times \hat{e}_y \right] \sin kz \qquad \text{(A-60)}$$

As $k \to 0$, equation (A-60) gives

$$\lim_{k=0} \underline{J}^+_{inc}(\underline{r}^+) = 0 \text{ everywhere on } S_+ \qquad \text{(A-61)}$$

and from equation (A-2)

$$\lim_{k=0} \underline{J}^+(\underline{r}^+) = 0 \text{ everywhere on } S+ \qquad \text{(A-62)}$$

From equations (A-54) and (A-62) we then see that

$$\underline{J}(r^+) = -\underline{\underline{R}}_z \cdot \underline{J}(r^-) \qquad \text{(A-63)}$$

which is the vector relationship between the current densities at $\underline{r}^+$ and $\underline{r}^-$.

In order to show the first of equation (A-52) we form the inner product of equation (A-63) with $\hat{s}(r^+)$:

$$\hat{s}(\underline{r}^+) \cdot \underline{J}(\underline{r}^+) = J_s(\underline{r}^+) = -\hat{s}(\underline{r}^+) \cdot \underline{\underline{R}}_z \cdot \underline{J}(\underline{r}^-) \tag{A-64}$$

The right-hand side of equation (A-64) can be simplified by expanding $s(r^+)$. $\underline{\underline{R}}_z$

$$\begin{aligned} s(\underline{r}^+) \cdot \underline{\underline{R}}_z &= \left[\underline{s}_x(\underline{r}^+) + \underline{s}_y(\underline{r}^+) + \underline{s}_z(\underline{r}^+)\right] \cdot \underline{\underline{R}}_z \\ &= 0 + \underline{s}_y(r^+) - \underline{s}_z(r^+) \end{aligned} \tag{A-65}$$

From figure A4 we see that

$$\underline{s}_y(\underline{r}^+) = -\underline{s}_y(\underline{r}^-)$$

$$\underline{s}_z(\underline{r}^+) = \underline{s}_z(\underline{r}^-)$$

and equation (A-65) gives

$$\hat{s}(r^+) \cdot \underline{\underline{R}}_z = -s(\underline{r}^-) \tag{A-66}$$

Thus the right hand side of equation (A-64) gives, by virtue of equation (A-66),

$$J_s(\underline{r}^+) = J_s(\underline{r}^-) \quad \text{Q.E.D.}$$

The second of equations (A-52) can be shown similarly by inner multiplication of equation (A-63) with $\hat{t}(\underline{r}^+)$ and noticing that (see figure A4)

$$\underline{t}_x(\underline{r}^+) = \underline{t}_x(\underline{r}^-)$$

$$\underline{t}_y(\underline{r}^+) = \underline{t}_y(\underline{r}^-)$$

$$\underline{t}_z(\underline{r}^+) = -\underline{t}_z(\underline{r}^-)$$

that is

$$\hat{\underline{t}}(\underline{r}^+) \cdot \underline{\underline{R}}_z = \hat{\underline{t}}(\underline{r}^-).$$

APPENDIX B

A PERFECTLY CONDUCTING ELLIPSOID IN A MAGNETOSTATIC FIELD

In this appendix we calculate the surface current density induced on a perfectly conducting ellipsoid immersed in a magnetostatic-like field, i.e. we assume that the frequency of the incident electromagnetic plane wave is high enough to cause negligible penetration but low enough to decouple the magnetostatic and electrostatic interactions (see reference 2 page 5 for a discussion). The current density induced due to the electrostatic interaction will not be considered. Thus we will solve the magnetostatic problem depicted in figure B1 where the incident magnetic field is

$$\underline{H}_{inc} = H_o \hat{e}_y \tag{B-1}$$

and the normal component of the total magnetic field on the surface of the ellipsoid ($b < a < c$) vanishes.

First we briefly explain the meaning of the ellipsoidal coordinates ξ, η, ζ, defined by the following relationships.

$$\frac{x^2}{a^2+\xi} + \frac{y^2}{b^2+\xi} + \frac{z^2}{c^2+\xi} = 1 \qquad \infty > \xi > -b^2 \tag{B-2}$$

$$\frac{x^2}{a^2+\eta} + \frac{y^2}{b^2+\eta} + \frac{z^2}{c^2+\eta} = 1 \qquad -b^2 > \eta > -a^2 \tag{B-3}$$

$$\frac{x^2}{a^2+\zeta} + \frac{y^2}{b^2+\zeta} + \frac{z^2}{c^2+\zeta} = 1 \qquad -a^2 > \zeta > -c^2 \tag{B-4}$$

The first family of surfaces represents confocal ellipsoids defined by ξ = const. ($\xi = 0$ corresponds to our perfectly conducting ellipsoid.)

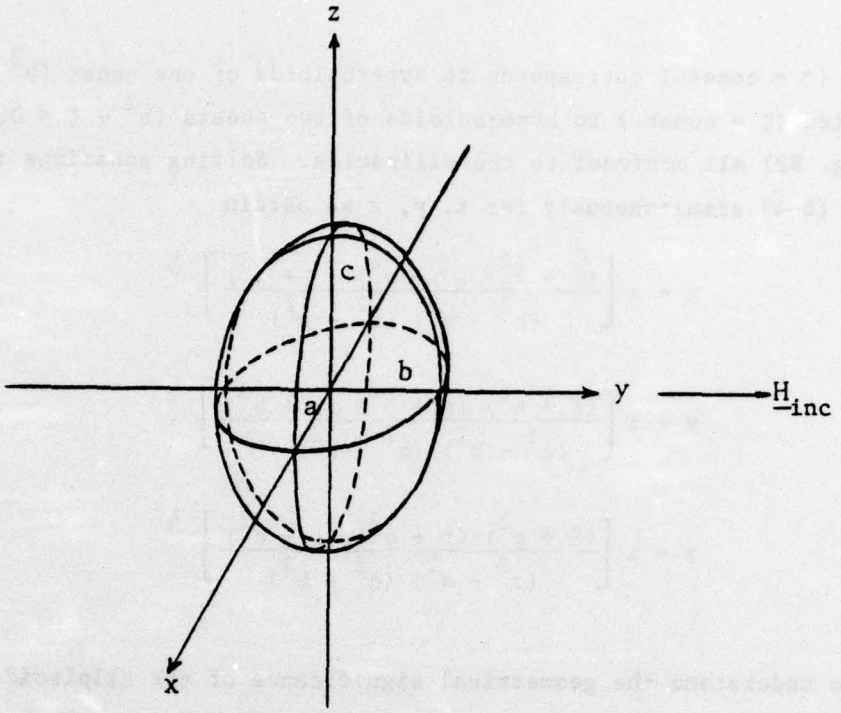

$$\frac{x^2}{a^2} + \frac{y^2}{b^2} + \frac{z^2}{c^2} = 1$$

Figure B1: A perfectly conducting ellipsoid (c>a>b) in a magnetostatic field $\underline{H}_{inc} = H_o \hat{e}_y$.

The second (η = const.) corresponds to hyperboloids of one sheet ($b^2 + \eta < 0$) and the third (ζ = const.) to hyperboloids of two sheets ($b^2 + \zeta < 0$, $a^2 + \zeta < 0$) (fig. B2) all confocal to the ellipsoids. Solving equations (B-2), (B-3), and (B-4) simultaneously for x, y, z we obtain

$$x = \pm \left[\frac{(\xi + a^2)(\eta + a^2)(\zeta + a^2)}{(b^2 - a^2)(c^2 - a^2)} \right]^{1/2} \tag{B-5}$$

$$y = \pm \left[\frac{(\xi + b^2)(\eta + b^2)(\zeta + b^2)}{(c^2 - b^2)(a^2 - b^2)} \right]^{1/2} \tag{B-6}$$

$$z = \pm \left[\frac{(\xi + c^2)(\eta + c^2)(\zeta + c^2)}{(c^2 - a^2)(c^2 - b^2)} \right]^{1/2} \tag{B-7}$$

In order to understand the geometrical significance of the ellpisoidal coordinates we trace how the above conicoids come into being. From equation (B-2) we see that for $\xi > -b^2$ all three forms are positive and the resulting surfaces are confocal ellipsoids ranging from a sphere at infinity for $\xi \to \infty$ ($x^2 + y^2 + z^2 \to \xi^2$) to an elliptical disk with semi-axes $a^2 - b^2$, $c^2 - b^2$ lying in the xz-plane for $\xi = -b^2 + \delta^2 (\delta \to 0)$. As ξ (which we call η for the range $-a^2$, $-b^2$) passes from $-b^2 + \delta^2$ to $-b^2 - \delta^2$ the sign of the second term in equation (B-3) becomes negative and the resulting surfaces are hyperboloids of one sheet. For $\eta = -b^2 - \delta^2$ ($\delta \to 0$) the hyperboloid degenerates into the region in the xz-plane that lies outside the elliptical disk. For $\eta = -a^2 + \delta^2$ ($\delta \to 0$) the hyperboloid is flattened into the region in the yz-plane "inside" the hyperbola $-y/(a^2 - b^2) + z^2/(c^2 - a^2) = 1$. As η (which we call ζ for the range $-c^2$, $-a^2$) passes from $-a^2 + \delta^2$ to $-a^2 - \delta^2$ the first two terms in equation (B-4) become negative and the resulting hyperboloids now have two sheets. For $\eta = -a^2 - \delta^2$ ($\delta \to 0$) the corresponding hyperboloid is the region in the yz-plane outside the hyperbola $-y^2/(a^2 - b^2) + z^2/(c^2 - a^2) = 1$, i.e., it has two separate sheets. Finally, as $\zeta = -c^2 + \delta^2$ ($\delta \to 0$) the two sheets are flattened into the entire xy-plane, i.e., the two sheets coalesce. The above

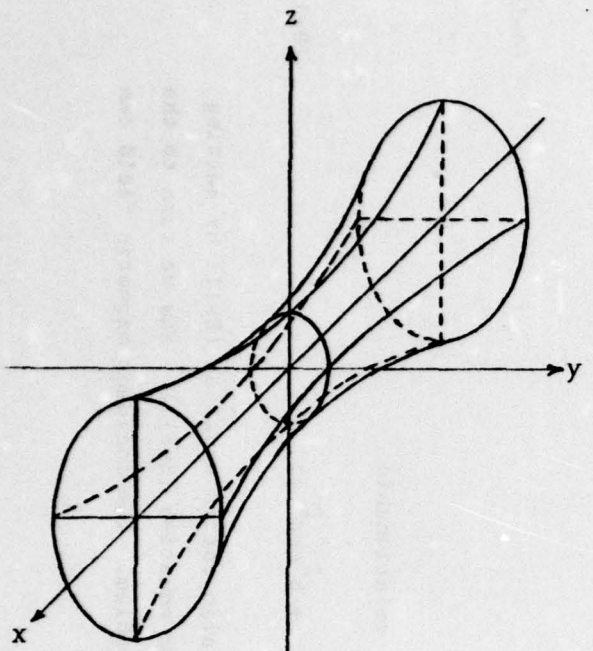

$$\frac{x^2}{a^2+\eta} + \frac{y^2}{|b^2+\eta|} + \frac{z^2}{c^2+\eta} = 1$$

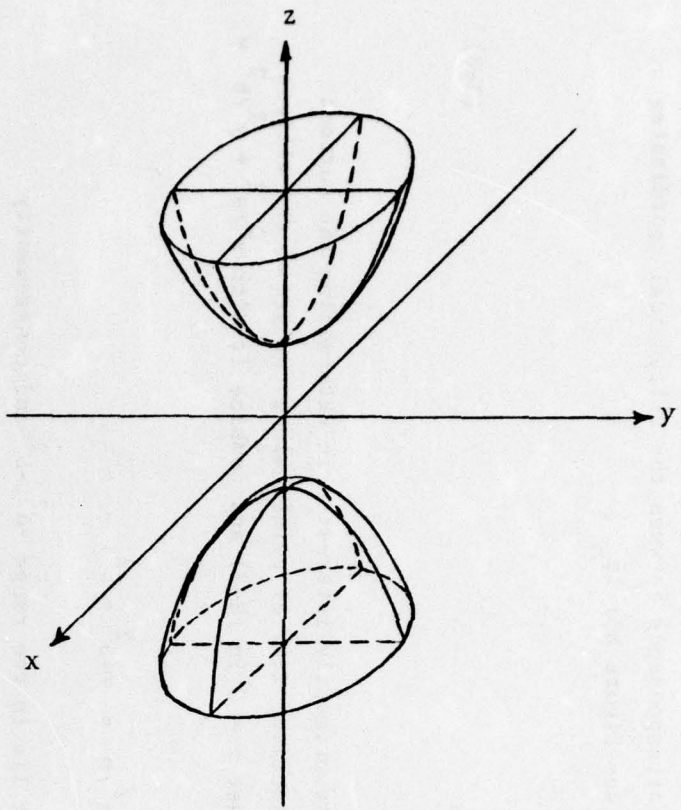

$$-\frac{x^2}{|a^2+\zeta|} - \frac{y^2}{|b^2+\zeta|} + \frac{z^2}{c^2+\zeta} = 1$$

Figure B2: Hyperboloids of one and two sheets.

discussion shows that the correspondence between the ellipsoidal coordinates and spherical coordinates (see figure B3) is

$$\begin{aligned} \xi &\leftrightarrow r \\ \eta &\leftrightarrow \phi_p \\ \zeta &\leftrightarrow \theta \end{aligned} \tag{B-8}$$

In this appendix we are primarily interested in determining the current density at the z = 0 intersection, i.e. at points along the arc of the ellipse $x^2/a^2 + y^2/b^2 = 1$. If we set z = 0 in (B-3) and combine it with $x^2/a^2 + y^2/b^2 = 1$ we obtain

$$(x^2 + y^2)\eta = \eta(a^2 + b^2) + \eta^2$$

The solution $\eta = 0$ does not lie in the range $-a^2,-b^2$ and consequently

$$\eta = x^2 + y^2 - (a^2 + b^2) \tag{B-9}$$

If we define ϕ such that (see figure 3)

$$\begin{aligned} x &= a \cos \phi \\ y &= b \sin \phi \end{aligned} \tag{B-10}$$

we can derive the following useful relationship

$$\eta = -(a^2 \sin^2\phi + b^2\cos^2 \phi) \tag{B-11}$$

which we will use later. (We can also obtain equation (B-11) by setting $\zeta = -c^2$ to either equation (B-5) or equation (B-6).) Now we turn to the formulation and solution of the problem. The incident magnetic field can be derived from a scalar potential

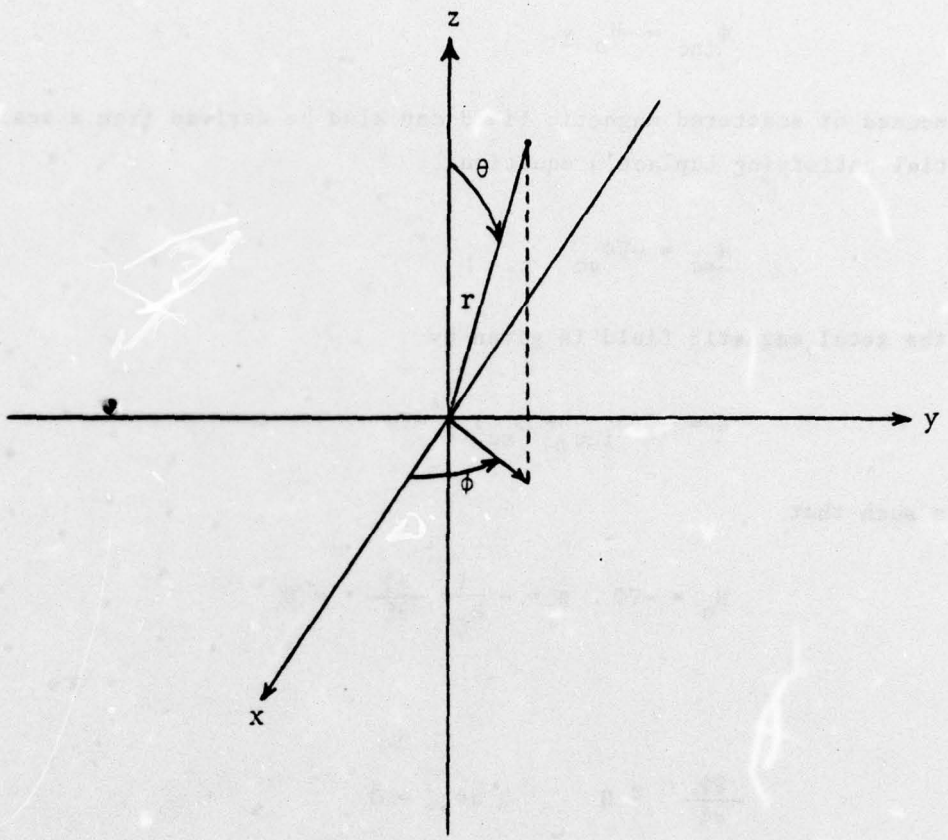

Figure B3: The spherical coordinate system.

$$\Phi_{inc} = -H_o\ y \tag{B-12}$$

The induced or scattered magnetic field can also be derived from a scalar potential satisfying Laplace's equation

$$\underline{H}_{sc} = -\nabla\Phi_{sc} \tag{B-13}$$

Thus the total magnetic field is given by

$$\underline{H} = -\nabla(\Phi_{inc} + \Phi_{sc}) = -\nabla\Phi \tag{B-14}$$

and is such that

$$H_n = -\nabla\Phi \cdot \hat{n} = -\frac{1}{h_\xi}\frac{\partial\Phi}{\partial\xi} = 0$$

i.e.

$$\frac{\partial\Phi}{\partial\xi} = 0 \qquad \text{at } \xi = 0 \tag{B-15}$$

($\hat{n}$ is the unit vector normal to the surface of the ellipsoid.)

If we recall equation (B-6), equation (B-12) can be rewritten as

$$\left.\begin{aligned}\Phi_{inc} &= \mp H_o\left[\frac{(\xi + b^2)(\eta + b^2)(\zeta + b^2)}{(c^2 - b^2)(a^2 - b^2)}\right]^{\frac{1}{2}} \\ &= Af(\xi)f(\eta)f(\zeta)\end{aligned}\right\} \tag{B-16}$$

where

$$f(p) = p + b^2$$

$$p = \xi, \eta, \zeta \tag{B-17}$$

$$A = \mp \frac{H_o}{\left[(a^2-b^2)\ (c^2-b^2)\right]^{1/2}}$$

In view of equation (B-16) and the boundary condition (B-15) the scattered potential Φ_{sc} should have the form

$$\Phi_{sc} = Bg(\xi)f(\eta)f(\zeta) \tag{B-18}$$

where the functional form of $g(\xi)$ will be determined by requiring that Φ_{sc} satisfy Laplace's equation.

From equations (B-15), (B-16) and (B-18) we find

$$B = -A \left[\frac{df/d\xi}{dg/d\xi}\right]_{\xi=0} \tag{B-19}$$

and

$$\Phi = Af(\eta)f(\zeta)\left\{f(\xi)-g(\xi)\left[\frac{df/d\xi}{dg/d\xi}\right]_{\xi = 0}\right\} \tag{B-20}$$

The two surface components of the surface current density $\underline{J}$ are

$$J_\zeta = H_\eta = -\frac{1}{h_\eta}\ \frac{\partial\Phi}{\partial\eta} \quad , \quad \xi = 0 \tag{B-21}$$

$$J_\eta = H_\zeta = -\frac{1}{h_\zeta}\ \frac{\partial\Phi}{\partial\zeta} \quad , \quad \xi = 0 \tag{B-22}$$

where

$$h_\eta = \frac{1}{2} \frac{\left[(\eta-\zeta)\ (\eta-\xi)\right]^{\frac{1}{2}}}{R(\eta)} \quad , \quad \xi = 0 \tag{B-23}$$

$$h_\zeta = \frac{1}{2} \frac{\left[(\zeta-\xi)\ (\zeta-\eta)\right]^{\frac{1}{2}}}{R(\zeta)} \quad , \quad \xi = 0 \tag{B-24}$$

and

$$R(p) = \left[(p + a^2)\ (p + b^2)\ (p + c^2)\right]^{\frac{1}{2}} \tag{B-25}$$

Thus

$$J_\zeta = -\frac{A}{h_\eta}\ f'(\eta) f(\zeta) \left[W(f,g) / \left[dg/d\xi\right]\right]_{\xi=0}$$

$$J_\eta = -\frac{A}{h_\zeta}\ f(\eta)\ f'(\zeta)\ \left[W(f,g) / \left[dg/d\xi\right]\right]_{\xi=0} \tag{B-26}$$

where

$$f'(p) = \frac{1}{2} \frac{1}{(p + b^2)^{\frac{1}{2}}} \ , \ p = \zeta, \eta \tag{B-27}$$

and W(f,g) is the Wronskian of f and g:

$$W(f,g) = f \frac{dg}{d\xi} - g \frac{df}{d\xi} \tag{B-28}$$

Next we determine g(ξ). Laplace's equation in ellipsoidal coordinates has the form (ref. 8, page 59)

$$(\eta - \zeta)\ R_\xi \frac{\partial}{\partial\xi}\left(R_\xi \frac{\partial \Phi_{sc}}{\partial\xi}\right) + (\zeta-\xi) R_\eta \frac{\partial}{\partial\eta}\left(R_\eta \frac{\partial \Phi_{sc}}{\partial\eta}\right)$$

$$+ (\xi-\eta)\ R_\zeta \frac{\partial}{\partial\zeta}\left(R_\zeta \frac{\partial \Phi_{sc}}{\partial\zeta}\right) = 0 \tag{B-28}$$

Substituting Φ_{sc} in equation (B-28) by its form given by equation (B-18) we obtain the following equation

$$R_\xi \frac{d}{d\xi}\left(R_\xi \frac{dg}{d\xi}\right) - \left(\frac{b^2 + c^2}{4} + \frac{\xi}{2}\right) g = 0 \qquad \text{(B-29)}$$

Noticing that $f(\xi)$ also satifies equation (B-29) we invoke a well-known result for a second-order linear equation that allows one to obtain a solution if an independent solution of the same equation is known, i.e.

$$g(\xi) = f(\xi)\int \frac{d\xi}{f^2(\xi)\, R_\xi} \qquad \text{(B-30)}$$

$$= (\xi + b^2)^{\frac{1}{2}} \int_\xi^\infty \frac{d\xi}{(\xi + b^2)\sqrt{(\xi + a^2)\,(\xi + b^2)\,(\xi + c^2)}}$$

The scattered field is due to localized currents, i.e., $\Phi(\xi)$ must vanish at $\xi = \infty$. This is secured by making the upper integration limit in equation (B-30) infinite. Now we are in a position to evaluate $\left[dg/d\xi\right]\xi = 0$ and the Wronskian at $\xi = 0$. From equation (B-30)

$$\left[\frac{dg}{d\xi}\right]_{\xi = 0} = \frac{1}{2b}\int_0^\infty \frac{d\xi}{(\xi + b^2)\sqrt{(\xi + a^2)\,(\xi + b^2)\,(\xi + c^2)}} - \frac{1}{ab^2c} \qquad \text{(B-31)}$$

$$= \frac{1}{2ab^2c}(a_o - 2)$$

---

8. Stratton, J. A., Electromagnetic Theory, McGraw-Hill Book Company, Inc. New York and London, 1941.

where

$$a_o = abc \int_0^\infty \frac{d\xi}{(\xi + b^2)\sqrt{(\xi + a^2)(\xi + b^2)(\xi + c^2)}} \qquad \text{(B-32)}$$

The Wronskian can be evaluated by recalling that g and f satisfy equation (B-29), which is of the Sturm-Liouville type, i.e.

$$W(f,g) = C/R_\xi \qquad \text{(B-33)}$$

where C is a constant to be determined. If we evaluate f and g for $\xi \to \infty$ we have

$$f(\xi) = (\xi + b^2)^{1/2} \to \xi^{1/2}$$

$$g(\xi) = f(\xi) \int_\xi^\infty \frac{d\xi}{f(\xi)\, R\xi} \to \xi^{1/2} \int_\xi^\infty \frac{d\xi}{\xi^{5/2}} = \frac{2}{3}\,\frac{1}{\xi}$$

and

$$W(f,g) = \xi^{1/2}\left(-\frac{2}{3}\frac{1}{\xi 2}\right) - \frac{2}{3}\,\frac{1}{\xi}\,\frac{1}{2}\xi^{-1/2} = -\xi^{-3/2} = C\,\xi^{-3/2}$$

Thus

$$C = -1$$

and

$$\left.\begin{aligned} W(f,g) &= -\frac{1}{R_\xi} \\ \left[W(f,g)\right]_{\xi = 0} &= -\frac{1}{abc} \end{aligned}\right\} \qquad \text{(B-34)}$$

We can now rewrite equations (B-26) as

$$\left.\begin{aligned} J_\zeta &= \pm \frac{2H_o b}{a_o - 2} \frac{1}{\left[(c^2-b^2)\,(a^2-b^2)\right]^{1/2}} \left[\frac{(\eta+a^2)\,(\eta+c^2)\,(\zeta+b^2)}{(\eta-\zeta)\,\eta}\right]^{-1/2} \\ J_\eta &= \pm \frac{2H_o b}{a_o - 2} \frac{1}{\left[(c^2-b^2)\,(a^2-b^2)\right]^{1/2}} \left[\frac{(\zeta+a^2)\,(\zeta+c^2)\,(\nu+b^2)}{(\zeta-\eta)\,\zeta}\right]^{1/2} \end{aligned}\right\} \quad \text{(B-35)}$$

where the + sign corresponds to $y < 0$ and the - sign to $y > 0$.

Let's now evaluate the current component at points $z = 0$, $x = a\cos\phi$, $y = b\sin\phi$. In this case $\zeta = -c^2$ and from (B-11) $\eta = -(a^2\sin^2\phi + b^2\cos^2\phi)$. Thus,

$$\left.\begin{aligned} J_\zeta\,(z=0) &= \pm \frac{2H_o b}{a_o - 2} \frac{|\cos\phi|}{(a^2\sin^2\phi + b^2\cos^2\phi)^{1/2}} \\ J_\eta\,(z=0) &= 0 \end{aligned}\right\} \quad \text{(B-36)}$$

Equation (B-36) shows that the surface current density at the $z = 0$ intersection is perpendicular to the $z = 0$ plane. To translate J_ζ into J_z we recall equation (B-11) and that $J_\zeta = -(1/h_\eta)\,\partial\Phi/\partial\eta$, $J_\theta = -(1/h_{\phi_p})\,\partial\Phi/\partial\phi_p$ ($= -J_z$, at $z = 0$). (As one can see from figure 3 the angle ϕ is not the usual polar angle ϕ_p such that $x = \rho(\phi_p)\cos\phi_p$ and $y = \rho(\phi_p)\sin\phi_p$. However, $\tan\phi = \frac{a}{b}\tan\phi_p$ and $\partial/\partial\phi, \partial/\partial\phi_p$ have the same sign.) Thus equation (B-36) gives

$$0 \le \phi \le \pi/2 \qquad J_\zeta = -J_\theta = J_z > 0$$

$$\pi/2 \le \phi \le \pi \qquad J_\zeta = J_\theta = -J_z > 0$$

$$\pi \leq \phi \leq 3\pi/2 \qquad J_\zeta = -J_\theta = J_z < 0$$

$$3\pi/2 \leq \phi < 2\pi \qquad J_\zeta = J_\theta = -J_z < 0$$

Thus the sign of J_z is the same as the sign of $\cos\phi$.

Parameter a_o given by equation (B-32) can be expressed in terms of an elliptic integral of the second kind. This can be accomplished by making the substitution

$$\cos\phi = \frac{x + b^2}{x + c^2}$$

which transforms equation (B-32) into

$$a_o = \frac{2abc}{(c^2 - b^2)^{3/2}} \int_0^{\phi} \frac{\tan^2\theta \; d\theta}{(1-k^2\sin^2\theta)^{\frac{1}{2}}} \qquad \text{(B-37)}$$

where

$$\cos\phi = b/c$$

$$k^2 = \frac{c^2 - a^2}{c^2 - b^2}$$

Using reference 9 No. 782.03 we obtain

$$a_o = \frac{2a\cos\phi}{c \sin^3\phi} \left[\frac{\tan\phi}{1 - k^2} \sqrt{1 - k^2\sin^2\phi} - \frac{E(\phi,k)}{1 - k^2} \right] \qquad \text{(B-38)}$$

where

$$E(\phi,k) = \int_0^{\phi} (1 - k^2\sin^2\theta)^{\frac{1}{2}} \, d\theta \qquad \text{(B-39)}$$

---

9. Dwight, H.B., Tables of Integrals and Other Mathematical Data, The Macmillan Company, New York, Fourth Edition, 1964.

is the elliptic integral of the second kind. Certain limiting cases are of interest.

1. INFINITE CYLINDER OF ELLIPTICAL CROSS SECTION

By letting $c \to \infty$ in equation (B-38) one can easily obtain

$$a_o = \frac{2a}{a + b} \tag{B-40}$$

The same expression can be derived by using equation (B-32), i.e.

$$a_o = \lim_{c\to\infty} ab \int_0^{\infty} \frac{d\xi}{(\xi+b^2)^{3/2}\sqrt{(\xi+a^2)(\xi/c^2+1)}} \tag{B-41}$$

$$= ab\left\{\int_0^M \frac{d\xi}{(\xi+b^2)^{3/2}\sqrt{\xi+a^2}} + \lim_{c\to\infty}\int_M^{\infty} \frac{d\xi}{(\xi+b^2)^{3/2}\sqrt{(\xi+a^2)(\xi/c^2+1)}}\right\}$$

The second integral which we call I is positive and smaller than I_1 where

$$I_1 = \int_M^{\infty} \frac{d\xi}{(\xi+b^2)^{3/2}\sqrt{\xi+a^2}}$$

i.e.

$$0 < I < I_1$$

As $M \to \infty$ $I_1 \to 0$ and $I = 0$

The first integral in equation (B-41) can be rewritten as $\int_{b^2}^{\infty} \frac{dx}{x\sqrt{x(x+a^2-b^2)}}$ and it is elementary (ref. 9, No. 383.1)

$$a_o = ab \left\{ -\frac{2}{(a^2-b^2)x} \left[x^2 + (a^2-b^2)x \right]^{\frac{1}{2}} \right\}_{b^2}^{\infty} = \frac{2a}{a+b}$$

Thus for an infinite elliptical cylinder

$$\left.\begin{aligned} J_z &= H_o(a+b) \frac{\cos\phi}{(a^2\sin^2\phi + b^2\cos^2\phi)^{\frac{1}{2}}} \\ J_\phi &= 0 \end{aligned}\right\} \qquad \text{(B-42)}$$

with

$$\underline{H}_{inc} = H_o \hat{e}_y$$

and ϕ defined in figure 3.

Notice that $J_z(\phi = 0) = H_o(1 + a/b)$. When a = b, $J_z = 2H_o \cos\phi$ a well-known result. It is interesting to note that

$$J_z(\phi=0,\ a\neq b)/J_z(\phi=0, a=b) = (1+a/b)/2 > 1$$

In order to see how much the infinite cylinder solution differs from the ellipsoid solution (which can be made to look like a finite cylinder of elliptic cross section for c much larger than a), we cast equation (B-38) into the following form

$$a_o = \frac{2a}{a+b} - \frac{2ab}{(1-b^2/c^2)^{\frac{1}{2}}(a^2-b^2)} \left[E(\phi,k) - (1-b^2/c^2)^{\frac{1}{2}} \right] \qquad \text{(B-43)}$$

2. PROLATE SPHEROID

If we recall definition (B-32) for a_o and set a=b the resulting integral is identical to the one obtained by Sancer et al (ref. 1) for a prolate spheroid

immersed in a magnetic field. To verify that expression (B-38) is also correct we must consider the limit carefully because if we set a=b, i.e. $k^2=1$, we obtain the indeterminate expression 0/0. Thus we set

$$a^2=b^2(1+\delta^2) \quad , \quad a=b(1+\tfrac{1}{2}\delta^2+0(\delta^4))$$

and noting that

$$\frac{b}{c} = \cos\phi \quad , \quad (1 - \frac{b^2}{c^2})^{\frac{1}{2}} = \sin\phi$$

$$1 - k^2 = \frac{\delta^2}{\tan^2\phi}$$

$$(1 - k^2\sin^2\theta)^{\frac{1}{2}} = (\cos^2\theta + \frac{\delta^2}{\tan^2\phi} \sin^2\theta)^{\frac{1}{2}}$$

$$= \cos\theta \, (1 + \frac{\delta^2}{2\tan^2\phi} \sin^2\theta + 0(\delta^4))$$

we obtain

$$a_o = \frac{2\cos^2\phi}{\sin^3\phi} (1 + \tfrac{1}{2}\delta^2 + 0(\delta^4))$$

$$\left\{\frac{\tan^3\phi}{\delta^2} \cos\phi \, (1 + \tfrac{1}{2}\delta^2 + 0(\delta^4)) \right.$$

$$- \frac{\tan^2\phi}{\delta^2} \left[\sin\phi + \frac{\delta^2}{2\tan^2\phi} (-\sin\phi + \frac{1}{2} \ln \frac{1 + \sin\phi}{1 - \sin\phi} \right)$$

$$\left. \left. + 0(\delta^4)\right]\right\}$$

$$= \frac{2\cos^2\phi}{\sin^3\phi}\left\{\frac{1}{2}\sin\phi\tan^2\phi + \frac{1}{2}\sin\phi - \frac{1}{4}\ln\frac{1+\sin\phi}{1-\sin\phi}\right\} + O(\delta^2)$$

and as $\delta \to 0$

$$a_o = \frac{1}{1-\varepsilon^2}\left(1 + \frac{1}{2}\frac{\varepsilon^2}{(1-\varepsilon^2)^{\frac{1}{2}}}\ln\frac{1-\sqrt{1-\varepsilon^2}}{1+\sqrt{1-\varepsilon^2}}\right) \qquad \text{(B-44)}$$

where $\varepsilon = b/c$. Equation (B-44) is identical to equation (4) in reference 1.

APPENDIX C

NUMERICAL SOLUTION FOR THE MAGNETIC FIELD INTEGRAL EQUATION FOR AIRCRAFT

1. MODEL

Our model for an aircraft is depicted in figure 1. The fuselage as well as the rest of the aircraft components are modeled as elliptical cylinders of major axis $2a_i$ and minor axis $2b_i$ where i denotes the component or body under consideration.

2. ZONING

Our aircraft is symmetric about the xz-plane and as we explained in Section I we can utilize this symmetry to transform the integral equation for the current density $\underline{J}$ into two integral equations for $\underline{J}^{\pm}$ defined over half of the aircraft ($y \geq 0$). Thus we will only zone the aircraft for $y \geq 0$.

The half airplane for $y \geq 0$ consists of four sections or bodies. Body 1 is the fuselage, body 2 is the wing corresponding to $y \geq 0$, body 3 is the horizontal stabilizer ($y \geq 0$) and the vertical stabilizer is body 4. Each body is treated independently in this appendix. The intersections are treated in Appendix D.

Because we treat the bodies independently, we define the orthonormal triad $\hat{n}$, $\hat{s}$, $\hat{t}$ accordingly, i.e. $\hat{s}$ corresponds to the azimuthal direction defined by the angle ϕ (fig. 3), $\hat{n}$ is the normal to the surface and $\hat{t} = \hat{n} \times \hat{s}$. Analytically,

$$\hat{s} = \frac{\partial \underline{r}}{\partial \phi} \Big/ \left| \frac{\partial \underline{r}}{\partial \phi} \right| \tag{C-1}$$

where $\underline{r}$ is the radius vector.

Thus at each point on the surface of a body we have a pair of orthonormal surface vectors $\hat{s}$ and $\hat{t}$ which define two orthogonal directions and for this

reason we introduce a convenient surface coordinate system (ϕ,ℓ) where ϕ corresponds to the s-direction and ℓ to the t-direction on the walls but the radial direction on the caps. Each body will be divided into ϕ-strips and ℓ-strips. The ϕ-strips are bounded by ℓ = constant lines and the ℓ-strips by ϕ = constant lines. For each zone a reference point is taken and it represents the central point of a zone. The coordinates of this central point are given in Section 4 of this appendix. The meaning of ϕ and ℓ can be clarified by considering a specific body, say the fuselage. Any point on the surface of the fuselage can be described in terms of three parameters: ϕ, x and r where $x = x$, $y = a_1\ r \sin\phi$, $z = -b_1\ r \cos\phi$. On the caps ($x = 0$, $x = \ell_1$) r ranges between 0 and 1 and on the walls $r = 1$. Now ℓ can be defined as follows. On the walls, that is for $0 < x < \ell_1$, let $\ell = x$. For $x = 0$, $0 \leq r \leq 1$ let $\ell = \ell_1$ $1 + r$. For the rest of the bodies, which only have one endcap at x = length of body, ℓ = length + r for the endcap.

We are now in a position to exhibit our zone numbering scheme. As we mentioned earlier we have four bodies which we have numbered from 1 to 4. Zone no. 1 is assigned to body no. 1 (the fuselage) and corresponds to the t-strip defined by $\phi = 0$, $\phi = \phi_1 > 0$ and $\ell = 0$, $\ell = \ell' > 0$. The subsequent zones are numbered in the direction of increasing ℓ until we reach $\ell = \ell_1 + 2$. Then we go back to the t-strip defined by $\phi = \phi_1$, $\phi = \phi_2 > \phi_1$ and $\ell = 0$, $\ell = \ell' > 0$ and the subsequent zones are numbered in the direction of increasing ℓ until we reach $\ell = \ell_1 + 2$ and so forth. When we have covered the fuselage we continue with the wing (body no. 2) following the same procedure, i.e., using the same numbering scheme in the local ϕ,ℓ space. Figure C1 illustrates the numbering scheme we just outlined. (Figure C1 should not be interpreted as providing any information with respect to the relative sizes of bodies 1 and 2 or the size, number and uniformity of zones).

3. MATRIX EQUATIONS FOR CURRENT DENSITY

Throughout the following discussion α denotes a zone number, i denotes a body number, j denotes a strip index defined by two ϕ = constant boundaries,

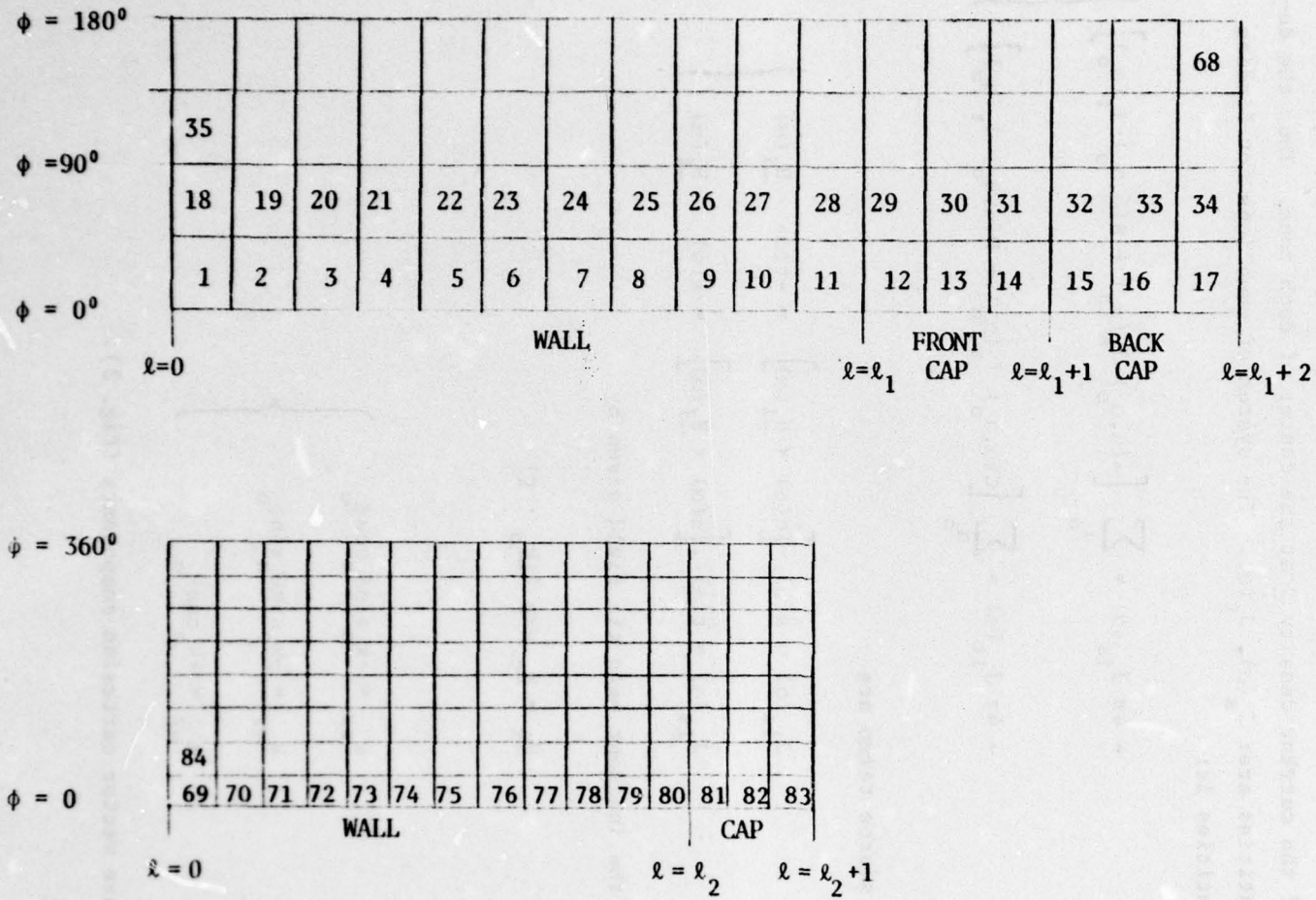

Figure C1: Numbering scheme for zones on the aircraft component. Two components are shown: the fuselage and the wing.

and k denotes a strip index defined by two l = constant boundaries. For example, zone 28 in figure 16 corresponds to $\alpha = 28$, $i = 1$, $j = 2$, $k = 11$. The relationship between α and i, j, k will be exhibited separately for each body in section 4 of this appendix. We wish to evaluate the s and t-components of the current density $\underline{J}$ at the center of each zone. Thus the desired quantities are: $J_s(\alpha)$, $J_t(\alpha)$. The system of equations for finding these quantities is:

$$\left.\begin{aligned} -4\pi J_{is}(\alpha) &= \sum_{\alpha_o} \left[A(\alpha,\alpha_o)\, J_s(\alpha_o) + B(\alpha,\alpha_o)\, J_t(\alpha_o)\right] \\ -4\pi J_{it}(\alpha) &= \sum_{\alpha_o} \left[C(\alpha,\alpha_o)\, J_s(\alpha_o) + D(\alpha,\alpha_o)\, J_t(\alpha_o)\right] \end{aligned}\right\} \quad (C\text{-}2)$$

where the source terms are

$$\left.\begin{aligned} J_{is}(\alpha) &= \hat{s}(\alpha) \cdot \left[\hat{n}(\alpha) \times \underline{H}_i(\alpha)\right] = -\hat{t}(\alpha) \cdot \underline{H}_i(\alpha) \\ J_{it}(\alpha) &= \hat{t}(\alpha) \cdot \left[\hat{n}(\alpha) \times \underline{H}_i(\alpha)\right] = \hat{s}(\alpha) \cdot \underline{H}_i(\alpha) \end{aligned}\right\} \quad (C\text{-}3)$$

and $\underline{H}_i$ is the incident magnetic field given by

$$\underline{H}_i = \underline{H}_o \exp\left(i\underline{k}_o \cdot \underline{r}\right) \quad (C\text{-}4)$$

and

$$\left.\begin{aligned} k_{ox} &= -k_o \sin\theta_o \cos\phi_o \\ k_{oy} &= -k_o \sin\theta_o \sin\phi_o \\ k_{oz} &= -k_o \cos\theta_o \end{aligned}\right\} \quad (C\text{-}5)$$

are the wave vector cartesian components (fig. 2).

To find the cartesian components of $\underline{H}_o$ we have to define the polarization direction of the electric field $\underline{E}_i$: If we consider the axis perpendicular to $\underline{k}$ and lying in the $\underline{k}$, z=axis plane, say x", then $\underline{E}_i$ forms an angle $\pi-\phi_p$ with x" (fig. 2). ($\underline{E}_i$, $\underline{H}_i$ and x" lie in a plane perpendicular to $\underline{k}$. We can now calculate the cartesian components of $\underline{H}_o$ by making three successive rotations as follows. We assume that the $\underline{k}$, $\underline{E}_i$, $\underline{H}_i$ system initially coincides with the -z, -x, y system and we bring it to its final position by first rotating about z by ϕ (rotation matrix A) then about y' by θ (rotation matrix B) and finally about z" by $-\phi$ (rotation matrix C) (fig. C2). Thus

$$\begin{pmatrix} H_{ox} \\ H_{oy} \\ H_{oz} \end{pmatrix} = A^{-1}B^{-1}C^{-1} \begin{pmatrix} 0 \\ H_o \\ 0 \end{pmatrix}$$

$$= \begin{pmatrix} \cos\phi_o & -\sin\phi_o & 0 \\ \sin\phi_o & \cos\phi_o & 0 \\ 0 & 0 & 1 \end{pmatrix} \begin{pmatrix} \cos\theta_o & 0 & \sin\theta_o \\ 0 & 1 & 0 \\ -\sin\theta_o & 0 & \cos\theta_o \end{pmatrix} \begin{pmatrix} \cos\phi_p & \sin\phi_p & 0 \\ -\sin\phi_p & \cos\phi & 0 \\ 0 & 0 & 1 \end{pmatrix} \begin{pmatrix} 0 \\ H_o \\ 0 \end{pmatrix}$$

or

$$\left.\begin{aligned} H_{ox} &= H_o(\cos\phi_o\cos\theta_o\sin\phi_p - \sin\phi_o\cos\phi_p) \\ H_{oy} &= H_o(\sin\phi_o\cos\theta_o\sin\phi_p + \cos\phi_o\cos\phi_p) \\ H_{oz} &= -H_o\sin\theta_o\sin\phi_p \end{aligned}\right\} \qquad (C\text{-}6)$$

The matrix terms in equation (C-2) are given by the following expressions.

$$A(\alpha,\alpha_o) = -.5\delta_{\alpha\alpha_o} + \int_{S(\alpha_o)} \underline{R}(\alpha,\alpha_o) \cdot (\hat{t}_\alpha \times \hat{s}_{a_o}) Q(\alpha,\alpha_o) dS'$$

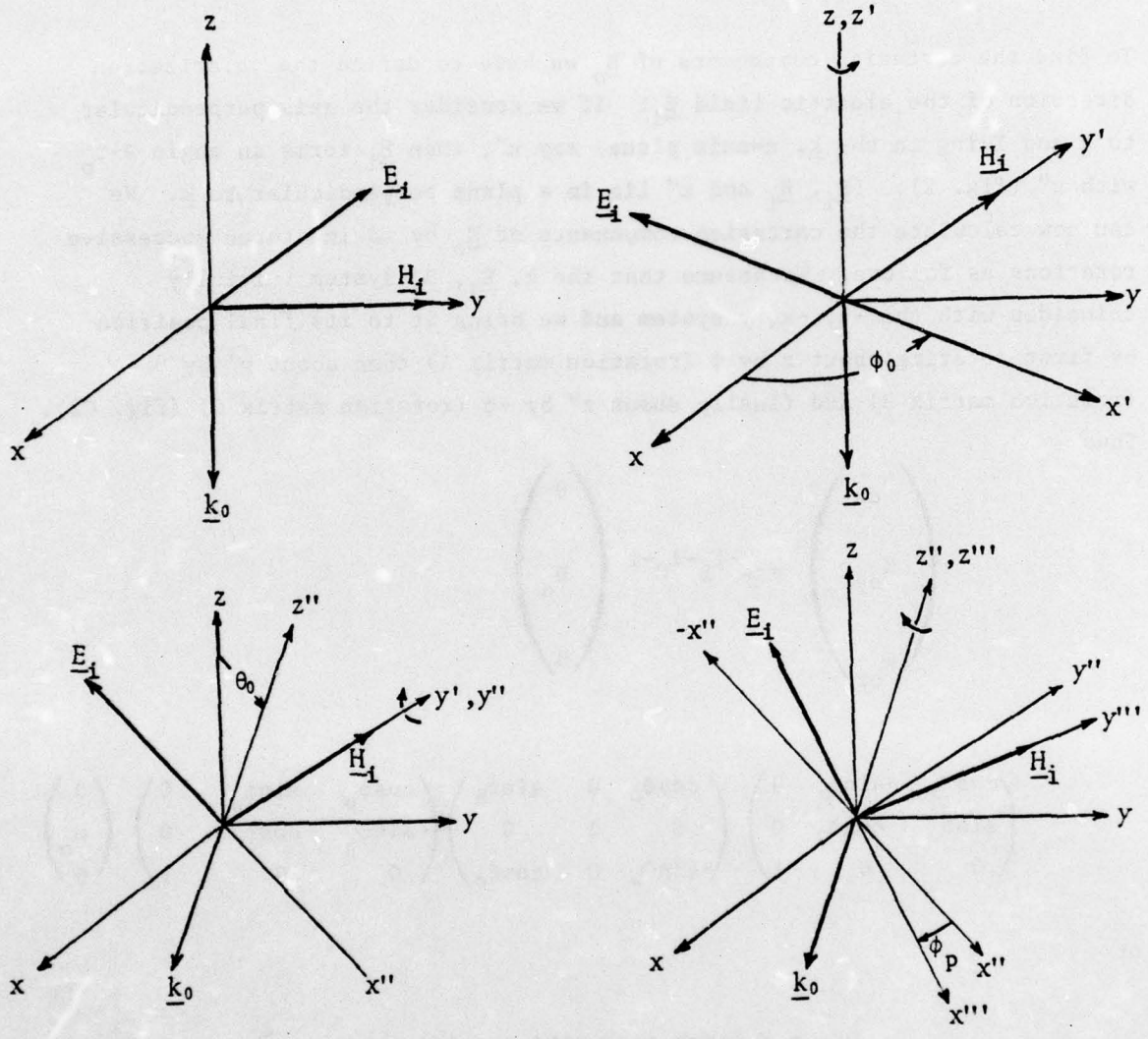

Figure C2: Three successive rotations used in the definition and derivation of the incident magnetic field components.

$$B(\alpha,\alpha_o) = \int_{S(\alpha_o)} \underline{R}(\alpha,\alpha_o) \cdot (\hat{t}_\alpha \times \hat{t}_{\alpha_o}) Q(\alpha,\alpha_o) dS$$

$$C(\alpha,\alpha_o) = -\int_{S(\alpha_o)} \underline{R}(\alpha,\alpha_o) \cdot (\hat{s}_\alpha \times \hat{s}_{\alpha_o}) Q(\alpha,\alpha_o) dS \qquad \text{(C-7)}$$

$$D(\alpha,\alpha_o) = -.5\delta_{\alpha\alpha_o} - \int_{S(\alpha_o)} \underline{R}(\alpha,\alpha_o) \cdot (\hat{s}_\alpha \times \hat{t}_{\alpha_o}) Q(\alpha,\alpha_o) dS$$

$$Q(\alpha,\alpha_o) = \left[-1 + ik_o R(\alpha,\alpha_o)\right] \exp\left[ik_o R(\alpha,\alpha_o)\right] / R^3(\alpha,\alpha_o)$$

$$\underline{R}(\alpha,\alpha_o) = \underline{r}_\alpha - \underline{r}_{\alpha_o} \qquad \text{(C-8)}$$

$$R(\alpha,\alpha_o) = |\underline{r}_\alpha - \underline{r}_{\alpha_o}|$$

As we mentioned earlier our aircraft is symmetric about the xz-plane, and we can utilize this symmetry to transform (C-2) into a pair of equations for two fictitious current densities defined over only half the surface of the aircraft, i.e. $y \geq 0$. These equations are

$$\left.\begin{aligned} -4\pi J^{\pm}_{is}(\alpha) &= \sum_{\alpha_o} \left[A^{\pm}(\alpha,\alpha_o)\, J^{\pm}_s(\alpha_o) + B^{\pm}(\alpha,\alpha_o)\, J^{\pm}_t(\alpha_o)\right] \\ -4\pi J^{\pm}_{it}(\alpha) &= \sum_{\alpha_o} \left[C^{\pm}(\alpha,\alpha_o)\, J^{\pm}_s(\alpha_o) + D^{\pm}(\alpha,\alpha_o) J^{\pm}_t(\alpha_o)\right] \end{aligned}\right\} \qquad \text{(C-9)}$$

where

$$
\begin{aligned}
J_s(\alpha) &= J_s^-(\alpha) + J_s^+(\alpha) \\
J_s(-\alpha) &= J_s^-(\alpha) - J_s^+(\alpha) \\
J_t(\alpha) &= J_t^+(\alpha) + J_t^-(\alpha) \\
J_t(-\alpha) &= J_t^+(\alpha) - J_t^-(\alpha)
\end{aligned}
\qquad \text{(C-10)}
$$

Equations (C-10) show that from a knowledge of $\underline{J}^{\pm}$ over zones corresponding to $y \geq 0$ one can calculate the real current density $\underline{J}$ over the entire surface, i.e. over zones corresponding to α and $-\alpha$.

The source terms are given by

$$
\left.
\begin{aligned}
J_{is}^{\pm}(\alpha) &= -\hat{t}(\alpha) \cdot \underline{H}_i^{\pm}(\alpha)\, e^{-i(\theta+\psi)} \\
J_{it}^{\pm}(\alpha) &= \hat{s}(\alpha) \cdot \underline{H}_i^{\pm}(\alpha)\, e^{-i(\theta+\psi)}
\end{aligned}
\right\} \qquad \text{(C-11)}
$$

where

$$
\left.
\begin{aligned}
\underline{H}_i^+(\alpha) &= -i\sin\phi\,(H_{ox}\hat{e}_x + H_{oz}\hat{e}_z) + \cos\phi\, H_{oy}\hat{e}_y \\
\underline{H}_i^-(\alpha) &= -i\sin\phi\, H_{oy}\hat{e}_y + \cos\phi\,(H_{ox}\hat{e}_x + H_{oz}\hat{e}_z)
\end{aligned}
\right\} \qquad \text{(C-12)}
$$

$$
\left.
\begin{aligned}
\theta &= k_o z(\alpha)\cos\theta_o \\
\psi &= k_o x(\alpha)\sin\theta_o\cos\phi_o \\
\phi &= k_o y(\alpha)\sin\theta_o\sin\phi_o
\end{aligned}
\right\} \qquad \text{(C-13)}
$$

The above equations are derived by first recalling that

$$
\underline{J}_i^{\pm}(\alpha) = \frac{1}{2}\left[\underline{J}_i(\alpha) \pm \underline{R}_y \cdot \underline{J}_i(-\alpha)\right] \qquad \text{(C-14)}
$$

where

$$\underline{J}_i(\pm\alpha) = \hat{n}(\pm\alpha) \times \underline{H}_o(\pm\alpha) e^{-\underline{k}_o \cdot \underline{r}(\pm\alpha)}$$

If we define

$$\underline{k}_o \cdot \underline{r}(\alpha) = -(\theta+\psi+\phi)$$

and use the following relationships

$$t_x(\alpha) - t_x(-\alpha)$$

$$t_y(\alpha) = -t_y(-\alpha)$$

$$t_z(\alpha) = t_z(-\alpha)$$

$$s_x(\alpha) = -s_x(-\alpha)$$

$$s_y(\alpha) = s_y(-\alpha)$$

$$s_z(\alpha) = -s_z(-\alpha)$$

which can easily be demonstrated, one can show that

$$\underline{H}_i^{\pm}(\alpha) = \frac{1}{2} \left[H_{ix}(\alpha) \mp H_{ix}(-\alpha) \right] \hat{e}_x + \left[H_{iz}(\alpha) \mp H_{iz}(-\alpha) \right] \hat{e}_z + \left[H_{iy}(\alpha) \pm H_{iy}(-\alpha) \right] \hat{e}_y$$

and equations (C-11), (C-12) can then easily be verified.

Finally, we give the expressions for the matrix terms on equation (C-9)

$$A^{\pm}(\alpha,\alpha_o) = -0.5\delta_{\alpha\alpha o} + \int_{S(\alpha_o)} [\underline{R}^{+}(\alpha,\alpha_o) \cdot (\hat{t}_\alpha \times \hat{s}_{\alpha o})\, Q(R^{+})$$

$$\underline{R}^{-}(\alpha,\alpha_o) \cdot (\hat{t}_\alpha \times \underline{\underline{R}}_y \cdot \hat{s}_{\alpha o})\, Q(R^{-})]\, dS$$

$$B^{\pm}(\alpha,\alpha_o) = \int_{S(\alpha_o)} [\underline{R}^{+}(\alpha,\alpha_o) \cdot (\hat{t}_\alpha \times \hat{t}_{\alpha o})\, Q(R^{+}) \pm \underline{R}^{-}(\alpha,\alpha_o)$$

$$\cdot (\hat{t}_\alpha \times \underline{\underline{R}}_y \cdot t_{\alpha o})\, Q(R^{-})]\, dS$$

$$C^{\pm}(\alpha,\alpha_o) = -\int_{S(\alpha_o)} [\underline{R}^{+}(\alpha,\alpha_o) \cdot (\hat{s}_\alpha \times \hat{s}_{\alpha o})\, Q(R^{+}) \pm \underline{R}^{-}(\alpha,\alpha_o)$$

$$\cdot (\hat{s}_\alpha \times \underline{\underline{R}}_y \cdot \hat{s}_{\alpha o})\, Q(R^{-})]\, dS$$

$$D^{\pm}(\alpha,\alpha_o) = -0.5\delta_{\alpha\alpha o} - \int_{S(\alpha_o)} [\underline{R}^{+}(\alpha,\alpha_o) \cdot (\hat{s}_\alpha \times \hat{t}_{\alpha o})\, Q(R^{+})$$

$$\pm \underline{R}^{-}(\alpha,\alpha_o) \cdot (\hat{s}_\alpha \times \underline{\underline{R}}_y \cdot t_{\alpha o})\, Q(R^{-})]\, dS \qquad \text{(C-15)}$$

$$Q(R^{\pm}) = [-1+ik_o R^{\pm}(\alpha,\alpha_o)]\, \exp[ik_o R^{\pm}(\alpha,\alpha_o)]/[R^{\pm}(\alpha,\alpha_o)]^3$$

$$\underline{R}^{+}(\alpha,\alpha_o) = \underline{R}(\alpha,\alpha_o) = \underline{r}(\alpha) - \underline{r}(\alpha_o)$$

$$\underline{R}^{-}(\alpha,\alpha_o) = \underline{r}(\alpha) - \underline{\underline{R}}_y \cdot \underline{r}(\alpha_o) \qquad \text{(C-16)}$$

In Section 5 of this appendix we present a detailed calculation for $A^{\pm}$, $B^{\pm}$, $C^{\pm}$ and $D^{\pm}$.

4. DEFINITION OF COORDINATES OF CENTERS AND BOUNDARIES OF ZONES

In this section we give the coordinates of the centers of zones that are not adjacent to the intersections. Assuming that we have N_{ℓ_i} transverse strips (defined by ℓ = constant boundaries) on the walls of the ith body, N_{r_i} transverse strips (defined by ℓ = constant boundaries) in the end cap of the ith body, N_{si} longitudinal strips (defined by ϕ = constant boundaries) on the ith body and N_i zones on the ith body we can now present the defining relationships for the coordinates of the centers of zones that are not adjacent to intersections (Appendix D).

a. Fuselage (Body No. 1)

One can easily show that

$$\alpha = \alpha(i=1,j,k) = (j-1)(N_{\ell_i} + 2N_{r_i}) + k \tag{C-17}$$

where α, i, j and k were defined in Section 3 of this appendix. The index j varies from 1 to N_{s_1} and k from 1 to $N_{\ell_1} + 2N_{r_1}$ depending on whether we are on the walls ($k = 1,\ldots,N_{\ell_1}$), on the front cap ($k = N_{\ell_1} + 1,\ldots,N_{\ell_1} + N_{r_1}$) or the back end cap ($k = N_{\ell_1} + N_{r_1},\ldots,N_{\ell_1} + 2N_{r_1}$).

$$j\epsilon[1,N_{s_1}], \quad k\epsilon[1,N_{\ell_1}]$$

$$\phi_j = \frac{180}{N_{s_1}}\left(j - \frac{1}{2}\right) \qquad x_k = \frac{\ell_1}{N_{\ell_1}}\left(k - \frac{1}{2}\right)$$

$$x(\alpha) = x_k \qquad s_x(\alpha) = 0 \qquad t_x(\alpha) = 1$$

$$y(\alpha) = b_1 \sin\phi_j \qquad s_y(\alpha) = \frac{b_1 \cos\phi_j}{N_1(\phi_j)} \qquad t_y(\alpha) = 0$$

$$z(\alpha) = -a_1 \cos\phi_j \qquad s_z(\alpha) = \frac{a_1 \sin\phi_j}{N_1(\phi_j)} \qquad t_z(\alpha) = 0 \tag{C-18a}$$

where $N_1(\phi_j) = (b_1^2 \cos^2\phi_j + a_1^2 \sin^2\phi_j)^{1/2}$

$j \epsilon [1, N_{s_1}]$, $k - N_{\ell_1} \epsilon [1, N_{r_1}]$

$$r_k = \left[\frac{1}{N_{r_1}}\left(k - N_{\ell_1} - \frac{1}{2}\right)\right]^{1/2} \qquad \phi_j = \frac{180}{N_{s_1}}\left(j - \frac{1}{2}\right)$$

$$N_1(\phi_j) = (a_1^2 \sin^2\phi_j + b_1^2 \cos^2\phi_j)^{1/2}$$

$$x(\alpha) = 0 \qquad s_x(\alpha) = 0 \qquad t_x(\alpha) = 0$$

$$y(\alpha) = b_1 r_k \sin\phi_j \qquad s_y(\alpha) = \frac{b_1 \cos\phi_j}{N_1(\phi_j)} \qquad t_y(\alpha) = \frac{a_1 \sin\phi_j}{N_1(\phi_j)}$$

$$z(\alpha) = -a_1 r_k \cos\phi_j \qquad s_z(\alpha) = \frac{a_1 \sin\phi_j}{N_1 \phi_j)} \qquad t_z(\alpha) = \frac{-b_1 \cos\phi_j}{N_1(\phi_j)}$$

(C-19a)

$j \epsilon [1, N_{s_1}]$, $k - N_{\ell_1} - N_{r_1} \epsilon [1, N_{r_1}]$

$$r_k = \left[\frac{1}{N_{r_1}}\left(k - N_{\ell_1} - N_{r_1} - \frac{1}{2}\right)\right]^{1/2}, \qquad \phi_j = \frac{180}{N_{s_1}}\left(j - \frac{1}{2}\right)$$

$$N_1(\phi_j) = (b_1^2 \cos^2\phi_j + a_1^2 \sin^2\phi_j)^{1/2}$$

$$x(\alpha) = \ell_1 \qquad s_x(\alpha) = 0 \qquad t_x(\alpha) = 0$$

$$y(\alpha) = b_1 r_k \sin\phi_j \qquad s_y(\alpha) = \frac{b_1 \cos\phi_j}{N_1(\phi_j)} \qquad t_y(\alpha) = \frac{-a_1 \sin\phi_j}{N_1(\phi_j)}$$

$$z(\alpha) = -a_1 r_k \cos\phi_j \qquad s_z(\alpha) = \frac{a_1 \sin\phi_j}{N_1(\phi_j)} \qquad t_z(\alpha) = \frac{b_1 \cos\phi_j}{N_1(\phi_j)}$$

(C-20)

b. Wing (Body No. 2)

$$\alpha = \alpha(i=2,j,k) = (j-1)\ (N_{\ell_2} + N_{r_2}) + k + N_1 \qquad \text{(C-21)}$$

where N_1 is the total number of zones on the fuselage (body no. 1), i.e., $(N_{\ell_1} + 2N_{r_1})\ N_{s_1}$.

$$j \epsilon [1, N_{s_2}], \quad k \epsilon [1, N_{\ell_2}]$$

$$\phi_j = \frac{360}{N_{s_2}} \left(j - \frac{1}{2}\right) \qquad N_2(\phi_j) = (a_2^2 \sin^2\phi_j + b_2^2 \cos^2\phi_j)^{1/2}$$

$$y_k = \frac{\ell_2}{N_{\ell_2}} \left(k - \frac{1}{2}\right) + b_1$$

$$x(\alpha) = x_{02} + a_2 \cos\phi_j \qquad s_x(\alpha) = \frac{-a_2 \sin\phi_j}{N_2(\phi_j)} \qquad t_x(\alpha) = 0$$

$$y(\alpha) = y_k \qquad s_y(\alpha) = 0 \qquad t_y(\alpha) = 1$$

$$z(\alpha) = -b_2 \sin\phi_j \qquad s_z(\alpha) = -\frac{b_2 \cos\phi_j}{N_2(\phi_j)} \qquad t_z(\alpha) = 0 \qquad \text{(C-22)}$$

$$j \epsilon [1, N_{s_2}], \quad k - N_{\ell_2} \epsilon [1, N_{r_2}]$$

$$\phi_j = \frac{360}{N_{s_2}} \left(j - \frac{1}{2}\right) \qquad N_2(\phi_j) = (a_2^2 \sin^2\phi_j + b_2^2 \cos^2\phi_j)^{1/2}$$

$$r_k = \left[\frac{1}{N_{r_2}} \left(k - N_{\ell_2} - \frac{1}{2}\right)\right]^{1/2}$$

(C-23)

$$x(\alpha) = x_{02} + a_2 r_k \cos\phi_j \qquad s_x(\alpha) = -\frac{a_2 \sin\phi_j}{N_2(\phi_j)} \qquad t_x(\alpha) = -\frac{b_2 \cos\phi_j}{N_2(\phi_j)}$$

$$y(\alpha) = \ell_2 + a_1 \qquad s_y(\alpha) = 0 \qquad t_y(\alpha) = 0$$

$$z(\alpha) = -b_2 r_k \sin\phi_j \qquad s_z(\alpha) = -\frac{b_2 \cos\phi_j}{N_2(\phi_j)} \qquad t_z(\alpha) = \frac{a_2 \sin\phi_j}{N_2(\phi_j)} \qquad \text{(C-23)}$$

c. Horizontal Stabilizer (Body No. 3)

$$\alpha = \alpha(i=3,j,k) = (j-1)(N_{\ell_3} + N_{r_2}) + k + N_1 + N_2 \qquad \text{(C-24)}$$

where N_1, N_2 are the total number of zones on bodies 1 and 2, respectively.

$j \epsilon [1, N_{s_3}]$, $k \epsilon [1, N_{\ell_3}]$

$$\phi_j = \frac{360}{N_{s_3}} \left(j - \frac{1}{2}\right) \qquad N_3(\phi_j) = (b_3^2 \cos^2\phi_j + a_3^2 \sin^2\phi_j)^{1/2}$$

$$y_k = \frac{\ell_3}{N_{\ell_3}} \left(k - \frac{1}{2}\right) + a_1$$

$$x(\alpha) = x_{03} + a_3 \cos\phi_j \qquad s_x(\alpha) = \frac{-a_3 \sin\phi_j}{N_3(\phi_j)} \qquad t_x(\alpha) = 0$$

$$y(\alpha) = y_k \qquad s_y(\alpha) = 0 \qquad t_y(\alpha) = 1$$

$$z(\alpha) = -b_3 \sin\phi_j \qquad s_z(\alpha) = -\frac{b_2 \cos\phi_j}{N_3(\phi_j)} \qquad t_z(\alpha) = 0 \qquad \text{(C-25)}$$

$$j \epsilon [1, N_{s_L}], \quad k - N_{\ell_3} \epsilon [1, N_{r_3}]$$

$$\phi_j = \frac{360}{N_{s_3}} \left(j - \frac{1}{2}\right) \qquad N_3(\phi_j) = (b_3^2 \cos^2\phi_j + a_3^2 \sin^2\phi_j)^{1/2}$$

$$r_k = \left[\frac{1}{N_{r_3}} \left(k - N_{\ell_3} - \frac{1}{2}\right)\right]^{1/2}$$

$$x(\alpha) = x_{03} + a_3 r_k \cos\phi_j \qquad s_x(\alpha) = -\frac{a_3 \sin\phi_j}{N_3(\phi_j)} \qquad t_x(\alpha) = -\frac{b_3 \cos\phi_j}{N_3(\phi_j)}$$

$$y(\alpha) = \ell_3 + a_1 \qquad s_y(\alpha) = 0 \qquad t_y(\alpha) = 0$$

$$z(\alpha) = -b_3 r_k \sin\phi_j \qquad s_z(\alpha) = -\frac{b_3 \cos\phi_j}{N_3(\phi_j)} \qquad t_z(\alpha) = \frac{a_3 \sin\phi_j}{N_3(\phi_j)}$$

(C-26)

d. Vertical Stabilizer (Body No. 4)

$$\alpha = \alpha(i=4,j,k) = (j-1)(N_{\ell_4} + N_{r_4}) + k + N_1 + N_2 + N_3 \qquad \text{(C-27)}$$

where N_1, N_2, N_3 are the total number of zones on bodies 1, 2, and 3, respectively.

$$j \epsilon [1, N_{s_4}], \quad k \epsilon [1, N_{\ell_4}]$$

$$\phi_j = \frac{180}{N_{s_4}} \left(j - \frac{1}{2}\right) \qquad N_4(\phi_j) = (a_4^2 \sin^2\phi_j + b_4^2 \cos^2\phi_j)^{1/2}$$

$$z_k = \frac{\ell_4}{N_{\ell_4}} \left(k - \frac{1}{2}\right) + a_1 \qquad \text{(C-28)}$$

AD-A039 953 TDR INC LOS ANGELES CALIF F/G 1/3
FOUNDATION OF THE MAGNETIC FIELD INTEGRAL EQUATION CODE FOR THE--ETC(U)
APR 77 M I SANCER, S SIEGEL, A D VARVATSIS F29601-75-C-0067
UNCLASSIFIED AFWL-TR-76-279 NL

2 OF 2
AD
A039953

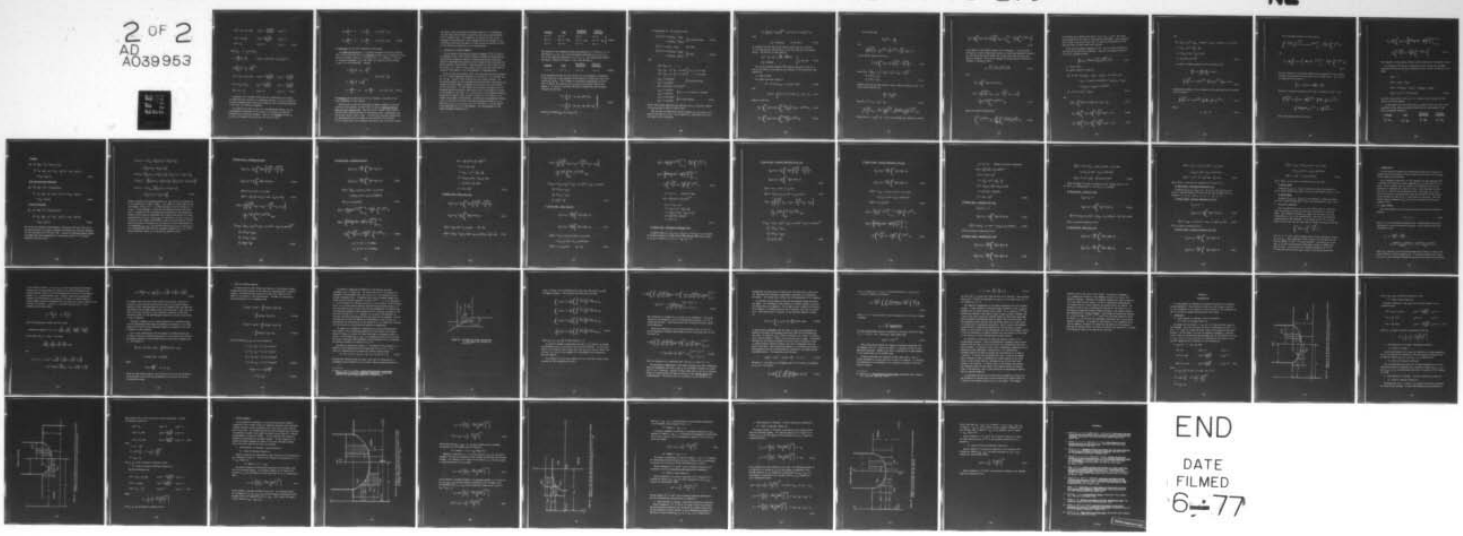

END
DATE
FILMED
6-77

$$x(\alpha) = x_{04} + a_4 \cos\phi_j \qquad s_x(\alpha) = -\frac{a_4 \sin\phi_j}{N_4(\phi_j)} \qquad t_x(\alpha) = 0$$

$$y(\alpha) = b_4 \sin\phi_j \qquad s_y(\alpha) = \frac{b_4 \cos\phi_j}{N_4(\phi_j)} \qquad t_y(\alpha) = 0$$

$$z(\alpha) = z_k \qquad s_z(\alpha) = 0 \qquad t_z(\alpha) = 1 \qquad \text{(C-28)}$$

$$j \in [1, N_{s_4}], \quad k - N_{\ell_4} \in [1, N_{r_4}]$$

$$\phi_j = \frac{380}{N_{s_4}}\left(j - \frac{1}{2}\right) \qquad N_4(\phi_j) = (a_4^2 \sin^2\phi_j + b_4^2 \cos^2\phi_j)^{1/2}$$

$$r_k = \left[\frac{1}{N_{r_4}}\left(k - N_{\ell_4} - \frac{1}{2}\right)\right]^{1/2}$$

$$x(\alpha) = x_{04} + a_4 r_k \cos\phi_j \qquad s_x(\alpha) = -\frac{a_4 \sin\phi_j}{N_4(\phi_j)} \qquad t_x(\alpha) = -\frac{b_4 \cos\phi_j}{N_4(\phi_j)}$$

$$y(\alpha) = b_4 r_k \sin\phi_j \qquad s_y(\alpha) = \frac{b_4 \cos\phi_j}{N_4(\phi_j)} \qquad t_y(\alpha) = -\frac{a_4 \sin\phi_j}{N_4(\phi_j)}$$

$$z(\alpha) = \ell_4 + a_1 \qquad s_z(\alpha) = 0 \qquad t_z(\alpha) = 0 \qquad \text{(C-29)}$$

Equations (C-17) through (C-29) give the coordinates at the centers of zones that will be used in our numerical solution. For the calculation of matrix elements given in the next section we need to know the boundaries of the zones over which we integrate.

For zones on the walls we can, in a straightforward manner, use the corresponding coordinates for the centers to calculate the limits of integration for the matrix elements. Thus for the <u>fuselage</u> we refer to x_k and ϕ_j in equation $(C\text{-}18)_a$ and for the (i=1,j,k) zone

$$x_1 = \frac{\ell_1}{N_{\ell_1}}(k-1) \qquad x_2 = \frac{\ell_1}{N_{\ell_1}} k \qquad x_k = \frac{1}{2}(x_1 + x_2)$$

$$\phi_1 = \frac{180}{N_{s_1}}(j-1) \qquad \phi_2 = \frac{180}{N_{s_1}} j \qquad \phi_j = \frac{1}{2}(\phi_1 + \phi_2) \qquad (C\text{-}18)_b$$

and <u>similarly</u> for the other components of our model.

<u>For zones on the caps</u> the ϕ = constant boundaries are easily obtained. Thus for the front end cap on the <u>fuselage</u> we refer to ϕ_j in equation $(C\text{-}19)_a$ and we can readily obtain $\phi_1 = (180/N_{s_1})(j-1)$, $\phi_2 = (180/N_{s_1})j$. For the r = constant boundaries, r_k at the center of a zone is not the average of the r's of the boundaries. Instead:

$$r_1 = \left[\frac{1}{N_{r_1}}\left(k - N_{\ell_1} - 1\right)\right]^{1/2}$$

$$r_k^2 = \frac{1}{2}(r_1^2 + r_2^2)$$

$$r_2 = \left[\frac{1}{N_{r_1}}\left(k - N_{\ell_1}\right)\right]^{1/2}$$

$$\phi_1 = \frac{180}{N_{s_1}}(j-1) \qquad \phi_2 = \frac{180}{N_{s_1}} j \qquad \phi_k = \frac{1}{2}(\phi_1 + \phi_2) \qquad (C\text{-}19)_b$$

and <u>similarly</u> on the back end cap of the fuselage or the caps of the other components of the aircraft.

Before we go on with the calculation of matrix elements in the next section of this appendix, we would like to state an <u>important feature built into our computer code</u>. Equations (C-17) through (C-29) dictate the rule that a given zone obeys in relationship with a neighboring zone on the same surface (wall or cap). To allow for sufficient nonuniformity for experimenting with the zoning the code provides that equations (C-17) through (C-29) can be applied sectionally; that is we first divide

the walls or caps in sections by drawing selected ϕ, t, r-boundaries and then within the sections we apply the rules that govern equations (C-17) through (C-29). For example we can divide the wall of the fuselage in three sections in the x-direction and two sections in the ϕ-direction and choose any number of zones within each section to allow for the desired nonuniformity of our zoning scheme.

5. CALCULATION OF MATRIX ELEMENTS

In this section we calculate the matrix elements $A^{\pm}$, $B^{\pm}$, $C^{\pm}$ and $D^{\pm}$ in equation (C-15). First we will outline the method of derivation and then perform a sufficient number of calculations that will allow the reader to understand how equations (C-62) through (C-92), which give the matrix elements, were obtained. These equations are still valid for the self-terms, i.e., when α is the central point of the zone over which we integrate (see Appendix D for zones adjacent to instersections).

As we can see from equation (C-15) the calculation of matrix elements $A^{\pm}$, $B^{\pm}$, $C^{\pm}$ and $D^{\pm}$ involves integrands of the form $\underline{R}^{+} \cdot (\hat{p} \times \hat{q}_o) Q(R^{+})$ and $\underline{R}^{-} \cdot (\hat{p} \times \underline{\underline{R}}_y \cdot \hat{q}_o) Q(R^{-})$ where $\hat{p}$ and $\hat{q}_o$ are unit surface vectors. The integrated variable has the subscript zero and runs over a particular zone whereas the free variable corresponds to the center of a zone anywhere on the four bodies. All four bodies are elliptical cylinders and as we explained earlier the surface unit vectors $\hat{s}$ and $\hat{t}$ are chosen to conform to the geometry of the body, i.e., $\hat{s}$ is defined in the azimuthal direction defined by the angle ϕ (fig. 3) and $\hat{t}$ is equal to $\hat{n} \times \hat{s}$ where $\hat{n}$ is the outward unit normal to the surface. To facilitate our subsequent calculations, to each body we attach a cartesian coordinate system x_1, x_2, x_3 such that $x_1 = x_1$, $x_2 = ar\cos\phi$, $x_3 = br\sin\phi$ where $r = 1$ on the walls of the body and $0 \leq r \leq 1$ on the endcaps. The correspondence to the global coordinate systems xyz is

Fuselage	Wing	Horizontal Stabilizer	Vertical Stabilizer	
$x_1 = x$	$x_1 = y$	$x_1 = y$	$x_1 = z$	
$x_2 = -z$	$x_2 = x - x_{02}$	$x_2 = x - x_{03}$	$x_2 = x - x_{04}$	(C-30a)
$x_3 = y$	$x_3 = -z$	$x_3 = -z$	$x_3 = y$	

The endcaps of the fuselage are then determined by $x_1 = 0$ and $x_1 = \ell_1$, of the wing by $x_1 = a_1 + \ell_2$, of the horizontal stabilizer by $x_1 = a_1 + \ell_3$ and of the vertical stabilizer by $x_1 = b_1 + \ell_4$. The relationship between the angle ϕ depicted in figure 1 and ϕ just defined is

Fuselage	Wing	Horizontal Stabilizer	Vertical Stabilizer	
$\phi \leftrightarrow \phi$	$\phi \leftrightarrow \phi$	$\phi \leftrightarrow \phi$	$\phi \leftrightarrow \phi$	(C-30b)

As we mentioned earlier the free variable in the integrands corresponds to the center of a zone anywhere on the surface of a body with local unit vectors $\hat{s}_\alpha$ and $\hat{t}_\alpha$. For a number of subsequent calculations we do not have to specify the form for $\hat{s}_\alpha$ or $\hat{t}_\alpha$ and we will denote them by the symbol $\hat{v}$. In order to calculate the matrix elements we must calculate integrals of the form

$$\left.\begin{aligned} I^+ &= \int_{S_o} \underline{R}^+ \cdot (\hat{v} \times \hat{q}_o)\, Q(R^+)\, dS_o, \\ I^- &= \int_{S_o} \underline{R}^- \cdot (\hat{v} \times R_y \cdot \hat{q}_o)\, Q(R^-)\, dS_o \end{aligned}\right\} \qquad \text{(C-31)}$$

where $\hat{q}_o$ is either $\hat{s}_{\alpha o} \equiv \hat{s}_o$ or $\hat{t}_{\alpha o} \equiv \hat{t}_o$.

We start with I^+. For a zone on a body

$$\left.\begin{aligned}\underline{R}^+(\hat{v} \times \hat{s}) &= \Delta x_1(v_2 s_{30} - v_3 s_{20}) \\ &\quad - v_1(\Delta x_2 s_{30} - \Delta x_3 s_{20})\end{aligned}\right\} \text{On walls and caps} \qquad \text{(C-32a)}$$

$$\left.\underline{R}^+(\hat{v} \times \hat{t}) = \Delta x_2 v_3 - \Delta x_3 v_2\right\} \text{On walls}$$

$$\left.\begin{aligned}\underline{R}^+(\hat{v} \times \hat{t}) &= \Delta x_1(v_2 t_{30} - v_3 t_{20}) \\ &\quad - v_1(\Delta x_2 t_{30} - \Delta x_3 t_{20})\end{aligned}\right\} \text{On caps} \qquad \text{(C-32b)}$$

and

$$\left.\begin{aligned}\Delta x_1 &= x_{1\alpha} - x_1 \\ \Delta x_2 &= x_{2\alpha} - x_2 = x_{2\alpha} - ar\cos\phi, \\ \Delta x_3 &= x_{3\alpha} - x_3 = x_{3\alpha} - br\sin\phi,\end{aligned}\right\} \begin{array}{l} 0 \le r \le 1 \text{ for caps} \\ r = 1 \text{ for walls}\end{array}$$

$$\left.\begin{aligned}s_{20} &= -a\sin\phi/N(\phi) \\ s_{30} &= b\cos\phi/N(\phi)\end{aligned}\right\} \text{On walls and caps}$$

$$N(\phi) = (a^2\sin^2\phi + b^2\cos^2\phi)^{1/2}$$

$$\left.\begin{aligned}t_{20} &= b\cos\phi/N(\phi) \\ t_{30} &= a\sin\phi/N(\phi)\end{aligned}\right\} \text{On } x_1 = x = 0 \text{ endcap of fuselage}$$

$$\left.\begin{aligned}t_{20} &= -b\cos\phi/N(\phi) \\ t_{30} &= -a\sin\phi/N(\phi)\end{aligned}\right\} \text{All other endcaps} \qquad \text{(C-33)}$$

Notice that we have simplified the notation and $\underline{r}_o = (x_1, x_2, x_3)$ instead of (x_{10}, x_{20}, x_{30}) to which we return later.

Next we need the differential surface element dS_o for a zone on the walls or the caps of a body. On the walls $dS_o = dx_1 ds$ where ds is the arc length in the ϕ-direction

$$ds = \left[(dx_2)^2 + (dx_3)^2\right]^{1/2} = (a^2 \sin^2\phi + b^2 \cos^2\phi)^{1/2}\, d\phi$$

Thus

$$dS_o = N(\phi)dx_1 d\phi \qquad \text{on the walls} \tag{C-34}$$

To calculate the area dS_o on the caps we recall that $x_2 = ar\cos\phi$, $x_3 = br\sin\phi$ and $\underline{r}_o = r(a\cos\phi\ \hat{e}_2 + b\sin\phi\ \hat{e}_3)$ where $\underline{r}_o$ is the radius vector. The area dS_o is thus given by

$$\left.\begin{aligned} dS_o &= |\underline{ds} \times d\underline{r}_o| = \left|\frac{\partial \underline{r}_o}{\partial \phi} \times \frac{\partial \underline{r}_o}{\partial r}\right| d\phi dr \\ dS_o &= abrdrd\phi \end{aligned}\right\} \text{on the caps} \tag{C-35}$$

Let us now evaluate integral $I^+(\hat{s})$ given by equation (C-31) for a zone on the walls and the caps but not adjacent to an intersection (see Appendix D).

a. Zone on Walls

We rewrite equation (C-32a) as

$$\underline{R}^+ \cdot (\hat{v} \times \hat{s}) = (x_{1\alpha} - x_1)\, M_1(\phi) + M_2(\phi) \tag{C-36}$$

Thus

$$I_w^+(\hat{s}) = \int_{S_o} \underline{R}^+ \cdot (\hat{v} \times \hat{s})\, Q(R^+)\, dS_o = I_{w1}^+ + I_{w2}^+ \tag{C-37}$$

where w = wall and

$$I_{w1}^+ = \int_{\phi_1}^{\phi_2} M_1(\phi)\, N(\phi)\, d\phi \int_{x_{11}}^{x_{12}} \frac{x_{1\alpha} - x_1}{4\pi R^3} (ik_o R - 1) e^{ik_o R}\, dx_1 \tag{C-38}$$

$$I_2^+ = \int_{\phi_1}^{\phi_2} M_2(\phi)\, N(\phi)\, d\phi \int_{x_{11}}^{x_{12}} \frac{ik_o R - 1}{4\pi R^3} e^{ik_o R}\, dx_1 \tag{C-39}$$

If we notice that

$$\frac{x_{1\alpha} - x_1}{R} = -\frac{\partial R}{\partial x_1}$$

and

$$\frac{d}{dR}\left(\frac{e^{ik_oR}}{R}\right) = -\frac{1}{R^2}e^{ik_oR} + \frac{ik_o}{R}e^{ik_oR} = \frac{e^{ik_oR}}{R^2}(ik_oR - 1)$$

we can rewrite equation (C-39) as

$$I_1^+ = \frac{1}{4\pi}\int_{\phi_1}^{\phi_2} M_1(\phi)\, N(\phi)\left[\frac{e^{ik_oR_2}}{R_2} - \frac{e^{ik_oR_1}}{R_1}\right]d\phi \qquad \text{(C-40)}$$

where $R(x_1) = \left[\left(x_{1\alpha} - x_1\right)^2 + \left(x_{2\alpha} - x_2\right)^2 + \left(x_{3\alpha} - x_3\right)^2\right]^{1/2}$

$R_1 = R(x_1 = x_{11})$

$R_2 = R(x_1 = x_{12})$ (C-41)

Integral I_{w2}^+ does not lend itself to such a simple treatment as I_{w1}^+. As a first step we observe that

$$\frac{dx_1}{R^3} = \frac{x_1 - x_{1\alpha}}{a^2R}$$

where $R^2 = a^2 + (x_1 - x_{1\alpha})^2$ and (C-42)

$$-\int \frac{e^{ik_oR}}{R^3}dx_1 = -\frac{\left(x_1 - x_{1\alpha}\right)e^{ik_oR}}{a^2R} + \int \frac{ik_oR\left(x_1 - x_{1\alpha}\right)^2 e^{ik_oR}}{a^2R^2}dx_1$$

Noting that $\left(x_1 - x_{1\alpha}\right)^2 = R^2 - a^2$ we can rearrange this equation to obtain

$$I_{w2}^{+} = \frac{1}{4\pi}\int_{\phi_1}^{\phi_2} M_2(\phi)\, N(\phi)\, d\phi \left\{ \frac{e^{ik_o R}}{a^2 R}\left(x_{1\alpha} - x_1\right)\Big|_{x_{11}}^{x_{12}} + \frac{ik_o}{a^2}\int_{x_{11}}^{x_{12}} e^{ik_o R}\, dx_1 \right\} \tag{C-43}$$

The integral in the angular bracket is not elementary. One can expand $\exp(ik_o R)$ in a Taylor series and evaluate the resulting elementary integrals but too many terms will be needed for a zone remote from the zone over which we integrate. This can be remedied by multiplying and dividing the integral by $\exp(ik_o R_o)$ where

$$R_o = \frac{R(x = x_{11}) + R(x = x_{12})}{2} \tag{C-44}$$

Thus

$$I_{w2}^{+} = \frac{1}{4\pi}\int_{\phi_1}^{\phi_2} M_2(\phi)\, N(\phi)\, K(\phi)\, d\phi$$

$$K(\phi) = \frac{1}{a^2}\left[\frac{e^{ik_o R_2}}{R_2}\left(x_{1\alpha} - x_{12}\right) - \frac{e^{ik_o R_1}}{R_1}\left(x_{1\alpha} - x_{11}\right)\right]$$

$$+ \frac{ik_o}{a^2} e^{ik_o R_o}\int_{x_{11}}^{x_{12}} e^{ik_o(R-R_o)}\, dx_1 \tag{C-45}$$

Now we can expand $\exp[ik_o(R-R_o)]$:

$$\int_{x_{11}}^{x_{12}} e^{ik_o(R-R_o)}\, dx_1 = \sum_{n=0}^{n_m}\int_{x_{11}}^{x_{12}} \frac{\left[ik_o(R - R_o)\right]^n}{n!}\, dx_1 \tag{C-46}$$

To determine n_m we observe that $\max|R - R_o| \approx |x_{11} - x_{12}|/2$ and recall that we require on the order of ten zones per wavelength. This translates into $k \max|R - R_o|$ being of the order of unity and consequently we only need few terms to secure sufficient accuracy.

If we use the binomial expansion for $(R - R_o)^n$ we obtain integrals of the form $\int R^n \, dx_1$ which are elementary. They can be evaluated with the aid of the recursion formula

$$\int R^n \, dx_1 = \frac{(x_{1\alpha} - x_1) R^n + n \int R^{n-2} \, dx_1}{n + 1} \tag{C-47}$$

b. Zone on Caps

We rewrite equation (C-32a) as

$$\underline{R}^+ \cdot (\hat{v} \times \hat{s}) = \Delta x_1 (v_2 s_{30} - v_3 s_{20}) - v_1 [(x_{2\alpha} - ar\cos\phi)(b\cos\phi)$$

$$- (x_{3\alpha} - br\sin\phi)(-a\sin\phi)]/N(\phi) = \Delta x_1 (v_2 s_{30} - v_3 s_{20})$$

$$- v_1 (x_{2\alpha} s_{30} - x_{3\alpha} s_{20}) + v_1 rab/N(\phi)$$

$$\underline{R}^+ \cdot (\hat{v} \times \hat{s}) = K_1(\phi) + rK_2(\phi) \tag{C-48}$$

and

$$I_c^+(\hat{s}) = \int_{S_o} \underline{R}^+ (\hat{v} \times \hat{s}) \, Q(R^+) \, dS_o = I_{c1}^+ + I_{c2}^+ \tag{C-49}$$

$$I_{c1}^+ = \frac{ab}{4\pi} \int_{\phi_1}^{\phi_2} K_1(\phi) \, d\phi \int_{r_1}^{r_2} \frac{re^{ik_o R}}{R^3} (ik_o R - 1) \, dr \tag{C-50}$$

$$I_{c2}^+ = \frac{ab}{4\pi} \int_{\phi_1}^{\phi_2} K_2(\phi) \, d\phi \int_{r_1}^{r_2} \frac{r^2 e^{ik_o R}}{R^3} (ik_o R - 1) \, dr \tag{C-51}$$

and

$$R^2 = (x_{1\alpha} - x_1)^2 + (x_{2\alpha} - ra\cos\phi)^2 + (x_{3\alpha} - rb\sin\phi)^2 = f + gr + hr^2$$

$$f = (x_{1\alpha} - x_1)^2 + x_{2\alpha}^2 + x_{3\alpha}^2$$

$$g = -2(x_{2\alpha}\, a\cos\phi + x_{3\alpha}\, b\sin\phi)$$

$$h = a^2\cos^2\phi + b^2\sin^2\phi \qquad \text{(C-52)}$$

In order to simplify equation (C-50) we observe that

$$\frac{rdr}{R^3} = -d\,\frac{2gr + 4f}{(4fh - g^2)R} \equiv -dP(r)$$

$$\int \frac{re^{ik_oR}}{R^3}\,dr = -P(R)e^{ik_oR} + \int P(R)ik_oe^{ik_oR}\,\frac{1}{2R}(g + 2hr)dr \qquad \text{(C-53)}$$

Performing the algebra in the integrand on the right-hand side of equation (C-53) we obtain

$$\int \frac{re^{ik_oR}}{R^3}\,dr = -P(r)e^{ik_oR} + \int \left(\frac{2g}{\Delta} + \frac{r}{R^2}\right) ik_oe^{ik_oR}\,dr \qquad \text{(C-54)}$$

where

$$\Delta = 4fh - g^2. \qquad \text{(C-55)}$$

If we rearrange equation (C-54) we obtain

$$\int_{r_1}^{r_2} \frac{r(ik_oR - 1)\, e^{ik_oR}}{R^3}\, dr = P(r)\, e^{ik_oR}\Big|_{r_1}^{r_2} - \frac{2ik_og}{\Delta} \int_{r_1}^{r_2} e^{ik_oR}\, dr$$

and

$$I_{c1}^{+} = \frac{ab}{4\pi} \int_{\phi_1}^{\phi_1} K_1(\phi)\, d\phi \left\{ \frac{2gr + 4f}{\Delta}\, e^{ik_oR}\Big|_{r_1}^{r_2} - \frac{2ik_og}{\Delta} \int_{r_1}^{r_2} e^{ik_oR}\, dr \right\} \tag{C-56}$$

The last integral in the angular bracket can be evaluated by the procedure outlined in connection with equations (C-43) through (C-46). I_{c2}^{+} can also be simplified by noting that

$$\frac{r^2}{R^3}\, dr = d\left[-rP(r) + \frac{2gR}{h\Delta}\right] + \frac{1}{h}\frac{dr}{R}$$

where P(r) is given by equation (C-53) and Δ by equation (C-55). Thus

$$\int \frac{r^2 e^{ik_oR}}{R^3}\, dr = \left[-rp(r) + \frac{2gR}{h\Delta}\right] e^{ik_oR} + \int r\left(\frac{2g}{\Delta} + \frac{r}{R^2}\right) ik_o\, e^{ik_oR}\, dr$$

$$-\int \frac{g(2hr + g)}{h\Delta}\, ik_o\, e^{ik_oR}\, dr + \frac{1}{h}\int \frac{e^{ik_oR}}{R}\, dr$$

This relationship allows us to write:

$$I_{c2}^{+} = \frac{ab}{4\pi} \int_{\phi_1}^{\phi_2} K_2(\phi)\, d\phi \left\{ \left[\frac{2r(gr + 2f)}{R} - \frac{2gR}{h} \right] \frac{e^{ik_o R}}{\Delta} \Bigg|_{r = r_1}^{r = r_2} \right.$$

$$\left. - \frac{1}{h} \int_{r_1}^{r_2} \frac{e^{ik_o R}}{R}\, dr + \frac{ik_o g^2}{h\Delta} \int_{r_1}^{r_2} e^{ik_o R}\, dr \right\} \qquad \text{(C-57)}$$

The integrals in the angular brackets can be evaluated as in equation (C-56).

To calculate $I^{+}(\hat{t})$ given by equation (C-31) we follow the procedure employed for $I^{+}(\hat{s})$ and arrive at equations (C-40), (C-45), (C-56) and (C-57) where

$$M_1(\phi) = 0$$

$$M_2(\phi) = \Delta x_2 v_3 - \Delta x_3 v_2$$

$$K_1(\phi) = \Delta x_1 (v_2 t_{30} - v_3 t_{20}) - v_1 (x_{2\alpha} t_{30} - x_{3\alpha} t_{20})$$

$$K_2(\phi) = \pm v_1 (a^2 - b^2) \sin\phi \cos\phi \qquad \text{(C-58)}$$

and the + sign refers to the $x_1 = x = 0$ endcap of the fuselage and the - sign to all other endcaps.

To calculate $I^{-}(\hat{t})$ and $I^{-}(\hat{s})$ given by equation (C-31) we observe that $\underline{R}_y$ refers to the global coordinate system and its relationship to the local coordinate systems is

Fuselage	Wing	Horizontal Stabilizer	Vertical Stabilizer
$\underline{R}_y = \underline{R}_{x3}$	$\underline{R}_y = \underline{R}_{x1}$	$\underline{R}_y = \underline{R}_{x1}$	$\underline{R}_y = \underline{R}_{x3}$

Fuselage

$$\underline{R}_y \cdot \hat{q}_o = \underline{R}_{x2} \cdot \hat{q}_o = (q_{o1}, q_{o2}, -q_{o3})$$

$$\underline{R}^- = \underline{r}_\alpha - \underline{R}_{x2} \cdot \underline{r}_o = (x_{1\alpha} - x_{10})\,\hat{e}_1 + (x_{2\alpha} - x_{20})\,\hat{e}_2 + (x_{3\alpha} \mp x_{30})\,\hat{e}_3 \qquad \text{(C-59)}$$

Wing and Horizontal Stabilizer

$$\underline{R}_y \cdot \hat{q}_o = \underline{R}_{x1} \cdot \hat{q}_o = (-q_{o1}, q_{o2}, q_{o3})$$

$$\underline{R}^- = \underline{r}_\alpha - \underline{R}_{x1} \cdot \underline{r}_o = (x_{1\alpha} + x_{10})\,\hat{e}_1 + (x_{2\alpha} - x_{20})\,\hat{e}_2 + (x_{3\alpha} - x_{30})\,\hat{e}_3 \qquad \text{(C-60)}$$

Vertical Stabilizer

$$\underline{R}_y \cdot \hat{q}_o = \underline{R}_{x3} \cdot \hat{q}_o = (q_{o1}, q_{o2}, -q_{o3})$$

$$\underline{R}^- = \underline{r}_\alpha - \underline{R}_{x2} \cdot \underline{r}_o = (x_{1\alpha} - x_{10})\,\hat{e}_1 + (x_{2\alpha} - x_{20})\,\hat{e}_2 + (x_{3\alpha} + x_{30})\,\hat{e}_3 \qquad \text{(C-61)}$$

We can use the previous relationships to calculate $I^-(\hat{t})$ and $I^-(\hat{s})$ on the walls and endcaps of the various bodies by following the procedure employed for the calculation of $I^+(\hat{t})$ and $I^+(\hat{s})$. Instead of exhibiting these results we present the final expressions for the matrix terms $A^\pm$, $B^\pm$, $C^\pm$ and $D^\pm$ defined by equation (C-15)

$$A^{\pm}(\alpha,\alpha_o) = -\frac{1}{2}\delta_{\alpha\alpha_o} + \left[I^{+}_{1ij}(t,s_o) + I^{+}_{2ij}(t,s_o)\right]$$

$$\pm \left[I^{-}_{1ij}(t,s_o) + I^{-}_{2ij}(t,s_o)\right]$$

$$B^{\pm}(\alpha,\alpha_o) = \left[I^{+}_{1ij}(t,t_o) + I^{+}_{2ij}(t,t_o)\right] \pm \left[I^{-}_{1ij}(t,t_o) + I^{-}_{2ij}(t,t_o)\right]$$

$$C^{\pm}(\alpha,\alpha_o) = -\left\{\left[I^{+}_{1ij}(s,s_o) + I^{+}_{2ij}(s,s_o)\right] \pm \left[I^{-}_{1ij}(s,s_o) + I^{-}_{2ij}(s,s_o)\right]\right\}$$

$$D^{\pm}(\alpha,\alpha_o) = -\frac{1}{2}\delta_{\alpha\alpha_o} - \left\{\left[I^{+}_{1ij}(s,t_o) + I^{+}_{2ij}(s,t_o)\right]\right.$$

$$\left. \pm \left[I^{-}_{1ij}(s,t_o) + I^{-}_{1ij}(s,t_o)\right]\right\} \qquad \text{(C-62)}$$

Before we present the defining equations for $I^{\pm}_{1ij}$ and $I^{\pm}_{2ij}$ an explanation of the notation is in order. Index i runs from 1 to 4 and refers to the four bodies. Index j refers to either the wall (w) or the endcap (c) of a body. In the fuselage, j refers to both endcaps (and also the wall). The $I^{\pm}$ in equation (C-62) are simplified expressions of the integrals in equation (C-15) which are evaluated over a zone on the surface of a body characterized by (ϕ_1,ϕ_2), (x_{101},x_{102}) on the walls or (ϕ_1,ϕ_2), (r_1,r_2) on a cap and by the surface unit vectors $\hat{t}_o$ and $\hat{s}_o$ given by equation (C-33). The free variable α corresponds to the center of a zone characterized by its coordinates $x_{1\alpha}$, $x_{2\alpha}$, $x_{3\alpha}$ and unit vectors $\hat{t}_\alpha(t_1,t_2,t_3)$, $\hat{s}_\alpha(s_1,s_2,s_3)$. The transformations from the local coordinate systems x_1, x_2, x_3 to the global coordinate system x,y,z are given by equation (C-30).

$A^{\pm}$ Matrix Term. Fuselage (i=1,j=w)

$$I^{\pm}_{11w}(t,s_o) = \frac{1}{4\pi}\int_{\phi_1}^{\phi_2} M^{\pm}_1(\phi)\left[\frac{e^{ik_oR^{\pm}_2}}{R^{\pm}_2} - \frac{e^{ik_oR^{\pm}_1}}{R^{\pm}_1}\right]d\phi$$

$$I^{\pm}_{21w}(t,s_o) = \frac{1}{4\pi}\int_{\phi_1}^{\phi_2} M^{\pm}_2(\phi)\, K^{\pm}(\phi)\, d\phi \qquad \text{(C-63)}$$

$$M^{\pm}_1(\phi) = \pm t_2\, b_1 \cos\phi + t_3\, a_1 \sin\phi$$

$$M^{\pm}_2(\phi) = t_1\left[\pm a_1 b_1 \mp x_{2\alpha}\, b_1 \cos\phi - x_{3\alpha}\, a_1 \sin\phi\right] \qquad \text{(C-64)}$$

$$K^{\pm}(\phi) = \frac{1}{a_1^2}\left[\frac{e^{ik_oR^{\pm}_2}}{R^{\pm}_2}(x_{1\alpha} - x_{102}) - \frac{e^{ik_oR^{\pm}_1}}{R^{\pm}_1}(x_{1\alpha} - x_{101})\right]$$

$$+ \frac{ik_o}{a_1^2}\, e^{ik_oR^{\pm}_o}\int_{x_{101}}^{x_{102}} e^{ik_o(R^{\pm}-R^{\pm}_o)}\, dx_{10}$$

$$R^{\pm}(x_{10}) = \left[(x_{1\alpha} - x_{10})^2 + (x_{2\alpha} - a_1\cos\phi)^2 + (x_{3\alpha} \mp b_1 \sin\phi)^2\right]^{1/2}$$

$$R^{\pm}_1 = R^{\pm}(x_{10} = x_{101})$$

$$R^{\pm}_2 = R^{\pm}(x_{10} = x_{102})$$

$$R^{\pm}_o = \tfrac{1}{2}(R^{\pm}_1 + R^{\pm}_2) \qquad \text{(C-65)}$$

$A^{\pm}$ Matrix Term. Fuselage (i=1, j=c)

$$I^{\pm}_{11c}(t,s_o) = \frac{a_1 b_1}{4\pi} \int_{\phi_1}^{\phi_2} K^{\pm}_1(\phi)\, H_1(\phi)\, d\phi$$

$$I^{\pm}_{21c}(t,s_o) = \frac{a_1 b_1}{4\pi} \int_{\phi_1}^{\phi_2} K^{\pm}_2(\phi)\, H_2(\phi)\, d\phi \qquad \text{(C-66)}$$

$$K^{\pm}_1(\phi) = \Big[(x_{1\alpha} - x_c)(\pm t_2\, b_1 \cos\phi + t_3\, a_1 \sin\phi)$$

$$-t_1(\pm x_{2\alpha}\, b_1 \cos\phi + x_{3\alpha}\, a_1 \sin\phi)\Big]/N(\phi)$$

$$K^{\pm}_2(\phi) = \pm t_1\, a_1 b_1 / N(\phi) \qquad \text{(C-67)}$$

$$H^{\pm}_1(\phi) = \frac{2g^{\pm}r + 4f}{\Delta^{\pm} R^{\pm}} e^{ik_o R^{\pm}} \Bigg|_{r=r_1}^{r=r_2} - \frac{2ik_o g^{\pm}}{\Delta^{\pm}} \int_{r_1}^{r_2} e^{ik_o R^{+}}\, dr$$

$$H^{\pm}_2(\phi) = \left[\left(\frac{2r(g^{\pm}r + 2f)}{R^{\pm}} - \frac{2g^{\pm}R^{\pm}}{h}\right) \frac{e^{ik_o R^{\pm}}}{\Delta^{\pm}}\right]_{r=r_1}^{r=r_2}$$

$$- \frac{1}{h} \int_{r_1}^{r_2} \frac{e^{ik_o R^{\pm}}}{R^{\pm}}\, dr + \frac{ik_o (g^{\pm})^2}{h\Delta^{\pm}} \int_{r_1}^{r_2} e^{ik_o R^{\pm}}\, dr \qquad \text{(C-68)}$$

$$x_c = 0 \quad \text{for} \quad x = 0 \text{ endcap}$$

$$x_c = \ell_1 \quad \text{for} \quad x = \ell_1 \text{ endcap} \qquad \text{(C-69)}$$

$$N(\phi) = \left(a_1^2 \sin^2\phi + b_1^2 \cos^2\phi\right)^{1/2}$$

$$R^{\pm} = f + g^{\pm} r + hr^2$$

$$f = (x_{1\alpha} - x_c)^2 + x_{2\alpha}^2 + x_{3\alpha}^2$$

$$g^{\pm} = \mp 2x_{3\alpha}\, b_1 \sin\phi - 2x_{2\alpha}\, a_1 \cos\phi$$

$$h = a_1^2 \cos^2\phi + b_1^2 \sin^2\phi$$

$$\Delta^{\pm} = 4fh - (g^{\pm})^2 \qquad \text{(C-70)}$$

<u>$A^{\pm}$ Matrix Term. Wing (i=2, j=w)</u>

$$I_{12w}^{\pm}(t, s_o) = \frac{1}{4\pi} \int_{\phi_1}^{\phi_2} M_1^{\pm}(\phi) \left[\frac{e^{ik_o R_2^{\pm}}}{R_2^{\pm}} - \frac{e^{ik_o R_1^{\pm}}}{R_1^{\pm}} \right] d\phi$$

$$I_{22w}^{\pm}(t, s_o) = \frac{1}{4\pi} \int_{\phi_1}^{\phi_2} M_2^{\pm}(\phi)\, K^{\pm}(\phi)\, d\phi \qquad \text{(C-71)}$$

$$M_1^{\pm}(\phi) = t_2 b_2 \cos\phi + t_3 a_2 \sin\phi, \qquad (M_1^{+} = M_1^{-})$$

$$M_2^{\pm}(\phi) = [a_2 b_2 - (x_{2\alpha}\, b_2 \cos\phi + x_{3\alpha}\, a_2 \sin\phi)]\, t_1, \quad (M_2^{+} = M_2^{-}) \qquad \text{(C-72)}$$

$$K^{\pm}(\phi) = \frac{1}{a_2^2}\left[\frac{e^{ik_o R_2^{\pm}}}{R_2^{\pm}}(x_{1\alpha} \mp x_{102}) - \frac{e^{ik_o R_1^{\pm}}}{R_1^{\pm}}(x_{1\alpha} \pm x_{101})\right]$$

$$+ \frac{ik_o}{a_2^2} e^{ik_o R_o^{\pm}} \int_{x_{101}}^{x_{102}} e^{ik_o(R^{\pm}-R_o^{\pm})}\, dx_{10}$$

$$R^{\pm}(x_{10}) = [(x_{1\alpha} \mp x_{10})^2 + (x_{2\alpha} - a_2\cos\phi)^2 + (x_{3\alpha} - b_2\sin\phi)^2]$$

$$R_1^{\pm} = R^{\pm}(x_{10} = x_{101})$$

$$R_2^{\pm} = R^{\pm}(x_{10} = x_{102})$$

$$R_o^{\pm} = \tfrac{1}{2}(R_1^{\pm} + R_2^{\pm}) \qquad \text{(C-73)}$$

<u>$A^{\pm}$ Matrix Term. Wing (i=2,j=c)</u>

$$I_{12c}^{\pm}(t,s_o) = \frac{a_2 b_2}{4\pi}\int_{\phi_1}^{\phi_2} K_1^{\pm}(\phi)\, H_1^{\pm}(\phi)\, d\phi$$

$$I_{22c}^{\pm}(t,s_o) = \frac{a_2 b_2}{4\pi}\int_{\phi_1}^{\phi_2} K_2^{\pm}(\phi)\, H_2^{\pm}(\phi)\, d\phi \qquad \text{(C-74)}$$

$$K_1^{\pm}(\phi) = [(x_{1\alpha} \mp x_c)(t_2\, b_2\cos\phi + t_3\, a_2\sin\phi)$$

$$- t_1(x_{2\alpha}\, b_2\cos\phi + x_{3\alpha}\, a_2\sin\phi)]/N(\phi)$$

$$K_2^{\pm}(\phi) = + t_1\, a_2 b_2/N(\phi), \qquad (K_2^{+} = K_2^{-}) \qquad \text{(C-75)}$$

$$H_1^{\pm}(\phi) = \frac{2gr + 4f^{\pm}}{\Delta^{\pm} R^{\pm}} e^{ik_o R^{\pm}} \Bigg|_{r = r_1}^{r = r_2} - \frac{2ik_o g}{\Delta^{\pm}} \int_{r_1}^{r_2} e^{ik_o R^{+}} dr$$

$$H_2^{\pm}(\phi) = \left[\left[\frac{2r(gr + 2f^{\pm})}{R^{\pm}} - \frac{2gR^{\pm}}{h} \right] \frac{e^{ik_o R^{\pm}}}{\Delta^{\pm}} \right]_{r = r_1}^{r = r_2}$$

$$- \frac{1}{h} \int_{r_1}^{r_2} \frac{e^{ik_o R^{\pm}}}{R^{\pm}} dr + \frac{ik_o g^2}{h\Delta^{\pm}} \int_{r_1}^{r_2} e^{ik_o R^{\pm}} dr \qquad \text{(C-76)}$$

$$x_c = a_1 + \ell_2 \qquad \text{(endcap of wing)}$$

$$N(\phi) = \left(a_2^2 \sin^2\phi + b_2^2 \cos^2\phi \right)^{1/2}$$

$$R^{\pm} = f^{\pm} + gr + hr^2$$

$$f^{\pm} = (x_{1\alpha} \mp x_c)^2 + x_{2\alpha}^2 + x_{3\alpha}^2$$

$$g = -2x_{3\alpha} b_2 \sin\phi - 2x_{2\alpha} a_2 \cos\phi$$

$$h = a_2^2 \cos^2\phi + b_2^2 \sin^2\phi$$

$$\Delta^{\pm} = 4f^{\pm}h - g^2 \qquad \text{(C-77)}$$

$\underline{A^{\pm} \text{ Matrix Term. Horizontal Stabilizer (i=3)}}$

Integrals $I_{13w}^{\pm}(t,s_o)$, $I_{13c}^{\pm}(t,s_o)$, $I_{23w}^{\pm}(t,s_o)$ and $I_{23c}^{\pm}(t,s_o)$ are given by formulas identical to those for the wing provided that a_2 is changed to a_3, b_2 to b_3 and $x_1 = y$, $x_2 = x - x_{03}$, $x_3 = -z$.

$\underline{A^{\pm}\text{ Matrix Term. Vertical Stabilizer (i=4, j=2)}}$

$$I^{\pm}_{14w}(t,s_o) = \frac{1}{4\pi}\int_{\phi_1}^{\phi_2} M^{\pm}_1(\phi)\left[\frac{e^{ik_oR^{\pm}_2}}{R^{\pm}_2} - \frac{e^{ik_oR^{\pm}_1}}{R^{\pm}_1}\right]d\phi$$

$$I^{\pm}_{24w}(t,s_o) = \frac{1}{4\pi}\int_{\phi_1}^{\phi_2} M^{\pm}_2(\phi)\,K^{\pm}(\phi)\,d\phi \qquad \text{(C-78)}$$

$$M^{\pm}_1(\phi) = \pm t_2\, b_4\cos\phi + t_3\, a_4 \sin\phi$$

$$M^{\pm}_2(\phi) = (\pm a_4 b_4 \mp x_{2\alpha}\, b_4\cos\phi - x_{3\alpha}\, a_4 \sin\phi)\, t_1 \qquad \text{(C-79)}$$

$$K^{\pm}(\phi) = \frac{1}{a_4^2}\left[\frac{e^{ik_oR^{\pm}_2}}{R^{\pm}_2}(x_{1\alpha} - x_{102}) - \frac{e^{ik_oR^{\pm}_1}}{R^{\pm}_1}(x_{1\alpha} - x_{101})\right]$$

$$+ \frac{ik_o}{a_4^2}\, e^{ik_oR^{\pm}_o}\int_{x_{101}}^{x_{102}} e^{ik_o(R^{\pm}-R^{\pm}_o)}\,dx_{10}$$

$$R^{\pm}(x_{10}) = [(x_{1\alpha} - x_{10})^2 + (x_{2\alpha} - a_4\cos\phi)^2 + (x_{3\alpha} \mp b_4\sin\phi)]^{1/2}$$

$$R^{\pm}_1 = R^{\pm}(x_{10} = x_{101})$$

$$R^{\pm}_2 = R^{\pm}(x_{10} = x_{102})$$

$$R^{\pm}_o = \frac{1}{2}(R^{\pm}_1 + R^{\pm}_2) \qquad \text{(C-80)}$$

$A^{\pm}$ Matrix Terms. Vertical Stabilizer (i=4,j=c)

$$I^{\pm}_{14c}(t,s_o) = \frac{a_4 b_4}{4\pi} \int_{\phi_1}^{\phi_2} K^{\pm}_1(\phi)\, H^{\pm}_1(\phi)\, d\phi$$

$$I^{\pm}_{24c}(t,s_o) = \frac{a_4 b_4}{4\pi} \int_{\phi_1}^{\phi_2} K^{\pm}_2(\phi)\, H^{\pm}_2(\phi)\, d\phi \qquad \text{(C-81)}$$

$$K^{\pm}_1(\phi) = [(x_{1\alpha} - x_c)(\pm t_2\, b_4 \cos\phi + t_3\, a_4 \sin\phi)$$

$$- t_1(\pm x_{2\alpha}\, b_4 \cos\phi + x_{3\alpha}\, a_4 \sin\phi)]/N(\phi)$$

$$K^{\pm}_2(\phi) = \pm t_1\, a_4 b_4 / N(\phi) \qquad \text{(C-82)}$$

$$H^{\pm}_1(\phi) = \frac{2g^{\pm}_r + 4f}{\Delta^{\pm} R^{\pm}}\, e^{ik_o R^{\pm}}\Big|_{r=r_1}^{r=r_2} - \frac{2ik_o g^{\pm}}{\Delta^{\pm}} \int_{r_1}^{r_2} e^{ik_o R^{+}}\, dr$$

$$H^{\pm}_2(\phi) = \left[\left[\frac{2r(g^{\pm}r + 2f)}{R^{\pm}} - \frac{2g^{\pm}R^{\pm}}{h}\right]\frac{e^{ik_o R^{\pm}}}{\Delta^{\pm}}\right]_{r=r_1}^{r=r_2}$$

$$= \frac{1}{h}\int_{r_1}^{r_2} \frac{e^{ik_o R^{\pm}}}{R^{\pm}}\, dr + \frac{ik_o (g^{\pm})^2}{h\Delta^{\pm}} \int_{r_1}^{r_2} e^{ik_o R^{\pm}}\, dr \qquad \text{(C-83)}$$

$$x_c = b_1 + \ell_4 \qquad \text{(endcap of vertical stabilizer)}$$

$$N(\phi) = \left(a_4^2 \sin^2\phi + b_4^2 \cos^2\phi\right)^{1/2}$$

$$R^{\pm} = f + g^{\pm} r + h r^2$$

$$f = (x_{1\alpha} - x_c)^2 + x_{2\alpha}^2 + x_3^2$$

$$g^{\pm} = -2x_{2\alpha}\, a_4 \cos\phi \mp 2x_{3\alpha}\, b_4 \sin\phi$$

$$h = a_4^2 \cos^2\phi + b_4^2 \sin^2\phi$$

$$\Delta^{\pm} = 4fh - (g^{\pm})^2 \qquad \text{(C-84)}$$

<u>$B^{\pm}$ Matrix Term. Fuselage (i=1, j=w)</u>

$$I_{11w}^{\pm}(t,t_o) = 0$$

$$I_{21w}^{+}(t,t_o) = \frac{1}{4\pi}\int_{\phi_1}^{\phi_2} M_2^{\pm}(\phi)\, K^{\pm}(\phi)\, d\phi \qquad \text{(C-85)}$$

$$M_2^{\pm}(\phi) = [t_3(x_{2\alpha} - a_1\cos\phi) - t_2(x_{3\alpha} \mp b_1 \sin\phi)]N(\phi) \qquad \text{(C-86)}$$

$K^{\pm}(\phi)$ are given by equations (C-65).

<u>$B^{\pm}$ Matrix Terms. Fuselage (i=1, j=c)</u>

$$I_{11c}^{\pm}(t,t_o) = \frac{a_1 b_1}{4\pi}\int_{\phi_1}^{\phi_2} K_1^{\pm}(\phi)\, H_1^{\pm}(\phi)\, d\phi$$

$$I_{21c}^{\pm}(t,t_o) = \frac{a_1 b_1}{4\pi}\int_{\phi_1}^{\phi_2} K_2^{\pm}(\phi)\, H_2^{\pm}(\phi)\, d\phi \qquad \text{(C-87)}$$

$$K_1^{\pm}(\phi) = (-1)^n \left[(x_{1\alpha} - x_c)\mp t_2\, a_1 \sin\phi - t_3\, b_1 \cos\phi\right)$$

$$-t_1(\pm x_{2\alpha}\, a_1 \sin\phi - x_{3\alpha}\, b_1 \cos\phi)]/N(\phi)$$

$$K_2^{\pm}(\phi) = \pm (-1)^n\, t_1\left(a_1^2 - b_1^2\right) \sin\phi \cos\phi/N(\phi) \qquad \text{(C-88)}$$

$H_1^{\pm}(\phi)$ and $H_2^{\pm}(\phi)$ are given by equation (C-68) through (C-70), $n = 0$ for the $x_c = 0$ endcap and $n = 1$ for the $x_c = \ell_1$ endcap.

<u>$B^{\pm}$ Matrix Term. Wing (i=2, j=w)</u>

$$I_{12w}^{\pm}(t,t_o) = 0$$

$$I_{22w}^{\pm}(t,t_o) = \frac{1}{4\pi}\int_{\phi_1}^{\phi_2} M_2^{\pm}(\phi)\, K^{\pm}(\phi)\, d\phi \qquad \text{(C-89)}$$

$$M_2^{\pm}(\phi) = [t_3(x_{2\alpha} - a_2 \cos\phi) - t_2(x_{3\alpha} - b_2 \sin\phi)]\, N(\phi), \quad (M_2^{+} = M_2^{-}) \qquad \text{(C-90)}$$

$K^{\pm}(\phi)$ is given by equation (C-73).

<u>$B^{\pm}$ Matrix Term. Wing (i=2, j=c)</u>

$$I_{12c}^{\pm}(t,t_o) = \frac{a_2 b_2}{4\pi}\int_{\phi_1}^{\phi_2} K_1^{\pm}(\phi)\, H_1^{\pm}(\phi)\, d\phi$$

$$I_{22c}^{\pm}(t,t_o) = \frac{a_2 b_2}{4\pi}\int_{\phi_1}^{\phi_2} K_2^{\pm}(\phi)\, H_2^{\pm}(\phi)\, d\phi \qquad \text{(C-91)}$$

$$K_1^{\pm}(\phi) = [(x_{1\alpha} \mp x_c)(t_3\, b_2 \cos\phi - t_2\, a_2 \sin\phi)$$

$$- t_1(x_{3\alpha}\, b_2 \cos\phi - x_{2\alpha}\, a_2 \sin\phi)]/N(\phi)$$

$$K_2^{\pm}(\phi) = -t_1(a^2 - b^2) \cos\phi \sin\phi, \quad (K_2^{+} = K_2^{-}) \tag{C-92}$$

$H_1^{\pm}(\phi)$, $H_2^{\pm}(\phi)$, x_c are given by equations (C-76) and (C-77).

$B^{\pm}$ Matrix Term. Horizontal Stabilizer (i=3)

Integrals $I_{13w}^{\pm}(t,t_o)$, $I_{23w}^{\pm}(t,t_o)$, $I_{13c}^{\pm}(t,t_o)$ and $I_{23c}^{\pm}(t,t_o)$ are given by formulas identical to those for the wing provided that a_2 is changed to a_3, b_2 to b_3 and $x_1 = y$, $x_2 = x - x_{03}$, $x_3 = -z$.

$B^{\pm}$ Matrix Terms. Vertical Stabilizer (i=4,j=w)

$$I_{14w}^{\pm}(t,t_o) = 0$$

$$I_{24w}^{\pm}(t,t_o) = \frac{1}{4\pi}\int_{\phi_1}^{\phi_2} M_2^{\pm}(\phi)\, K^{\pm}(\phi)\, d\phi \tag{C-93}$$

$$M_2^{\pm}(\phi) = [(x_{2\alpha} - a_4 \cos\phi)\, t_3 - (x_{3\alpha} \mp b_4 \sin\phi)\, t_2]\, N(\phi) \tag{C-94}$$

$K^{\pm}(\phi)$ is given by equation (C-80).

$B^{\pm}$ Matrix Terms. Vertical Stabilizer (i=4,j=c)

$$I_{14c}^{\pm}(t,t_o) = \frac{a_4 b_4}{4\pi}\int_{\phi_1}^{\phi_2} K_1^{\pm}(\phi)\, H_1^{\pm}(\phi)\, d\phi$$

$$I_{24c}^{\pm}(t,t_o) = \frac{a_4 b_4}{4\pi}\int_{\phi_1}^{\phi_2} K_2^{\pm}(\phi)\, H_2^{\pm}(\phi)\, d\phi \tag{C-95}$$

$$K_1^{\pm}(\phi) = [(x_{1\alpha} - x_c)(\mp t_2\, a_4 \sin\phi + t_3\, b_4 \cos\phi)$$

$$+ t_1(\pm x_{2\alpha}\, a_4 \sin\phi - x_{3\alpha}\, b_4 \cos\phi)]/N(\phi)$$

$$K_2^{\pm}(\phi) = \pm t_1(b^2 - a^2) \cos\phi \sin\phi/N(\phi) \qquad \text{(C-96)}$$

$H_1^{\pm}(\phi)$, $H_2^{\pm}(\phi)$, x_c are given by equations (C-83) and (C-84).

$C^{\pm}$ Matrix Terms

Integrals $I_{1ij}^{\pm}(s,s_o)$, $I_{2ij}^{\pm}$ are identical to those calculated for the $A^{\pm}$ terms provided that $t_m(m = 1,2,3)$ are substituted by $s_m(m = 1,2,3)$.

$D^{\pm}$ Matrix Terms

Integrals $I_{1ij}^{\pm}(s,t_o)$, $I_{2ij}^{\pm}(s,t_o)$ are identical to those calculated for the $B^{\pm}$ forms provided $t_m(m = 1,2,3)$ are substituted by $s_m(m = 1,2,3)$.

6. SELF-ZONE INTERACTION

When the observation point $\underline{r}_\alpha$ is the central point of a zone over which we integrate we talk about self-zone interaction or self-zone terms. The integration variable $\underline{r}_o$ ranges over the entire zone and consequently $\underline{r}_o = \underline{r}_\alpha$ at the central point. What about the resulting singularities in the integrand? If we examine the $A^{\pm}$, $B^{\pm}$, $C^{\pm}$ and $D^{\pm}$ matrix terms we see that the only terms of concern are those of the form

$$\int_{\phi_1}^{\phi_2} K_2^{+}(\phi)\, d\phi \int_{r_1}^{r_2} \frac{e^{ik_o R^{+}}}{R^{+}}\, dr$$

(The A^{+}, B^{-}, C^{-} and D^{-} matrix element cannot involve self-terms because $\underline{R} \cdot \underline{r}_o \neq \underline{r}_\alpha$.) The integration is over a zone on the cap $K_2^{+}(\phi)$ has the form $t_1\, ab/N(\phi)$ or $t_1(a^2 - b^2) \sin\phi \cos\phi/N(\phi)$. But when $\underline{r}_\alpha$ is on the cap, $t_1 \equiv 0$ and the potentially troublesome integral is identically equal to zero. In conclusion, all equations giving the $A^{\pm}$, $B^{\pm}$, $C^{\pm}$ $D^{\pm}$ terms are valid for both zone to zone or self-zone interactions.

7. INTERPOLATION

In this section we explain the interpolation scheme that allows us to evaluate the current density at points other than the centers of the zones on the surface of the aircraft.

As we discussed in Section 3 of this appendix one uses equations (C-9) to evaluate the fictitious current components $J^{\pm}_{s,t}$ at the centers of the zones. Notice, however that the variable α in equations (C-9) is not restricted to represent the center of a zone. Such restriction is true only for α_o. Thus we can use equations (C-9) to evaluate $J^{\pm}_{s,t}$ at any point (see section 9 for points near edges and junctions) on the surface of the aircraft in terms of $J^{\pm}_{s,t}$ at the centers of the zones. The real current density components $J_{s,t}$ can then be calculated with the aid of equation (C-10).

8. CHARGE DENSITY

The charge density σ can be calculated with the aid of the continuity equation

$$i\omega\sigma = \nabla_s \cdot \underline{J} \tag{C-99}$$

where $\nabla_s \cdot \underline{J}$ is the surface divergence of $\underline{J}$. We approximate directional derivatives by central difference quotients. We can therefore write the divergence of $\underline{J}$ as

$$\nabla_s \cdot \underline{J} \equiv \frac{\partial J_s(\underline{r})}{\partial s} + \frac{\partial J_t(\underline{r})}{\partial t}$$

$$\approx \frac{J_s(\phi+\Delta\phi,t) - J_s(\phi-\Delta\phi,t)}{(\Delta C)_s} + \frac{J_t(\phi,t+\Delta t) - J_t(\phi,t-\Delta t)}{(\Delta C)_t}$$

where $(\Delta C)_s$ and $(\Delta C)_t$ are the chords between points $(\phi+\Delta\phi,t)$, $(\phi-\Delta\phi,t)$ and points $(\phi,t+\Delta t)$, $(\phi,t-\Delta t)$ respectively. In the above equation the values of J_s and J_t are calculated through the interpolation scheme as we explained

in the previous section. If J_t and J_s could be calculated with unlimited accuracy and it were possible to calculate the desired differences with similar accuracy, then as Δt and $\Delta\phi$ approach zero the error of the approximation to $\nabla_s \cdot \underline{J}$ would approach zero. However, since the interpolation formula is an approximation to equations (6) based on a finite number of current density values we understand that $\Delta J_s/(\Delta C)_s$ and $\Delta J_t/(\Delta C)_t$ depend on the accuracy of $J_s(\phi+\Delta\phi,t)$, $J_s(\phi-\Delta\phi,t)$, $J_t(\phi,t+\Delta t)$ and $J_t(\phi,t-\Delta t)$. If we introduce the relative errors

$$\alpha_s = \frac{J_s^e - J_s}{J_s^e} \qquad \alpha_t = \frac{J_t^e - J_t}{J_t^e}$$

where the superscript e stands for exact, then:

$$\text{numerical divergence} \equiv \text{"}\nabla_s \cdot \underline{J}\text{"} = \frac{\Delta J_s^e}{(\Delta C)_s} + \frac{\Delta J_t^e}{(\Delta C)_t} - \frac{\Delta(\alpha_s J_s^e)}{(\Delta C)_s} - \frac{\Delta(\alpha_t J_t^e)}{(\Delta C)_t}$$

In the limit $(\Delta C)_s \to 0$, $(\Delta C)_t \to 0$ we have

$$\frac{\Delta J_s^e}{(\Delta C)_s} + \frac{\Delta J_t^e}{(\Delta C)_t} = \frac{\partial J_s^e}{\partial s} + \frac{\partial J_t^e}{\partial s} = i\omega\sigma^e$$

and

$$i\omega\sigma = \text{"}\nabla_s \cdot \underline{J}\text{"} = i\omega\sigma^e - \alpha_s \frac{\partial J_s^e}{\partial s} - J_s^e \frac{\partial \alpha_s}{\partial s} - \alpha_t \frac{\partial J_t^e}{\partial t} - J_t^e \frac{\partial \alpha_t}{\partial t}$$

$$= i\omega\sigma^e - i\omega\sigma^e\alpha_s + \frac{\partial J_t^e}{\partial t}(\alpha_s - \alpha_t) + J_s^e \frac{\partial \alpha_s}{\partial s} + J_t^e \frac{\partial \alpha_t}{\partial t}$$

$$\alpha_\sigma = \frac{\sigma^e - \sigma}{\sigma^e} = \alpha_s - \frac{1}{i\omega\sigma_e}\left[(\alpha_s - \alpha_t)\frac{\partial J_t^e}{\partial t} + J_s^e \frac{\partial \alpha_s}{\partial s} + J_t^e \frac{\partial \alpha_t}{\partial t}\right] \qquad \text{(C-100)}$$

For regions where the error varies slowly with position, $J_s^e(\partial\alpha_s/\partial s) + J_t(\partial\alpha_t/\partial t)$ can be smaller than the first term in the square brackets. Equation (C-100) then shows that in the low frequency limit the numerical calculation of the charge density can be very inaccurate. When $(\Delta C)_s$ and $(\Delta C)_t$ are finite the error α_s will be given by equation (C-100) plus correction terms, but the low-frequency problem will persist even though it may be lessened.

The above treatment is by no means complete but it provides insight into the difficulties that beset the numerical calculation of the charge density with the aid of the continuity equation as required in the work statement for this proposal.

Due to time constraints we did not explore a different method that is based on solving an integral equation for σ whose source term involves the normal component of the incident electric field and an integral over $\underline{J}$. The equation is

$$\frac{i\omega}{2}\sigma(\underline{r}) = i\omega\epsilon\,\hat{n}(\underline{r}) \cdot \underline{E}_i(\underline{r}) - \int_S \left[k_o^2 G(R)\,\hat{n}(\underline{r}) \cdot \underline{J}(\underline{r}_o)\right.$$

$$\left. + i\omega\sigma(\underline{r}_o)\,\hat{n}(\underline{r}) \cdot \nabla_s G(R)\right] dS_o$$

where

$$G(R) = \frac{e^{ik_oR}}{4\pi R} \qquad R = |\underline{r} - \underline{r}_o|$$

Using the same zoning scheme as for the solution for $\underline{J}$ we can calculate σ at the centers of the zones and subsequently at any point through our interpolation scheme.

9. EDGE AND JUNCTION BEHAVIOR

In this section we will discuss the behavior of the surface currents paying particular attention to the effects of discontinuities in surface normals. We define an edge (junction) to have more (less) air than metal in the vicinity of the discontinuity. We begin our discussion by rewriting equation (1) in component form

$$\frac{1}{2} J_s(\underline{r}) = J_{is}(\underline{r}) + \int_S K_A(\underline{r};\underline{r}_o)\, J_s(\underline{r}_o)\, dS_o + \int_S K_B(\underline{r};\underline{r}_o)\, J_t(\underline{r}_o)\, dS_o \qquad \text{(C-101a)}$$

$$\frac{1}{2} J_t(\underline{r}) = J_{it}(\underline{r}) + \int_S K_C(\underline{r};\underline{r}_o)\, J_s(\underline{r}_o)\, dS_o + \int_S K_D(\underline{r};\underline{r}_o)\, J_t(\underline{r}_o)\, dS_o \qquad \text{(C-101b)}$$

where the kernels K_A, K_B, K_C, K_D are defined as

$$K_A = (\underline{r} - \underline{r}_o) \cdot (\hat{t} \times \hat{s}_o)\, F(k_oR)/R^3$$

$$K_B = (\underline{r} - \underline{r}_o) \cdot (\hat{t} \times \hat{t}_o)\, F(k_oR)/R^3$$

$$K_C = -(\underline{r} - \underline{r}_o) \cdot (\hat{s} \times \hat{s}_o)\, F(k_oR)/R^3$$

$$K_D = -(\underline{r} - \underline{r}_o) \cdot (\hat{s} \times \hat{t}_o)\, F(k_oR)/R^3 \qquad \text{(C-102)}$$

$$F(k_oR) = (-1 + ik_oR)\frac{e^{ik_oR}}{4\pi}$$

$$R = |\underline{r} - \underline{r}_o| \qquad \text{(C-103)}$$

We proceed by examining the behavior of the kernels and their integrals $I_K(\underline{r}) = \int K(\underline{r};\underline{r}_o)\, dS_o$. We notice that each of the kernels are unbounded as R approaches zero, and, since $|F| \leq 2$ the kernels are well behaved everywhere else. In addition $I_K(\underline{r})$ will be bounded whenever the triple product involved decreases as fast as $R^{1+\varepsilon}$, $\varepsilon > 0$, as $\underline{r}_o$ approaches $\underline{r}$. If the surface has continuous curvature in the vicinity of the reference point, $\underline{r}$, the three vectors smoothly approach being coplanar making $\varepsilon \geq 1$. Thus our kernels vary no faster than 1/R and consequently the kernels have an integrable singularity (see reference 10 for a rigorous treatment of the case that results in $\varepsilon = 1$). However, if $\underline{r}$ is near a discontinuity in curvature the above reasoning may fail and $I_K(\underline{r})$ may be unbounded. We will now specifically treat the behavior of the kernels in the vicinity of a discontinuity in the direction of the normal (i.e., for edges and junctions) and then discuss the theoretical and numerical consequences.

We present our arguments by considering two plates intersecting at right angles. More complicated geometries as they appear in our model would not change our results but they would make our arguments harder to follow. If we expand $F(k_o|\underline{r} - \underline{r}_o|)$ in a MacLaurin series we see that only the zeroth order term will contribute to the singularity of our integrands. We therefore confine our attention to $k_o = 0$.

Our model is depicted in figure C3. We choose $\hat{s}$ on both plates to be parallel to the intersection of the plates and let $\hat{t} = \hat{n} \times \hat{s}$. If we treat our intersection as a junction our surface vectors become

$$\hat{s}_1 = \hat{s}_2 = \hat{e}_y,\ \hat{n}_1 = \hat{e}_z,\ \hat{n}_2 = -\hat{e}_x,\ \hat{t}_1 = -\hat{e}_x \text{ and } \hat{t}_2 = -\hat{e}_z \qquad \text{(C-104)}$$

We place the reference point on plate 1 and limit our attention to a rectangular patch (denoted by S_2) on plate 2 which includes the point on

---

10. Marin, L. and R. W. Latham, Analytical Properties of the Field Scattered by a Perfectly Conducting, Finite Body, Interaction Note 92, Air Force Weapons Laboratory, January 1972.

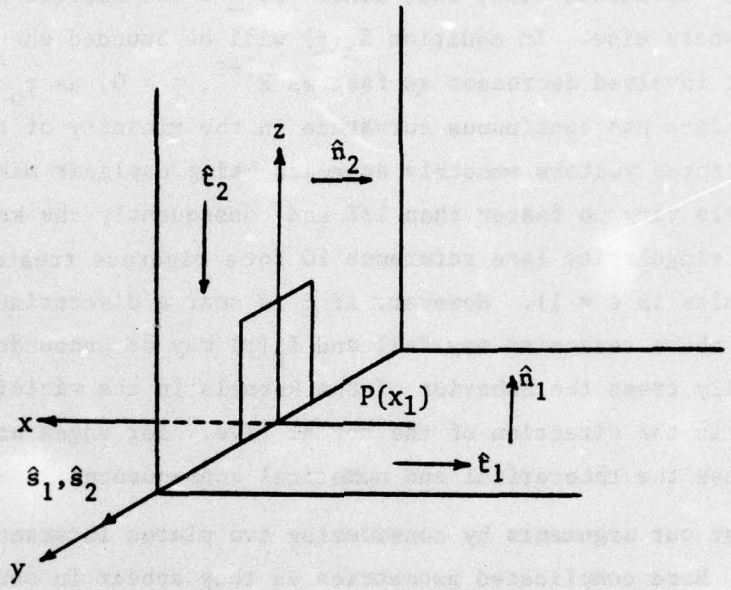

Figure C3: Two metallic plates intersecting at right angles and description of $\hat{n}$, $\hat{s}$, $\hat{t}$.

plate 2 closest to the reference point since only that patch can cause a singular integral. The integrals over that patch are then

$$\int_{S_2} K_A \, dS_o \equiv A = \frac{-1}{4\pi} \int_{-s}^{s} \int_{o}^{b} \frac{(\hat{t}_1 \times \hat{s}_2) \cdot \underline{r}_{12}}{R^3} \, dz_2 \, dy_2$$

$$\int_{S_2} K_B \, dS_o \equiv B = \frac{-1}{4\pi} \int_{-s}^{s} \int_{o}^{b} \frac{(\hat{t}_1 \times \hat{t}_2) \cdot \underline{r}_{12}}{R^3} \, dz_2 \, dy_2$$

$$\int_{S_2} K_C \, dS_o \equiv C = \frac{1}{4\pi} \int_{-s}^{s} \int_{o}^{b} \frac{(\hat{s}_1 \times \hat{s}_2) \cdot \underline{r}_{12}}{R^3} \, dz_2 \, dy_2$$

$$\int_{S_2} K_D \, dS_o \equiv D = \frac{1}{4\pi} \int_{-s}^{s} \int_{o}^{b} \frac{(\hat{s}_1 \times \hat{t}_2) \cdot \underline{r}_{12}}{R^3} \, dz_2 \, dy_2 \qquad \text{(C-105)}$$

where $\underline{r}_{12} = \underline{r}_1 - \underline{r}_2$, and we have chosen $y_1 = 0$.

$\hat{s}_1$ equals $\hat{s}_2$ making C identically zero and $\hat{t}_1 \times \hat{t}_2$ equals $-\hat{e}_y$ making K_B antisymmetric in y_2; thus both B and C are well behaved. For the geometries of our model it can be shown that both K_B and K_C vary no faster than $1/R$ as $\underline{r} \to \underline{r}_o$, even in the presence of a discontinuity and consequently are well behaved.

The integral D is also well behaved but for a much more subtle reason. Carrying out the integrations, we have

$$D = \frac{-1}{4\pi} \int_{-s}^{s} \int_{o}^{b} \frac{x_1 \, dz_2 \, dy_2}{(x_1^2 + y_2^2 + z_2^2)^{3/2}} = -2x_1 \int_{o}^{s} \frac{z_2 \, dy_2}{(x_1^2 + y_2^2)(x_1^2 + y_2^2 + z_2^2)^{1/2}} \Bigg|_{z_2 = 0}^{z_2 = b}$$

$$= \frac{1}{2\pi} \tan^{-1} \frac{y_2 \, z_2}{|x_1| \sqrt{x_1^2 + y_2^2 + z_2^2}} \Bigg|_{z_2 = 0}^{z_2 = b} \Bigg|_{y_2 = 0}^{y_2 = s} \qquad \text{(C-106)}$$

This expression is bounded for all values of the parameters. The saving feature of this integral is that the proportionality factor x_1 is not an integration variable. This feature will also be present for more complicated geometries.

Unlike the situation for D, the proportionality factor of $1/R^3$ in A is the integration variable whose limits are both on the same side of zero. The result is

$$A = \frac{-1}{4\pi} \int_{-s}^{s} \int_{o}^{b} \frac{z_2 \, dz_2 \, dy_2}{(x_1^2 + y_2^2 + z_2^2)^{3/2}} = \frac{1}{2\pi} \int_{o}^{s} \frac{dy_2}{(x_1^2 + y_2^2 + z_2^2)^{1/2}} \Bigg|_{z_2 = 0}^{z_2 = b}$$

$$= 2 \log \left[(z_2^2 + y_2^2 + x_1^2)^{1/2} + y_2 \right] \Bigg|_{z_2 = 0}^{z_2 = b} \Bigg|_{y_2 = 0}^{y_2 = s} \qquad \text{(C-107)}$$

which is unbounded as x_1 approaches zero, that is, $A \to 2\log |x_1| \to -\infty$.

The theoretical consequences of the above discussion are very interesting. Under the assumption that both J_s and J_t are everywhere integrable in either the "t" or "s" direction, equation (C-101a) shows that J_s may not be infinite except at a discontinuity and may be infinite or zero but not finite near a discontinuity. The latter point is true since if J_s is assumed to be

bounded away from zero but not infinite the left-hand side is finite yet the right-hand side displays a logarithmic singularity as $\underline{r}$ approaches the border. The former point follows from the boundedness of the integrals.

To continue our discussion we must now distinguish between junctions and edges. Our discussion of the behavior of a kernel assumed a junction and showed that A was negative. For an edge we must reverse the direction of $\hat{n}$ causing $\hat{t}$ to reverse direction and we therefore find that A is positive. This distinction is critical, for by rewriting equation (C-101a) as

$$\frac{1}{2} J_s(r) = \int_{s_2} K_A J_s(r_o) \, dS_o + \sum \text{finite terms} \qquad \text{(C-108)}$$

we see from the requirement that the limit of $J_s(\underline{r})$ as $\underline{r}$ approaches the border be the same if we approach from either side of the discontinuity that when A is negative $J_s(r_o)$ cannot be infinite, but, when A is positive $J_s(r_o)$ can be infinite. Thus J_s at the junction must be zero. Furthermore, the need for the singular behavior on the two sides of equation (C-108) to exactly balance, greatly restricts the type of singularity that can exist at the edge. This restriction enables us to determine the nature of the singularity as will be illustrated by returning to the wedge problem considered earlier. We assume that near the edge

$$J_s(\underline{x}_1) = c|x_1|^p \ , \quad J_s(z_2) = cz_2^p, \quad -1 < p < 0 \qquad \text{(C-109)}$$

(We want $-1 < p$ so that J_s is integrable and $p < 0$ so that J_s is singular at $x_1 = 0$.) We require

$$I_A \equiv \frac{-c}{4\pi} \int_{-s}^{s} \int_{o}^{b} \frac{z_2^{p+1} \, dz_2 \, dy_2}{(x_1^2 + y_2^2 + z_2^2)^{3/2}} = \frac{c}{2} |x_1|^p \qquad \text{(C-110)}$$

As $x_1 \to 0$ then $x_1/s \to 0$, $x_1/b \to 0$ and substitutions $y = y_2/|x_1|$ and $z = z_2/|x_1|$ transform the integral

$$I_A = \frac{c|x_1|^p}{4\pi} \int_{-\infty}^{\infty} \int_0^{\infty} \frac{z^{p+1}\, dz\, dy}{(1 + y^2 + z^2)^{3/2}} = \frac{c|x_1|^p}{2\pi} \int_0^{\infty} \frac{z^{p+1}\, dz}{1 + z^2} \tag{C-111}$$

Since $-1 < p < 0$ we can perform contour integration for the final integral obtaining

$$I_A = c\, \frac{|x_1|^p}{2}\, \frac{\sin[\pi/2(p+1)]}{\sin[\pi(p+1)]} \tag{C-112}$$

The only simultaneous solution to equations (C-112) and (C-110) for which $-1 < p < 0$ is $p = -1/3$. Thus near a right angled edge

$$J_s(x_1) = c|x_1|^{-1/3} \tag{C-113}$$

This result may be derived by a number of different approaches (see for example, ref. 11). Notice that when $c = 0$ equation (C-110) is automatically satisfied. Whether J_s is zero or infinite for an edge depends on the polarization of the incident wave.

A similar discussion for equation (C-101b) shows that J_t may not become unbounded at an edge since for an edge D is negative. To eliminate the possibility of an unbounded J_t at a junction, we appeal to the continuity equation

---

11. Collin, R. E., Field Theory of Guided Waves, McGraw-Hill Book Company, Inc., New York, 1969, pp. 18-20.

$$\nabla \cdot \underline{J} = i\omega\sigma, \quad \frac{\partial J_s}{\partial s} + \frac{\partial J_t}{\partial t} = i\omega\sigma \qquad \text{(C-114)}$$

and note that J_s, $\partial J_s/\partial s$, and σ must be zero for a junction. This requires that $\partial J_t/\partial t = 0$ which is impossible if $J_t(x_1)$ is to be finite for $|x_1| < 0$ and infinite at $x_1 = 0$.

The numerical consequences of the above discussions are very straightforward. A basic premise of the patch zoning technique is that J_s can be considered to be nearly constant over a patch. If J_s varies as $z^{-1/3}$ the patches must shrink to zero area in order to keep J_s nearly constant over a patch; this would require an infinite number of zones which would make costs prohibitive and probably make the matrix very ill-conditioned. We must therefore accept the fact that calculated values for J_s very close to the edge will be relatively inaccurate. Near a junction the boundary condition that J_s along the intersection be zero may make J_s change rapidly in the vicinity of the intersection, but since the change is finite it will be sufficient to slightly increase the zone density on both sides of the junction to obtain substantially accurate results.

The presence of junctions and edges has profound effects on our interpolation procedure. Since an interpolation procedure cannot be more reliable than the data it has to work with, the interpolation will fail near an endcap. In addition, since A has a logarithmic singularity as the observation point approaches a discontinuity, the interpolation procedure predicts an infinity whether the discontinuity is an edge or a junction. To avoid this troublesome fact near a junction we suggest that no attempt be made to determine the current density at any point closer to the junction than the reference points of the layer zones closest to the junction. If values close to the junction are desired the reference points on both sides of the junction should be equally close to the junction. Also a zone should not be significantly smaller than its nearest neighbors.

In concluding this section we would like to dispell any doubts that the prediction of currents away from the endcaps will greatly suffer as a result of the limited accuracy of J_s at the endcap. The integral

equation that we deal with is very stable. The kernel is singular at $\underline{r}_o = \underline{r}$ making the currents in the immediate vicinity of a point, the dominant influence. Therefore the singular behavior will tend to damp out as we move away from the endcap. The error committed by approximating the singularity by a finite quantity will barely effect the results. As evidence of what we say, we presented in Section IV, the results of an experimental comparison between uncapped cylinders, flat capped cylinders and hemispherically capped cylinders. Even though the theoretical behavior of J_s near the edge is $x^{-1/2}$, $x^{-1/3}$ and x^0 for the three respective cases the plots of J_t do not show any appreciable difference due to the varying boundary conditions. As evidence of the accuracy of our programm a quick look at figures 6 through 8 will show that the effects of the external edge did not greatly effect our ability to predict the currents on a cylinder at distances as close to the edge as our zone size.

APPENDIX D

INTERSECTIONS

In this appendix we consider the intersection between the elliptical bodies-components of the aircraft and show how their presence modifies (a) the coordinates at the centers of zones adjacent to the intersections and (b) the matrix element associated with these zones.

1. COORDINATES

a. Zones Adjacent to Fuselage - Wing Intersections

(1) Zones on Fuselage (figure D1)

We assume that the planes $x = x_{02}$ and $z = 0$ form walls for zones on the fuselage. Also only one layer of zones is intersected for both $z > 0$ and $z < 0$. (That is, zones that would exist in the absence of the intersection.) If the center of a zone (as defined in Appendix C, equation (C-18), where no intersections were assumed) has an x-coordinate such that $x < x_{02} - a_2$ or $x > x_{02} + a_2$ then the coordinates at the center of this zone are unaffected by the presence of the intersection.

If $x_{02} + a_2 > x > x_{02} - a_2$ then:

$$x(\alpha) = x_k \qquad s_x(\alpha) = 0 \qquad t_x(\alpha) = 1$$

$$y(\alpha) = b_1 \sin\phi \qquad s_y(\alpha) = \frac{b_1 \cos\phi}{N_1(\phi)} \qquad t_y(\alpha) = 0$$

$$z(\alpha) = -a_1 \cos\phi \qquad s_z(\alpha) = \frac{a_1 \sin\phi}{N_1(\phi)} \qquad t_z(\alpha) = 0 \qquad \text{(D-1)}$$

where

$$\phi = \phi_j \pm \frac{1}{2}\phi^* \quad (+ \text{ for } z > 0 \text{ and } - \text{ for } z < 0)$$

$$\phi^* = \sin^{-1}\frac{z^*}{a_1} \qquad z^* = b_2\left(1 - \frac{x^{*2}}{a_2^2}\right)^{1/2}$$

$$x^* = x_{02} - x_k$$

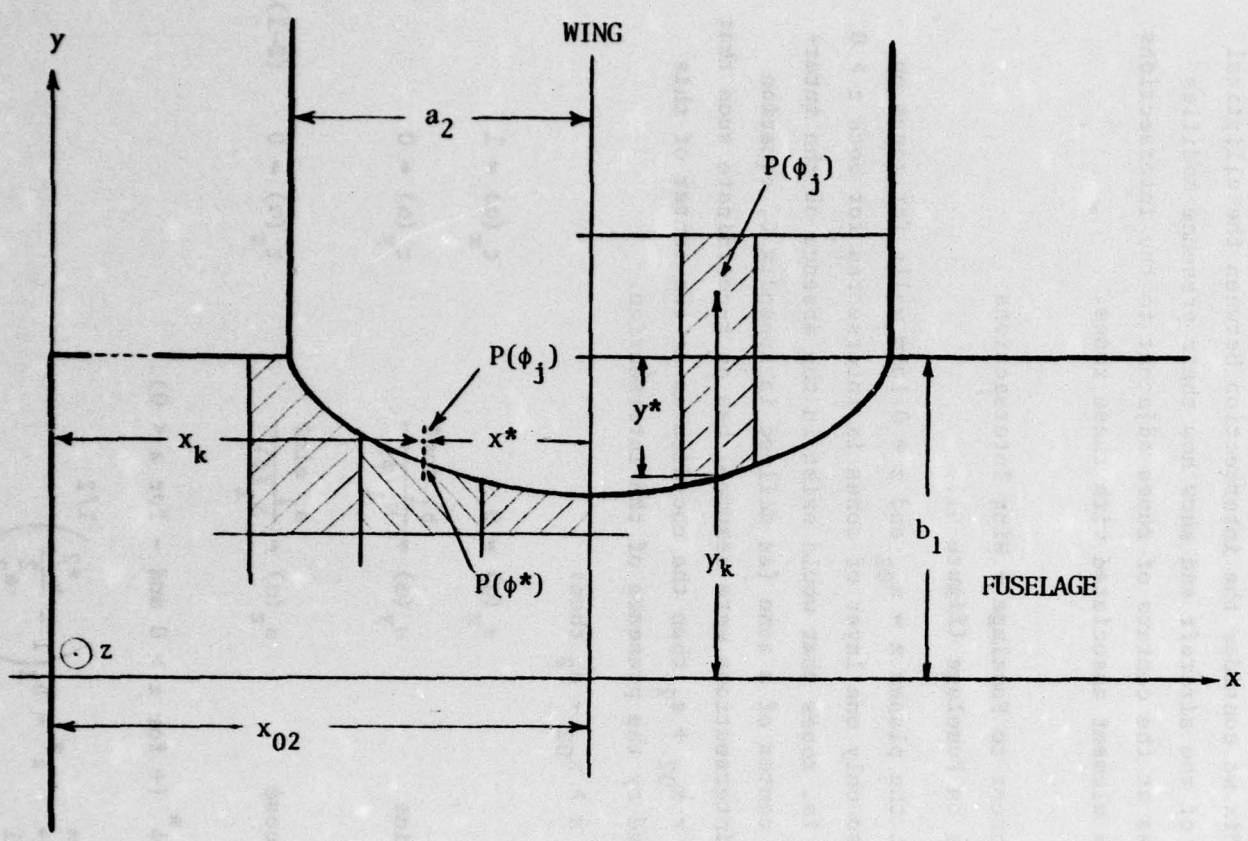

Figure D1: Geometry at the fuselage-wing intersection for the calculation of modified coordinates at the centers of zones near the junction.

and ϕ_j, x_k, $N_1(\phi)$ are given by equations (C-18).

(2) Zones on Wing (figure D1)

The new coordinates at the center of the zones adjacent to the intersection are

$$x(\alpha) = x_{02} + a_2 \cos\phi_j \qquad s_x(\alpha) = \frac{-a_2 \sin\phi_j}{N_2(\phi_j)}, \quad t_x(\alpha) = 0$$

$$y(\alpha) = y_k - \frac{1}{2} y^* \qquad s_y(\alpha) = 0, \quad t_y(\alpha) = 1$$

$$z(\alpha) = -b_2 \sin\phi_j \qquad s_z(\alpha) = -\frac{b_2 \cos\phi_j}{N_2(\phi_j)}, \quad t_z(\alpha) = 0 \qquad \text{(D-2)}$$

where ϕ_j, y_k, $N_2(\phi)$ are given by equations (C-22) and

$$y^* = b_1 \left[1 - \left(1 - \frac{b_2^2 \sin^2\phi_i}{a_1^2} \right)^{1/2} \right]$$

b. Zones Adjacent to Fuselage - Horizontal Stabilizer

(1) Zones on Fuselage

The new coordinates of the zones are derived by the same assumptions as for the wing and are identical to the ones given by equations (D-1) provided we replace x_{02}, b_2, a_2 by x_{03}, b_3, a_3 respectively.

(2) Zones on Horizontal Stabilizer

The new coordinates are derived by the same assumptions as for the wing and are given by equations (D-2) provided we replace x_{02}, a_2, b_2, N_2 by x_{03}, b_3, a_3, N_3 respectively and refer to equations (C-24) instead of (C-22).

c. Zones Adjacent to Fuselage - Vertical Stabilizer Intersection

(1) Zones on Fuselage (figure D2)

We assume that the $y = 0$ and $x = x_{04}$ planes form natural boundaries for zones on the fuselage. As with the fuselage-wing intersection we

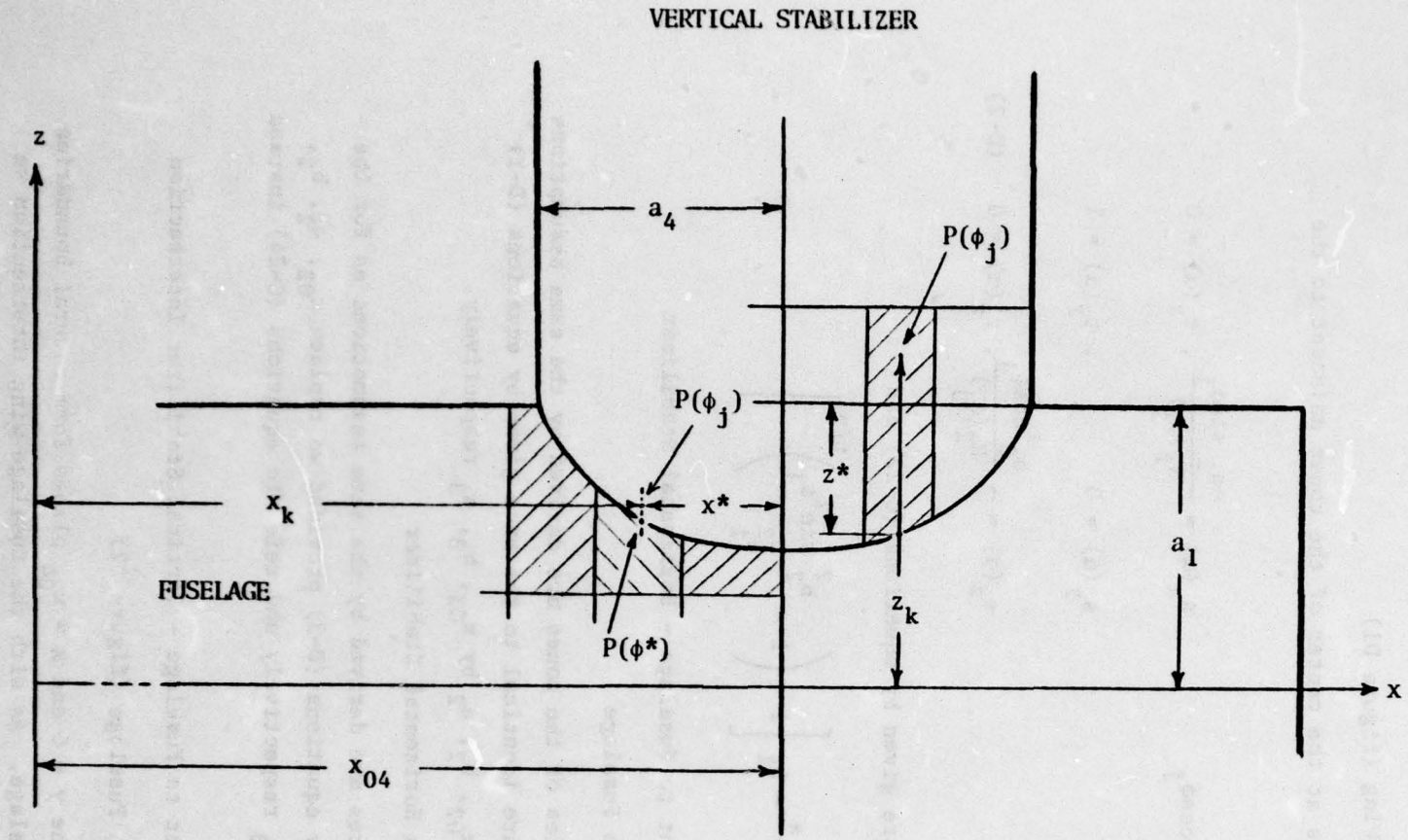

Figure D2: Geometry at the fuselage-vertical stabilizer intersection for the calculation of modified coordinates at the centers of zones near the junction.

again assume there is only one layer of zones intersected. The new coordinates are given by

$$x(\alpha) = x_k \qquad s_x(\alpha) = 0 \qquad , t_x(\alpha) = 1$$

$$y(\alpha) = a_1 \sin\phi \qquad s_y(\alpha) = \frac{a_1 \cos\phi}{N_1(\phi)} \quad , t_y(\alpha) = 0$$

$$z(\alpha) = -b_1 \cos\phi \qquad s_z(\alpha) = \frac{b_1 \sin\phi}{N_1(\alpha)} \quad , t_z(\alpha) = 0 \qquad \text{(D-3)}$$

where

$$\phi = \phi_j - \frac{1}{2}\phi^*$$

$$\phi^* = \sin^{-1}\frac{y^*}{a_1} \qquad y^* = b_4\left(1 - \frac{x^{*2}}{a_4^2}\right)^{1/2}$$

$$x^* = x_{04} - x_k$$

and ϕ_j, x_k, $N_1(\phi)$ are given by equations (C-18).

(2) Zones on Vertical Stabilizer (figure D2)

The new coordinates are

$$x(\alpha) = x_{04} + a_4 \cos\phi_j \qquad s_x(\alpha) = -\frac{a_4 \sin\phi_j}{N_4(\phi_j)} \quad , t_x(\alpha) = 0$$

$$y(\alpha) = b_4 \sin\phi_j \qquad s_y(\alpha) = \frac{b_4 \cos\phi_j}{N_4(\phi_j)} \quad , t_y(\alpha) = 0$$

$$z(\alpha) = z_k - \frac{1}{2}z^* \qquad s_z(\alpha) = 0 \qquad , t_z(\alpha) = 1 \qquad \text{(D-4)}$$

where

$$z^* = a_1\left[1 - \left(1 - \frac{b_4^2 \sin^2\phi_j}{b_1^2}\right)^{1/2}\right]$$

and ϕ_j, z_k, N_4 are given by equation (C-28).

2. MATRIX ELEMENTS

As we explained in Appendix C we calculated the matrix elements (equations (C-63) through (C-96)) by employing auxiliary local coordinate systems, attached to each cylindrical body, such that x_1 was along the axis of the body. The formulas giving the matrix elements must eventually be expressed in terms of the global coordinate system (figure 1) through transformation (C-30a) and (C-30b). (In the computer code the matrix elements are calculated in the global system.) In this subsection, we present the matrix elements in terms of the local coordinate systems. Notice that only zones on the walls are affected.

a. Zones Adjacent to Fuselage - Wing Intersection

(1) Zones on Fuselage (figure D3)

Figure 21 shows how we subdivide the zones adjacent to the intersection into subzones (1) and (2). First we will restrict our attention to $z > 0$, $x < x_{02}$ (figure 21).

(a) Region $z > 0$, $x < x_{02}$

The matrix elements $A^{\pm}$ are given by equations (C-63) through (C-65) with the following changes. For subzones labeled (1) in figure D3 we replace ϕ_1, ϕ_2 (as they appear in these equations) by ϕ_3, ϕ_2 respectively where

$$\phi_3 = \cos^{-1}\left[\frac{b_2}{a_1}\left(1 - \frac{(x_{02} - x_{102})^2}{a_2^2}\right)^{1/2}\right] \qquad \text{(D-5)}$$

and ϕ_2 defines a straight boundary of the zone. For subzones labeled (2) in figure 21, ϕ_1, ϕ_2, x_{101}, x_{102} (as they appear in equations (C-63) through (C-65)) are replaced by ϕ_1, ϕ_3, x_{101}, $x_1(\phi)$ (figure D3) respectively, where for $x_{02} - x_{101} \leq a_2$.

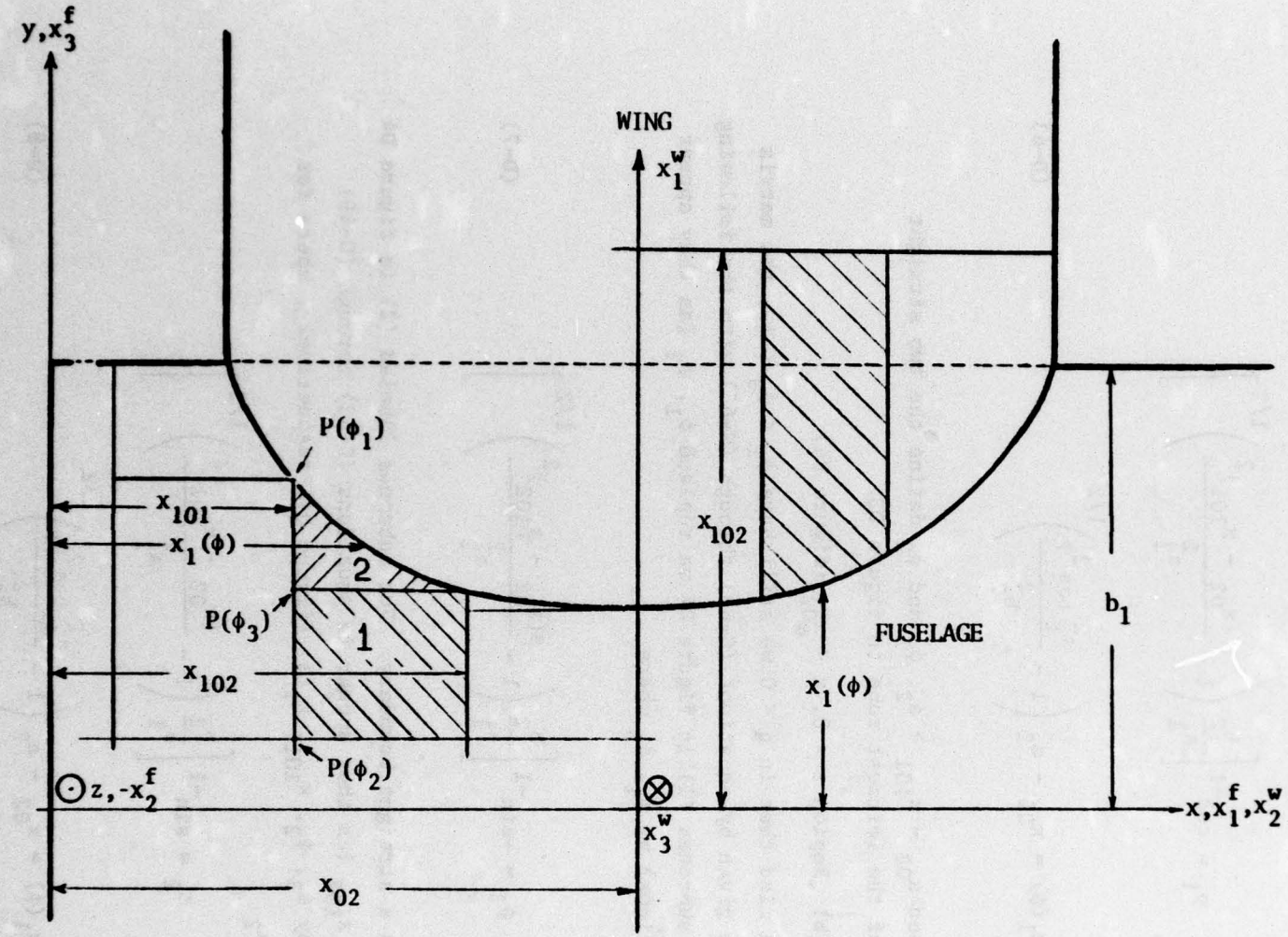

Figure D3: Geometry at the fuselage-wing intersection for the calculation of matrix elements involving zones near the junction. (Zones on fuselage correspond to $z > 0$, $x < x_{02}$.)

$$\phi_1 = \cos^{-1}\left[\frac{b_2}{a_1}\left(1 - \frac{(x_{02} - x_{101})^2}{a_2^2}\right)^{1/2}\right]$$

$$x_1(\phi) = x_{02} - a_2\left(1 - \frac{a_1^2 \cos^2\phi}{b_2^2}\right)^{1/2} \qquad \text{(D-6)}$$

Notice that when $x_{02} - x_{101} > a_2$, ϕ_1 and ϕ_2 define the two straight ϕ-boundaries of the leftmost zone in figure D3.

(b) Region $z < 0$, $x < x_{02}$ (figure D4)

Keeping in mind that in $q < 0$ we still have $\phi_1 < \phi_3 < \phi_2$, the matrix element $A^{\pm}$ are given by equations (C-63) through (C-65) with the following changes. For subzones (1) in figure D4 we replace ϕ_1, ϕ_2 (as they appear in these equations) by ϕ_1, ϕ_3 where

$$\phi_3 = -\sin^{-1}\left[\frac{b_2}{a_1}\left(1 - \frac{(x_{02} - x_{102})^2}{a_2^2}\right)^{1/2}\right] \qquad \text{(D-7)}$$

and ϕ_1 defines a straight boundary. For subzones labeled (2) in figure D4 ϕ_1, ϕ_2, x_{101}, x_{102} (as they appear in equations (C-63) through (C-65) are replaced by ϕ_3, ϕ_2, x_{101}, $x_1(\phi)$ (figure D4) respectively, where for $x_{02} - x_{101} \leq a_2$

$$\phi_2 = \sin^{-1}\left[\frac{b_2}{a_1}\left(1 - \frac{(x_{02} - x_{101})^2}{a_2^2}\right)^{1/2}\right]$$

$$x_1(\phi) = x_{02} - a_2\left(1 - \frac{a_1^2 \cos^2\phi}{b_2^2}\right)^{1/2} \qquad \text{(D-8)}$$

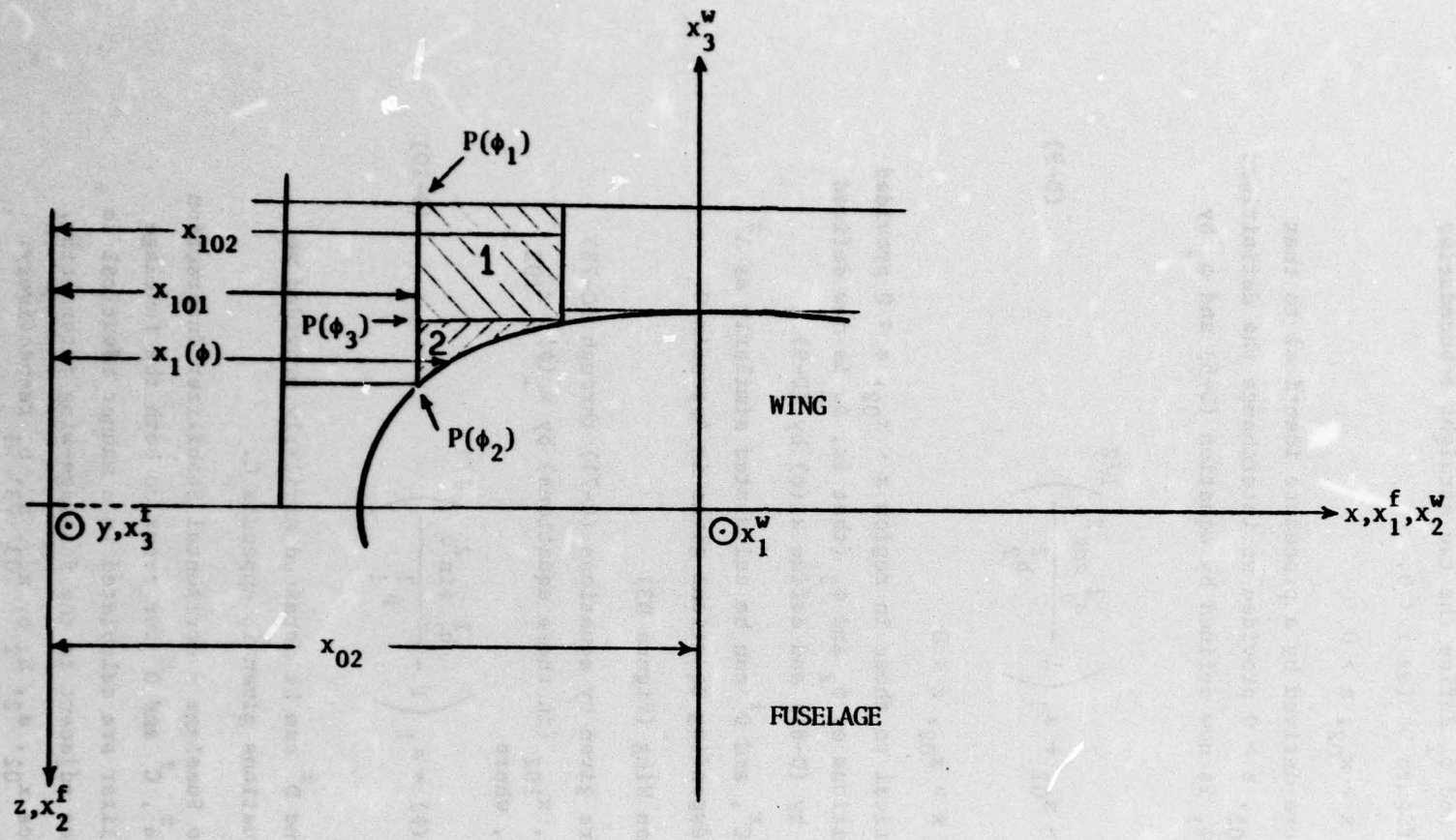

Figure D4: Geometry of the fuselage-wing intersection for the calculation of matrix elements involving zones near the junction on the fuselage for $z < 0$, $x < x_{02}$.

When $x_{02} - x_{101} > a_2$, ϕ_1 and ϕ_2 define the two straight ϕ-boundaries of the leftmost zone in figure D4 for $z < 0$.

(c) Region $x > x_{02}$, $z > 0$

The matrix elements are derived by a procedure identical to that employed in region $x < x_{02}$, $z > 0$ provided we interchange the definitions for ϕ_1 and ϕ_3 (that is, ϕ_1 is now defined by equation (D-5) and ϕ_3 by (D-6)) and define

$$x_1(\phi) = x_{02} + a_2 \left(1 - \frac{a_1^2 \cos^2\phi}{b_2^2}\right)^{1/2} \tag{D-9}$$

(d) Region $x > x_{02}$, $z < 0$

The results are identical to those in region $x < x_{02}$, $z < 0$ provided we interchange the definitions of ϕ_2 and ϕ_3 (that is, ϕ_2 is now defined by equation (D-7) and ϕ_3 by (D-8)) and define $x_1(\phi)$ by (D-9).

Matrix elements $B^{\pm}$, $C^{\pm}$, and $D^{\pm}$ can be calculated similarly as $A^{\pm}$ provided we use the corresponding equations given in Appendix C.

(2) Zones on Wing (figure D3)

Matrix elements $A^{\pm}$ are given by equations (C-71) through (C-73) provided we replace x_{101}, x_{102} (in these equations) by $x_1(\phi)$, x_{102} (figure D3) respectively, where

$$x_1(\phi) = a_1 \left(1 - \frac{b_2^2 \sin^2\phi}{b_1^2}\right)^{1/2} \tag{D-10}$$

Matrix elements $B^{\pm}$, $C^{\pm}$ and $D^{\pm}$ can be obtained similarly provided we use the corresponding equations given in Appendix C.

b. Zones Adjacent to Fuselage - Horizontal Stabilizer Interaction

Matrix elements $A^{\pm}$, $B^{\pm}$, $C^{\pm}$ and $D^{\pm}$ for zones on both the fuselage and the horizontal stabilizer are calculated in a manner identical to the one employed for zones adjacent to the fuselage-wing interaction. Naturally, we must replace x_{02}, a_2, b_2 by x_{03}, a_3, b_3 respectively.

c. Zones Adjacent to Fuselage - Vertical Stabilizer Intersection

(1) Zones on Fuselage (figure D5)

The matrix element $A^{\pm}$ are given by equations (C-63) through (C-65) with the following changes. For subzones labeled (1) in figure D5 we replace ϕ_1, ϕ_2 (as they appear in the equations) by ϕ_3, ϕ_2 (figure D5) respectively where

$$\phi_3 = \sin^{-1}\left[\frac{b_4}{b_1}\left(1 - \frac{(x_{04} - x_{102})^2}{a_4^2}\right)^{1/2}\right], \quad x < x_{04}$$

$$\phi_3 = \sin^{-1}\left[\frac{b_4}{b_1}\left(1 - \frac{(x_{04} - x_{101})^2}{a_4^2}\right)^{1/2}\right] \quad x > x_{04} \qquad \text{(D-11)}$$

and ϕ_2 defines the other boundary of the zone. For subzones labeled (2) in figure D5, we replace ϕ_1, ϕ_2 (as they appear in equations (C-63) through (C-65) by ϕ_1, ϕ_3 (figure D5) respectively and x_{101}, x_{102} (as they appear in equations (C-63) through (C-65)) by x_{101} (figure D5), $x_1(\phi)$ respectively where

$$x_1(\phi) = x_{04} \mp a_4\left(1 - \frac{b_1^2 \sin^2\phi}{b_4^2}\right)^{1/2}, \quad (-) \text{ for } x < x_{04}, \ (+) \text{ for } x > x_{04}$$

$$\phi_1 = \sin^{-1}\left[\frac{b_4}{a_1}\left(1 - \frac{(x_{04} - x_{101})^2}{a_4^2}\right)^{1/2}\right], \quad x < x_{04}, \ x_{04} - x_{101} < a_4$$

$$\phi_1 = \sin^{-1}\left[\frac{b_4}{a_1}\left(1 - \frac{(x_{04} - x_{102})^2}{a_4^2}\right)^{1/2}\right], \quad x > x_{04}, \ x_{04} - x_{101} < a_4$$

(D-12)

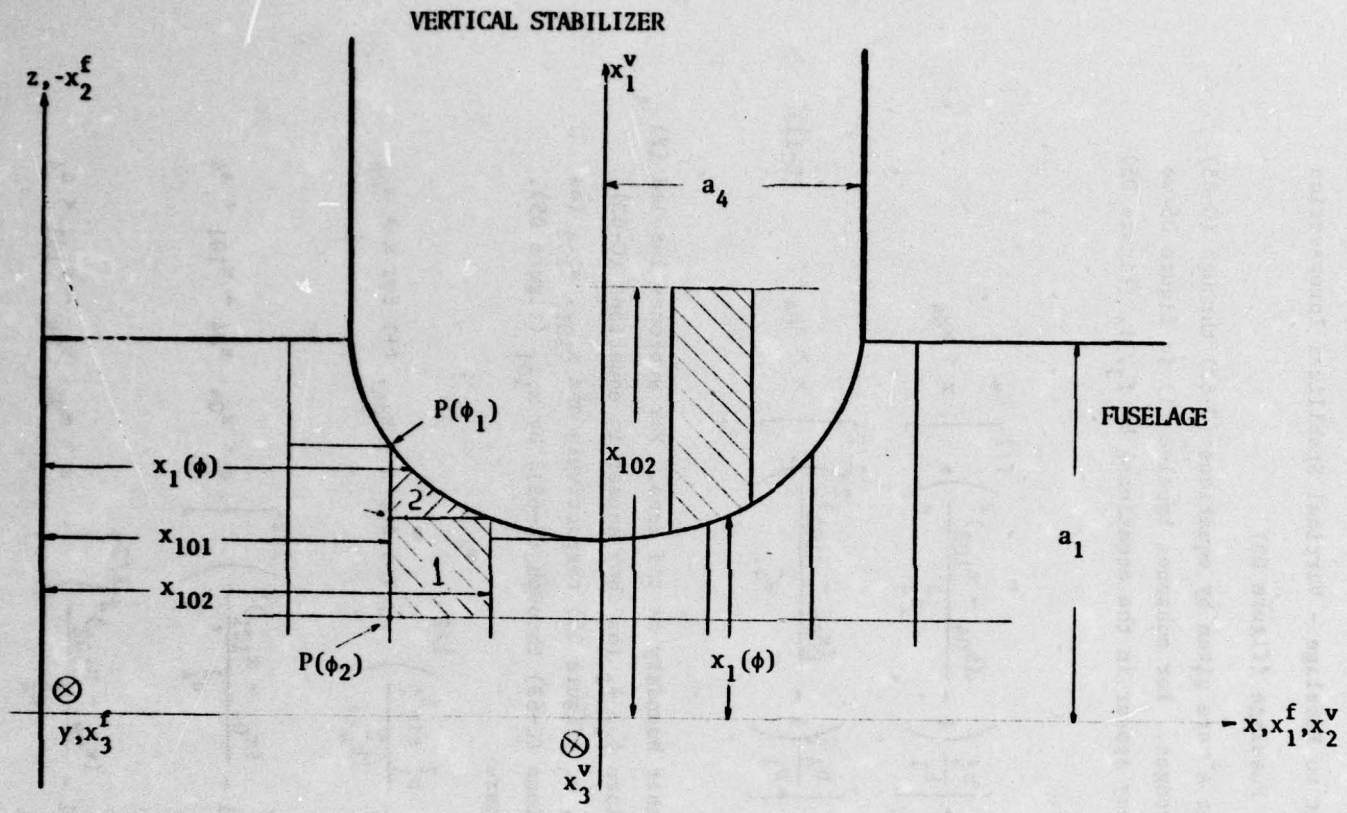

Figure D5: Geometry at the fuselage-vertical stabilizer for the calculation of matrix elements involving zones near the junction.

Notice that when $x_{04} - x_{101} > a_4$ in region $x < x_{04}$ or $x_{102} - x_{04} > a_4$ in region $x > x_{04}$, ϕ_1 and ϕ_2 define the two straight ϕ-boundaries for the leftmost zone in region $x < x_{04}$ or the rightmost zone in region $x > x_{04}$ (figure D5).

Matrix elements $B^{\pm}$, $C^{\pm}$, and $D^{\pm}$ can be derived similarly by using the same substitution as for $A^{\pm}$ in the relevant equation given in Appendix C.

(2) Zones on Vertical Stabilizer (figure D5)

Matrix elements $A^{\pm}$ are given by equations (C-78) through (C-80) provided we replace x_{101}, x_{102} (in these equations) by $x_1(\phi)$, x_{102} (figure D5) respectively, where

$$x_1(\phi) = a_1 \left(1 - \frac{b_4^2 \sin^2\phi}{b_1^2} \right)^{1/2} \qquad \text{(D-13)}$$

Matrix elements $B^{\pm}$, $C^{\pm}$ and $D^{\pm}$ can be derived similarly as we remarked right after equation (D-11).

REFERENCES

1. Sancer, M. I., R. W. Latham and A. D. Varvatsis, Relationship Between Total Currents and Surface Current Densities Induced on Aircraft and Cylinders, Interaction Note 194, Air Force Weapons Laboratory, August 1974.

2. Taylor, C. D., K. T. Chen and T. T. Crow, Electromagnetic Pulse Interaction with the EC-135 Aircraft, AFWL-TR-75-205, Air Force Weapons Laboratory, June 1976.

3. Sancer, M. I., Fundamental Errors Associated with the Gross Modeling of the Physical Features of Metallic Enclosures, AFWL-TR-76-297, Air Force Weapons Laboratory, December 1976.

4. Burton, R. W., R. W. P. King and D. Blejer, Surface Currents and Charges on a Thick Conducting Tube in an E-Polarized Plane-Wave Field, II. Measurements, progress report on contract F29601-75-C-0019, Air Force Weapons Laboratory/ELPE, Kirtland Air Force Base, New Mexico, 1976.

5. King, R. W. P., Surface Currents and Charges on a Thick Conducting Tube in an E-Polarized Plane-Wave Field, IV. Generalization to Cylinders of Various Lengths, progress report on contract F29601-75-C-0019, Air Force Weapons Laboratory/ELPE, Kirtland Air Force Base, New Mexico, 1976.

6. Sancer, M. I. and A. D. Varvatsis, Analytical and Numerical EMP Coupling Solutions for A Class of Structures Attached to the Wing of an Aircraft, AFWL-TR-74-298, July 1975 (also published as AFWL Interaction Note 197, October 1974).

7. Baum, C. E., Interaction of Electromagnetic Fields with an Object Which has an Electromagnetic Symmetry Plane, Interaction Note 63, Air Force Weapons Laboratory, March 1971.

8. Stratton, J. A., Electromagnetic Theory, McGraw-Hill Book Company, Inc., New York and London, 1941.

9. Dwight, H. B., Tables of Integrals and Other Mathematical Data, The Macmillan Company, New York, Fourth Edition, 1964.

10. Marin, L. and R. W. Latham, Analytical Properties of the Field Scattered by a Perfectly Conducting, Finite Body, Interaction Note 92, Air Force Weapons Laboratory, January 1972.

11. Collin, R. E., Field Theory of Guided Waves, McGraw-Hill Book Company, Inc., New York, 1969, pp. 18-20.